RESEARCH MEMORANDUM

THEORETICAL CHARACTERISTICS OF TWO-DIMENSIONAL

SUPERSONIC CONTROL SURFACES

By

Robert R. Morrissette and Lester F. Oborny

Langley Aeronautical Laboratory
Langley Field, Va.

NATIONAL ADVISORY COMMITTEE
FOR AERONAUTICS

WASHINGTON
July 27, 1948

JUN 1 6 1983

Reply to Attn of   139A

TO: Distribution

FROM: 180A/Security Classification Officer

SUBJECT: Authority to Declassify NACA/NASA Documents Dated Prior to
           January 1, 1960

Effective this date, all material *(informal, correspondence)* classified by this Center prior to
January 1, 1960, is declassified. This action does not include material
derivatively classified at the Center upon instructions from other Agencies.

Immediate re-marking is not required; however, until material is re-marked by
lining through the classification and annotating with the following statement,
it must continue to be protected as if classified:

        "Declassified by authority of LaRC Security Classification Officer (SCO)
        letter dated June 16, 1983," and the signature of person performing the
        re-marking.

If re-marking a large amount of material is desirable, but unduly burdensome,
custodians may follow the instructions contained in NHB 1640.4, subpart F,
section 1203.604, paragraph (h).

This declassification action complements earlier actions by the National
Archives and Records Service (NARS) and by the NASA Security Classification
Officer (SCO). In Declassification Review Program 807008, NARS declassified
the Center's "Research Authorization" files, which contain reports, Research
Authorizations, correspondence, photographs, and other documentation.
Earlier, in a 1971 letter, the NASA SCO declassified all NACA/NASA formal
series documents with the exception of the following reports, which must
remain classified:

Document No.	First Author
E-51A30	Nagey
E-53G20	Francisco
E-53G21	Johnson
E-53K18	Spooner
SL-54J21a	Westphal
E-55C16	Fox
E-56H23a	Himmel
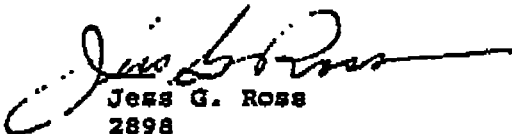
NATIONAL ADVISORY COMMITTEE FOR AERONAUTICS

RESEARCH MEMORANDUM

THEORETICAL CHARACTERISTICS OF TWO-DIMENSIONAL

SUPERSONIC CONTROL SURFACES

By Robert R. Morrissette and Lester F. Oborny

SUMMARY

The "Busemann second-order-approximation theory" for the pressure distribution over a two-dimensional airfoil in supersonic flow was used to determine some of the aerodynamic characteristics of uncambered symmetrical parabolic and double-wedge airfoils with leading-edge and trailing-edge flaps. The investigation was originally intended for application to aileron studies but, since the analysis is based on two-dimensional flow, the results are applicable to all types of control surfaces. The use of the term "aileron" may consequently be replaced in the present paper by the term "control surface." The characteristics presented and discussed are: aileron effectiveness factor, rate of change of hinge-moment coefficient with aileron deflection, rate of change of the pitching-moment coefficient about the midchord with aileron deflection, and the location of the center of pressure of the airfoil-aileron combination. In supersonic flow leading-edge ailerons were found to be much more effective than trailing-edge ailerons. Neither aileron, however, is as effective in supersonic flow as the trailing-edge aileron in subsonic flow. The calculations show that, for a given thickness ratio, trailing-edge ailerons are more effective on wedge airfoils than on parabolic airfoils; whereas leading-edge ailerons are more effective on parabolic airfoils than on wedge airfoils. The magnitude of the values of the rate of change of the hinge-moment coefficient with aileron deflection and the rate of change of pitching-moment coefficient about the midchord with aileron deflection is greater for leading-edge ailerons than for trailing-edge ailerons.

INTRODUCTION

In investigations of the aerodynamic characteristics of ailerons, the influence of certain factors is not found in the predictions based on a linearized solution. Higher-order solutions are therefore necessary and consequently the analysis must be made for a two-dimensional wing. The results are applicable not only to ailerons but to all types of control surfaces.

Several methods are in use at this time for calculating the pressure distribution over thin airfoils in a supersonic air stream. The prevailing methods are: the graphical method of references 1 and 2, the

Ackeret thin-airfoil theory, the Busemann second-order approximation used in reference 3, and the power series of references 2 and 4. None of these methods are exact as they do not consider the effect of the boundary layer on the airfoil.

In this paper the Busemann second-order approximation is used as the best compromise because this approximation gives expressions which are simple enough to be used in design work and which are probably as accurate as could be expected of any method that neglects the boundary-layer thickness. The Busemann approximation uses only the first two terms of the power series found in references 2 and 4. Figures 2, 12, and 13 of reference 2 show that the first two terms of the power series give results that are close approximations to the results obtained by use of the oblique-shock equations and the isentropic-expansion and compression equations. The method used herein is a closer approximation than the Ackeret theory as the Busemann approximation takes into account the effects of Mach number, airfoil thickness, and airfoil shape.

The second-order approximation is limited to small angles and thin airfoils. Reference 2 states that the theory used is not considered accurate for Mach numbers less than approximately 1.3. This lower limit has been used arbitrarily in this analysis. Also, the theory is not good for Mach numbers below that at which the shock wave detaches. Reference 2 gives values for the minimum Mach number for the existence of an attached shock as a function of the flow-deflection angle.

The factors varied in this analysis are airfoil thickness ratio, Mach number, airfoil shape, ratio of aileron chord to wing chord, and location of aileron. The characteristics investigated included aileron effectiveness factor, rate of change of hinge-moment coefficient with aileron deflection, rate of change of pitching-moment coefficient with aileron deflection, and location of center of pressure of the airfoil-aileron combination. The equations used herein and a sample derivation are found in the section entitled "ANALYSIS."

SYMBOLS

c	chord of airfoil (taken as = 1.0 herein)
c_a	chord of aileron, fraction of airfoil chord
C_1 and C_2	constants used in first and second terms of Busemann approximation for pressure coefficient in supersonic flow
c_{h_a}	aileron section hinge-moment coefficient $\left(h_a/q_0 c_a^2 \right)$

c_l airfoil section lift coefficient

$c_{m_{0.5}}$ airfoil section pitching-moment coefficient about midchord $\left(m_{0.5}/q_o c^2 \right)$

C_p center of pressure measured from leading edge, fraction of chord

h_a aileron section hinge moment

$m_{0.5}$ airfoil section pitching moment about midchord

M_o free-stream Mach number

q_o free-stream dynamic pressure $\left(\frac{1}{2}\rho_o V_o^2 \right)$

t maximum thickness of airfoil section

V_o free-stream velocity .

x distance behind leading edge, fraction of chord

y ordinate from chord line to any point on surface of airfoil, fraction of chord

$\Delta p/q$ pressure coefficient

$\dfrac{dc_{l_a}/d\delta_a}{dc_l/d\alpha}$ aileron effectiveness factor

α airfoil angle of attack

δ_a deflection of aileron relative to chord line (considered positive when it gives aileron a positive angle of attack)

δ_a/α geometric parameter used in determining center-of-pressure location

θ local angle between any point on surface of airfoil and free-stream direction

ρ_o free-stream density

γ ratio of specific heats (1.4)

Subscripts:

a   aileron

h   aileron hinge-line position $\left(\text{except when used in}\quad c_{h_a}\right)$

L   lower surface of airfoil

U   upper surface of airfoil
.

ANALYSIS

The analysis used in this paper is based on the Busemann second-order approximation for the pressure coefficient $\dfrac{\Delta p}{q}$ in supersonic flow. This coefficient is expressed in reference 3 in the following form:

$$\frac{\Delta p}{q} = C_1\theta + C_2\theta^2$$

where

$$C_1 = \frac{2}{\sqrt{M_o{}^2 - 1}}$$

$$C_2 = \frac{\gamma M_o{}^4 + \left(M_o{}^2 - 2\right)^2}{2\left(M_o{}^2 - 1\right)^2}$$

The procedure used in deriving the equations for the parameters considered is illustrated by the following derivation of the aileron effectiveness factor of a parabolic airfoil with a trailing-edge aileron. The other parameters are obtained by a similar analysis.
.

Aileron Effectiveness Factor

Parabolic airfoil with trailing-edge aileron. - The equation for the upper surface of a parabolic airfoil with the leading edge at the origin and the trailing edge at $x = 1.0$ is

$$y_U = 2\frac{t}{c}\left(x - x^2\right)$$

The slope at any point on the upper surface of the airfoil is

$$\left(\frac{dy}{dx}\right)_U = 2\frac{t}{c}(1 - 2x)$$

The local angle θ between any point on the surface of the airfoil and the free-stream direction, therefore, is

$$\theta_U = -\alpha + \left(\frac{dy}{dx}\right)_U$$

$$= -\alpha + 2\frac{t}{c}(1 - 2x)$$

and

$$\theta_L = \alpha - \left(\frac{dy}{dx}\right)_L$$

$$= \alpha + 2\frac{t}{c}(1 - 2x)$$

It follows then that

$$\left(\frac{\Delta p}{q}\right)_U = c_1\theta_U + c_2\theta_U^2$$

$$= c_1\left[-\alpha + 2\frac{t}{c}(1 - 2x)\right] + c_2\left[-\alpha + 2\frac{t}{c}(1 - 2x)\right]^2$$

and

$$\left(\frac{\Delta p}{q}\right)_L = C_1\left[\alpha + 2\frac{t}{c}(1 - 2x)\right] + C_2\left[\alpha + 2\frac{t}{c}(1 - 2x)\right]^2$$

The pressure coefficient for the airfoil then is

$$\frac{\Delta p}{q} = \left(\frac{\Delta p}{q}\right)_L - \left(\frac{\Delta p}{q}\right)_U$$

or

$$\frac{\Delta p}{q} = C_1(2\alpha) + C_2\left[8\alpha\frac{t}{c}(1 - 2x)\right]$$

The lift coefficient of the airfoil is

$$c_l = \int_0^{1.0} \frac{\Delta p}{q}\, dx$$

$$= 2\alpha \int_0^{1.0} \left[C_1 + 4C_2\frac{t}{c}(1 - 2x)\right] dx$$

$$= 2\alpha\left[C_1 x + 4C_2\frac{t}{c}\left(x - x^2\right)\right]_0^{1.0}$$

$$= 2\alpha C_1$$

The rate of change of lift coefficient with angle of attack therefore is

$$\frac{dc_l}{d\alpha} = 2C_1$$

The lift coefficient of the aileron c_{l_a} due to some aileron deflection δ_a can be found in a similar manner.

Because of the linear nature of the equations for pressure coefficient, the pressure coefficient at a point on the airfoil can be found by adding the pressure coefficient for the wing at angle of attack α with undeflected ailerons to the pressure coefficient for the wing at zero angle of attack with the aileron at angle of attack δ_a. The contribution of the aileron defines the control force on the wing and for that reason may be treated as a separate aileron pressure coefficient.

The pressure coefficient for the aileron $\left(\dfrac{\Delta p}{q}\right)_a$, therefore, is the same as that found for the airfoil except that the aileron deflection δ_a is used in place of the angle of attack α. Thus,

$$\left(\frac{\Delta p}{q}\right)_a = 2\delta_a\left[C_1 + 4C_2\frac{t}{c}(1 - 2x)\right]$$

Then, the lift coefficient for the aileron due to some deflection is

$$c_{l_a} = \int_{x_h}^{1.0} \left(\frac{\Delta p}{q}\right)_a dx$$

$$= 2\delta_a \int_{x_h}^{1.0} \left[C_1 + 4C_2\frac{t}{c}(1 - 2x)\right] dx$$

$$= 2\delta_a\left[C_1 x + 4C_2\frac{t}{c}\left(x - x^2\right)\right]_{x_h}^{1.0}$$

$$= 2\delta_a\left(1 - x_h\right)\left(C_1 - 4C_2\frac{t}{c}x_h\right)$$

and, therefore, the rate of change of lift coefficient of aileron with aileron deflection is

$$\frac{dc_{l_a}}{d\delta_a} = 2\left(1 - x_h\right)\left(C_1 - 4C_2\frac{t}{c}x_h\right)$$

The aileron effectiveness factor for a parabolic airfoil with trailing-edge aileron thus is

$$\frac{dc_{l_a}/d\delta_a}{dc_l/d\alpha} = \frac{2\left(1 - x_h\right)\left(C_1 - 4C_2\frac{t}{c}x_h\right)}{2C_1}$$

$$= \left(1 - x_h\right)\left(1 - 4\frac{C_2}{C_1}\frac{t}{c}x_h\right)$$

<u>Parabolic airfoil with leading-edge aileron</u>.- The aileron effectiveness factor for a parabolic airfoil with a leading-edge aileron is

$$\frac{dc_{l_a}/d\delta_a}{dc_l/d\alpha} = x_h\left[1 + 4\frac{C_2}{C_1}\frac{t}{c}\left(1 - x_h\right)\right]$$

<u>Wedge airfoil with trailing-edge aileron</u>.- The aileron effectiveness factor for a wedge airfoil with a trailing-edge aileron when $x_h \geqq 0.50$ is

$$\frac{dc_{l_a}/d\delta_a}{dc_l/d\alpha} = \left(1 - x_h\right)\left(1 - 2\frac{C_2}{C_1}\frac{t}{c}\right)$$

and when $x_h \leqq 0.50$,

$$\frac{dc_{l_a}/d\delta_a}{dc_l/d\alpha} = 1 - x_h\left(1 + 2\frac{C_2}{C_1}\frac{t}{c}\right)$$

Wedge airfoil with leading-edge aileron.- The aileron effectiveness factor for a wedge airfoil with a leading-edge aileron when $x_h \geqq 0.50$ is

$$\frac{dc_{l_a}/d\delta_a}{dc_l/d\alpha} = x_h + 2\frac{c_2}{c_1}\frac{t}{c}\left(1 - x_h\right)$$

and when $x_h \leqq 0.50$,

$$\frac{dc_{l_a}/d\delta_a}{dc_l/d\alpha} = x_h\left(1 + 2\frac{c_2}{c_1}\frac{t}{c}\right)$$

Rate of Change of Aileron Hinge-Moment Coefficient with Aileron

Deflection

Parabolic airfoil with trailing-edge aileron.- The equation for the rate of change of aileron hinge-moment coefficient with aileron deflection of a parabolic airfoil having a trailing-edge aileron is given as

$$\frac{\partial c_{h_a}}{\partial \delta_a} = -c_1 + \frac{4}{3}c_2\frac{t}{c}\left(1 + 2x_h\right)$$

Parabolic airfoil with leading-edge aileron.- The rate of change of aileron hinge-moment coefficient with aileron deflection of a parabolic airfoil with a leading-edge aileron is

$$\frac{\partial c_{h_a}}{\partial \delta_a} = c_1 + \frac{4}{3}c_2\frac{t}{c}\left(3 - 2x_h\right)$$

Wedge airfoil with trailing-edge aileron.- The rate of change of aileron hinge-moment coefficient with aileron deflection of a wedge airfoil with a trailing-edge aileron when $x_h \geqq 0.50$ is

$$\frac{\partial c_{h_a}}{\partial \delta_a} = -c_1 + 2c_2\frac{t}{c}$$

and when $x_h \leqq 0.50$,

$$\frac{\partial c_{h_a}}{\partial \delta_a} = -C_1 + C_2\frac{t}{c}\frac{\left(1 - 2x_h^2\right)}{\left(1 - x_h\right)^2}$$

<u>Wedge airfoil with leading-edge aileron</u>.- The rate of change of aileron hinge-moment coefficient with aileron deflection of a wedge airfoil having a leading-edge aileron when $x_h \geq 0.50$ is

$$\frac{\partial c_{h_a}}{\partial \delta_a} = C_1 - C_2\frac{t}{c}\frac{\left(1 - 4x_h + 2x_h^2\right)}{x_h^2}$$

and when $x_h \leqq 0.50$,

$$\frac{\partial c_{h_a}}{\partial \delta_a} = C_1 + 2C_2\frac{t}{c}$$

Rate of Change of Pitching-Moment Coefficient about Midchord with

Aileron Deflection

<u>Parabolic airfoil with trailing-edge aileron</u>.- The rate of change of pitching-moment coefficient about midchord with aileron deflection of a parabolic airfoil having a trailing-edge aileron is given as

$$\frac{\partial c_{m_{0.5}}}{\partial \delta_a} = C_1\left(x_h^2 - x_h\right) + \frac{4}{3}C_2\frac{t}{c}\left(-4x_h^3 + 6x_h^2 - 3x_h + 1\right)$$

<u>Parabolic airfoil with leading-edge aileron</u>.- The rate of change of pitching-moment coefficient about midchord with aileron deflection of a parabolic airfoil with a leading-edge aileron is

$$\frac{\partial c_{m_{0.5}}}{\partial \delta_a} = x_h\left[C_1\left(1 - x_h\right) + \frac{4}{3}C_2\frac{t}{c}\left(3 - 6x_h + 4x_h^2\right)\right]$$

Wedge airfoil with trailing-edge aileron.- The rate of change of
pitching-moment coefficient about midchord with aileron deflection for
a trailing-edge aileron when $x_h \geq 0.50$ is

$$\frac{\partial c_{m_{0.5}}}{\partial \delta_a} = \left(x_h^2 - x_h\right)\left(C_1 - 2C_2\frac{t}{c}\right)$$

and when $x_h \leq 0.50$,

$$\frac{\partial c_{m_{0.5}}}{\partial \delta_a} = C_1\left(x_h^2 - x_h\right) + C_2\frac{t}{c}\left(2x_h^2 - 2x_h + 1\right)$$

Wedge airfoil with leading-edge aileron.- The rate of change of
pitching-moment coefficient about midchord with aileron deflection for
a leading-edge aileron when $x_h \geq 0.50$ is

$$\frac{\partial c_{m_{0.5}}}{\partial \delta_a} = C_1\left(x_h - x_h^2\right) + C_2\frac{t}{c}\left(1 - 2x_h + 2x_h^2\right)$$

and when $x_h \leq 0.50$,

$$\frac{\partial c_{m_{0.5}}}{\partial \delta_a} = \left(x_h - x_h^2\right)\left(C_1 + 2C_2\frac{t}{c}\right)$$

Rate of Change of Pitching-Moment Coefficient about Midchord

with Angle of Attack

Parabolic airfoil.- The rate of change of pitching-moment coeffi-
cient about midchord with angle of attack for a parabolic airfoil is

$$\frac{\partial c_{m_{0.5}}}{\partial \alpha} = \frac{4}{3}C_2\frac{t}{c}$$

Wedge airfoil.- The equation for the rate of change of pitching-moment coefficient about midchord with angle of attack for a wedge airfoil is given as

$$\frac{\partial c_{m_{0.5}}}{\partial \alpha} = C_2 \frac{t}{c}$$

These equations were obtained from equations found in reference 3 and are given here for the sake of completeness.

Center of Pressure

Parabolic airfoil with trailing-edge aileron.- The center-of-pressure equation for a parabolic airfoil having a trailing-edge aileron is as follows:

$$c_p = \frac{1 - \frac{4}{3}\frac{C_2}{C_1}\frac{t}{c} + \frac{\delta_a}{\alpha}\left[1 - x_h{}^2 - \frac{4}{3}\frac{C_2}{C_1}\frac{t}{c}\left(1 + 3x_h{}^2 - 4x_h{}^3\right)\right]}{2 + \frac{\delta_a}{\alpha}\left(1 - x_h\right)\left(2 - 8\frac{C_2}{C_1}\frac{t}{c}x_h\right)}$$

Parabolic airfoil with leading-edge aileron.- The following center-of-pressure equation for a parabolic airfoil with a leading-edge aileron is expressed as:

$$c_p = \frac{1 - \frac{4}{3}\frac{C_2}{C_1}\frac{t}{c} + x_h{}^2\frac{\delta_a}{\alpha}\left[1 + \frac{4}{3}\frac{C_2}{C_1}\frac{t}{c}\left(3 - 4x_h\right)\right]}{2 + 2x_h\frac{\delta_a}{\alpha}\left[1 + 4\frac{C_2}{C_1}\frac{t}{c}\left(1 - x_h\right)\right]}$$

Wedge airfoil with trailing-edge aileron.- The center of pressure for a wedge airfoil with a trailing-edge aileron when $x_h \geqq 0.50$ is

$$c_p = \frac{1 - \dfrac{c_2}{c_1}\dfrac{t}{c} + \dfrac{\delta_a}{\alpha}\left[1 - x_h{}^2 + 2\dfrac{c_2}{c_1}\dfrac{t}{c}\left(x_h{}^2 - 1\right)\right]}{2 + \dfrac{\delta_a}{\alpha}\left(1 - x_h\right)\left(2 - 4\dfrac{c_2}{c_1}\dfrac{t}{c}\right)}$$

and when $x_h \leqq 0.50$,

$$c_p = \frac{1 - \dfrac{c_2}{c_1}\dfrac{t}{c} + \dfrac{\delta_a}{\alpha}\left[1 - x_h{}^2 - \dfrac{c_2}{c_1}\dfrac{t}{c}\left(1 + 2x_h{}^2\right)\right]}{2 + \dfrac{\delta_a}{\alpha}\left[2 - x_h\left(2 + 4\dfrac{c_2}{c_1}\dfrac{t}{c}\right)\right]}$$

<u>Wedge airfoil with leading-edge aileron</u>.- The center of pressure for a wedge airfoil with a leading-edge aileron when $x_h \geqq 0.50$ is

$$c_p = \frac{1 - \dfrac{c_2}{c_1}\dfrac{t}{c} + \dfrac{\delta_a}{\alpha}\left[x_h{}^2 + \dfrac{c_2}{c_1}\dfrac{t}{c}\left(1 - 2x_h{}^2\right)\right]}{2 + 2\dfrac{\delta_a}{\alpha}\left[x_h + 2\dfrac{c_2}{c_1}\dfrac{t}{c}\left(1 - x_h\right)\right]}$$

and when $x_h \leqq 0.50$,

$$c_p = \frac{1 - \dfrac{c_2}{c_1}\dfrac{t}{c} + x_h{}^2\dfrac{\delta_a}{\alpha}\left(1 + 2\dfrac{c_2}{c_1}\dfrac{t}{c}\right)}{2 + 2x_h\dfrac{\delta_a}{\alpha}\left(1 + 2\dfrac{c_2}{c_1}\dfrac{t}{c}\right)}$$

RESULTS

Drawings of the parabolic and wedge airfoil sections used in the calculations may be seen in figure 1. These two shapes were chosen because they are frequently considered for use in the wings of supersonic aircraft.

In figures 2 to 40 is shown the variation of the aerodynamic characteristics of ailerons with airfoil shape, location of aileron, airfoil thickness ratio, free-stream Mach number, ratio of aileron chord to wing chord, and the ratio of aileron deflection to the angle of attack. Table I is an index of the figures.

In figure 2 (fig. 9, reference 5 except Busemann curve) a comparison is shown of the results obtained by the method of calculation used herein and the results obtained by both the Ackeret theory and the method of reference 1. The method presented in this paper gives results that approach those of the method of reference 1 much closer than the Ackeret theory. This closer result is due to the fact that thickness ratio, Mach number, and airfoil shape are taken into consideration in the second-order approximation, whereas these factors are neglected in the Ackeret theory.

Figure 2 also shows that the aileron effectiveness for trailing-edge ailerons in subsonic flow is much higher than the aileron effectiveness of trailing-edge ailerons in supersonic flow. The reason for this result is that the flow ahead of the aileron is affected by the aileron in subsonic flow, whereas the flow in this region is not affected by the aileron in supersonic flow.

Unlike the Ackeret theory, the analysis used herein gives the following results for an airfoil-aileron combination in supersonic flow:

(1) Leading-edge ailerons are more effective than trailing-edge ailerons. (See figs. 3 to 7.)

(2) The magnitude of the values of $\partial c_{h_a}/\partial \delta_a$ and $\partial c_{m_{0.5}}/\partial \delta_a$ is greater for leading-edge ailerons than for trailing-edge ailerons. (See figs. 13 to 17 and 22 to 26.)

(3) The center of pressure of an airfoil-aileron combination having maximum thickness at the midchord and zero aileron deflection is ahead of the midchord (figs. 31 to 34).

Mach number. - An increase in the free-stream Mach number gives the following results:

(1) Above a Mach number of approximately 1.75 (depending on thickness ratio), the aileron effectiveness for leading-edge ailerons is

increased and the aileron effectiveness for trailing-edge ailerons is decreased. (See figs. 8 to 11.)

(2) The magnitude of the values of $\partial c_{h_a}/\partial \delta_a$ and $\partial c_{m_{0.5}}/\partial \delta_a$ is decreased for both leading-edge and trailing-edge ailerons (figs. 18 to 21 and 27 to 30).

(3) In general, above a Mach number of approximately 1.7 the center of pressure of an airfoil-aileron combination moves forward as shown in figures 31 to 34.

Thickness ratio.- The main difference between the first-order and second-order approximations is the thickness-ratio effect. The second-order approximation shows that an increase in airfoil thickness ratio:

(1) Increases the effectiveness of leading-edge ailerons and decreases the effectiveness of trailing-edge ailerons. When the thickness ratio is zero, the effectiveness is the same for both leading-edge and trailing-edge ailerons. (See fig. 12.)

(2). Increases the magnitude of the values of $\partial c_{h_a}/\partial \delta_a$ and $\partial c_{m_{0.5}}/\partial \delta_a$ for leading-edge ailerons and decreases the magnitude for trailing-edge ailerons as shown in figures 18 to 21 and 27 to 30.

(3) Moves the center of pressure of the airfoil-aileron combination forward (fig. 40).

Airfoil shape.- For a given thickness ratio of the airfoils considered herein, the surface slope near both the leading and trailing edges of the parabolic airfoil is greater than the slope at corresponding positions on the wedge airfoil. In these regions, therefore, the parabolic airfoil acts like an airfoil with a larger thickness ratio. It then follows that:

(1) For a given value of t/c, trailing-edge ailerons are more effective on wedge airfoils than on parabolic airfoils; whereas leading-edge ailerons are more effective on parabolic airfoils than on wedge airfoils. (See figs. 3 to 7.)

(2) The center of pressure is farther forward for the parabolic airfoil than for the wedge airfoil (figs. 31 to 39).

Ratio of aileron chord to wing chord.- An increase in the chord of the aileron increases the surface area of the aileron. As a result of this increase in aileron surface:

(1) The aileron effectiveness is increased (figs. 2 to 7).

(2) The magnitude of the value of $\partial c_{m_{0.5}}/\partial \delta_a$ increases until the aileron chord reaches a value of half the wing chord; then it decreases as the aileron chord is increased further. (See figs. 22 to 26.)

Since the pressure distribution over the wedge airfoil is independent of the chordwise location as long as the surface slope is a constant, the value of $\partial c_{h_a}/\partial \delta_a$ is independent of the ratio of the aileron chord to the wing chord. After the value of c_a/c exceeds 0.5, however, the surface slope changes and the pressure coefficient is no longer independent of the chordwise location. Thus, for further increases in c_a/c beyond this value, the value of $\partial c_{h_a}/\partial \delta_a$ then decreases for leading-edge ailerons and increases negatively for trailing-edge ailerons (figs. 14, 16, and 17).

The theory shows the pressure distribution over a parabolic airfoil to be a function of the chordwise location. As a result, when the ratio c_a/c is increased, the value of $\partial c_{h_a}/\partial \delta_a$ decreases for leading-edge ailerons and increases negatively for trailing-edge ailerons. (See figs. 13, 15, and 17.)

Ratio of aileron deflection to angle of attack.- Increasing the ratio of the aileron deflection to the angle of attack results in a relatively higher pressure on the aileron surfaces than on the rest of the airfoil. The center of pressure is thus shifted forward when leading-edge ailerons are used and backward when trailing-edge ailerons are used. (See figs. 31 to 34.)

CONCLUSIONS

The "Busemann second-order-approximation theory" for the pressure distribution over a two-dimensional airfoil in supersonic flow was used to determine some of the aerodynamic characteristics of uncambered symmetrical parabolic and double-wedge airfoils with leading-edge and trailing-edge ailerons. Within the limitations of the theory used, the following conclusions may be drawn about the effectiveness of ailerons in the Mach number range (1.3 to 4.0) investigated:

1. Neither leading-edge nor trailing-edge ailerons are as effective in supersonic flow as the trailing-edge aileron in subsonic flow.

2. For a given airfoil shape at high Mach numbers, leading-edge ailerons are much more effective than trailing-edge ailerons. However, the relative effectiveness of leading-edge and trailing-edge ailerons is a function of thickness ratio and the difference between the two becomes smaller with smaller thickness ratios.

3. For a given thickness ratio the aileron effectiveness is greater for leading-edge ailerons on parabolic airfoils than for leading-edge ailerons on symmetrical wedge-shape airfoils; however, trailing-edge ailerons are more effective on symmetrical wedge-shape airfoils than on parabolic airfoils.

4. An increase in airfoil thickness tends to decrease the aileron effectiveness when trailing-edge ailerons are used, whereas it increases the aileron effectiveness when leading-edge ailerons are used.

5. The magnitude of the values of the rate of change of the hinge-moment coefficient with aileron deflection and the rate of change of pitching-moment coefficient about the midchord with aileron deflection is greater for leading-edge ailerons than for trailing-edge ailerons.

Langley Memorial Aeronautical Laboratory
    National Advisory Committee for Aeronautics
        Langley Field, Va.

REFERENCES

1. Ivey, H. Reese, Stickle, George W., and Schuettler, Alberta: Charts for Determining the Characteristics of Sharp-Nose Airfoils in Two-Dimensional Flow at Supersonic Speeds. NACA TN No. 1143, 1947.

2. Laitone, Edmund V.: Exact and Approximate Solutions of Two-Dimensional Oblique Shock Flow. Jour. Aero. Sci., vol. 14, no. 1, Jan. 1947, pp. 25-41.

3. Bonney, E. Arthur: Aerodynamic Characteristics of Rectangular Wings at Supersonic Speeds. Jour. Aero. Sci., vol. 14, no. 2, Feb. 1947, pp. 110-116.

4. Busemann, A.: Aerodynamic Lift at Supersonic Speeds. 2844, Ae. Techl. 1201, British A.R.C., Feb. 3, 1937. (From Luftfahrtforschung, Bd. 12, Nr. 6, Oct. 3, 1935, pp. 210-220.)

5. Ivey, H. Reese: Notes on the Theoretical Characteristics of Two-Dimensional Supersonic Airfoils. NACA TN No. 1179, 1947.

TABLE I — INDEX OF FIGURES

Figure	Plot	Type of airfoil	Location of aileron	M_0	t/c	c_a/c	δ_a/α
1	Drawings of airfoil sections used	---------	------------	--------	----	----	---
2	$\dfrac{dc_{l_a}/d\delta_a}{dc_l/d\alpha}$ against c_a/c	Wedge	Trailing edge	4.0	0.05	0 to 1.0	---
3	$\dfrac{dc_{l_a}/d\delta_a}{dc_l/d\alpha}$ against c_a/c	Parabolic	Trailing edge	1.5,3.0, 4.0	.05, .10	0 to 1.0	---
4	$\dfrac{dc_{l_a}/d\delta_a}{dc_l/d\alpha}$ against c_a/c	Wedge	Trailing edge	1.5,3.0, 4.0	.05, .10	0 to 1.0	---
5	$\dfrac{dc_{l_a}/d\delta_a}{dc_l/d\alpha}$ against c_a/c	Parabolic	Leading edge	1.5,3.0, 4.0	.05, .10	0 to 1.0	---
6	$\dfrac{dc_{l_a}/d\delta_a}{dc_l/d\alpha}$ against c_a/c	Wedge	Leading edge	1.5,3.0, 4.0	.05, .10	0 to 1.0	---
7	$\dfrac{dc_{l_a}/d\delta_a}{dc_l/d\alpha}$ against c_a/c	Parabolic and wedge	Trailing and leading edges	4.0	.10	0 to 1.0	---
8	$\dfrac{dc_{l_a}/d\delta_a}{dc_l/d\alpha}$ against M_0	Parabolic	Trailing edge	1.3 to 4.0	0,.05, .10	.2	---
9	$\dfrac{dc_{l_a}/d\delta_a}{dc_l/d\alpha}$ against M_0	Wedge	Trailing edge	1.3 to 4.0	0,.05, .10	.2	---
10	$\dfrac{dc_{l_a}/d\delta_a}{dc_l/d\alpha}$ against M_0	Parabolic	Leading edge	1.3 to 4.0	0,.05, .10	.2	---
11	$\dfrac{dc_{l_a}/d\delta_a}{dc_l/d\alpha}$ against M_0	Wedge	Leading edge	1.3 to 4.0	0,.05, .10	.2	---
12	$\dfrac{dc_{l_a}/d\delta_a}{dc_l/d\alpha}$ against t/c	Parabolic	Trailing and leading edges	1.5,3.0, 4.0	0 to .10	.2	---
13	$\dfrac{\partial c_{h_a}}{\partial \delta_a}$ against c_a/c	Parabolic	Trailing edge	1.5,2.0, 4.0	.05, .10	0 to 1.0	---

NACA

TABLE I — INDEX OF FIGURES — Continued

Figure	Plot	Type of airfoil	Location of aileron	M_0	t/c	c_a/c	δ_a/α
14	$\dfrac{\partial c_{h_a}}{\partial \delta_a}$ against c_a/c	Wedge	Trailing edge	1.5, 2.0, 4.0	0.05, .10	0 to 1.0	---
15	$\dfrac{\partial c_{h_a}}{\partial \delta_a}$ against c_a/c	Parabolic	Leading edge	1.5, 2.0, 4.0	.05, .10	0 to 1.0	---
16	$\dfrac{\partial c_{h_a}}{\partial \delta_a}$ against c_a/c	Wedge	Leading edge	1.5, 2.0, 4.0	.05, .10	0 to 1.0	---
17	$\dfrac{\partial c_{h_a}}{\partial \delta_a}$ against c_a/c	Parabolic and wedge	Trailing and leading edges	4.0	.10	0 to 1.0	---
18	$\dfrac{\partial c_{h_a}}{\partial \delta_a}$ against M_0	Parabolic	Trailing edge	1.3 to 4.0	.05, .10	.2	---
19	$\dfrac{\partial c_{h_a}}{\partial \delta_a}$ against M_0	Wedge	Trailing edge	1.3 to 4.0	.05, .10	.2	---
20	$\dfrac{\partial c_{h_a}}{\partial \delta_a}$ against M_0	Parabolic	Leading edge	1.3 to 4.0	.05, .10	.2	---
21	$\dfrac{\partial c_{h_a}}{\partial \delta_a}$ against M_0	Wedge	Leading edge	1.3 to 4.0	.05, .10	.2	---
22	$\dfrac{\partial c_{m_{0.5}}}{\partial \delta_a}$ against c_a/c	Parabolic	Trailing edge	1.5, 2.0, 4.0	.05, .10	0 to 1.0	---
23	$\dfrac{\partial c_{m_{0.5}}}{\partial \delta_a}$ against c_a/c	Wedge	Trailing edge	1.5, 2.0, 4.0	.05, .10	0 to 1.0	---
24	$\dfrac{\partial c_{m_{0.5}}}{\partial \delta_a}$ against c_a/c	Parabolic	Leading edge	1.5, 2.0, 4.0	.05, .10	0 to 1.0	---
25	$\dfrac{\partial c_{m_{0.5}}}{\partial \delta_a}$ against c_a/c	Wedge	Leading edge	1.5, 2.0, 4.0	.05, .10	0 to 1.0	---
26	$\dfrac{\partial c_{m_{0.5}}}{\partial \delta_a}$ against c_a/c	Parabolic and wedge	Trailing and leading edges	2.0	.10	0 to 1.0	---

TABLE I — INDEX OF FIGURES — Concluded

Figure	Plot	Type of airfoil	Location of aileron	M_o	t/c	c_a/c	δ_a/α
27	$\dfrac{\partial c_{m_{0.5}}}{\partial \delta_a}$ against M_o	Parabolic	Trailing edge	1.3 to 4.0	0.05, .10	0.2	---
28	$\dfrac{\partial c_{m_{0.5}}}{\partial \delta_a}$ against M_o	Wedge	Trailing edge	1.3 to 4.0	.05, .10	.2	---
29	$\dfrac{\partial c_{m_{0.5}}}{\partial \delta_a}$ against M_o	Parabolic	Leading edge	1.3 to 4.0	.05, .10	.2	---
30	$\dfrac{\partial c_{m_{0.5}}}{\partial \delta_a}$ against M_o	Wedge	Leading edge	1.3 to 4.0	.05, .10	.2	---
31	C_p against M_o	Parabolic	Trailing edge	1.3 to 4.0	.10	.2	0 to ∞
32	C_p against M_o	Wedge	Trailing edge	1.3 to 4.0	.10	.2	0 to ∞
33	C_p against M_o	Parabolic	Leading edge	1.3 to 4.0	.10	.2	0 to ∞
34	C_p against M_o	Wedge	Leading edge	1.3 to 4.0	.10	.2	0 to ∞
35	C_p against c_a/c	Parabolic	Trailing edge	4.0	.05, .10	0 to 1.0	1.0
36	C_p against c_a/c	Wedge	Trailing edge	4.0	.05, .10	0 to 1.0	1.0
37	C_p against c_a/c	Parabolic	Leading edge	4.0	.05, .10	0 to 1.0	1.0
38	C_p against c_a/c	Wedge	Leading edge	4.0	.05, .10	0 to 1.0	1.0
39	C_p against c_a/c	Parabolic and wedge	Trailing and leading edges	4.0	.10	0 to 1.0	1.0
40	C_p against t/c	Parabolic	Trailing and leading edges	1.5, 3.0, 4.0	0 to .10	.2	1.0

NACA

NACA RM No. L8G12
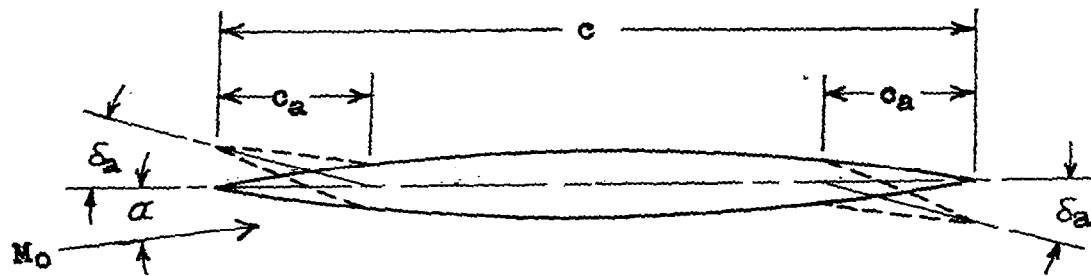
(a) Parabolic airfoil.
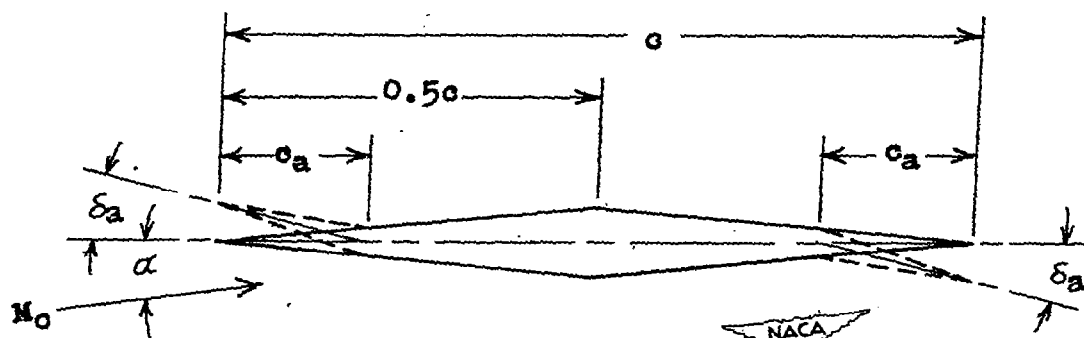
(b) Wedge airfoil.

Figure 1.— Airfoil sections used in calculations.
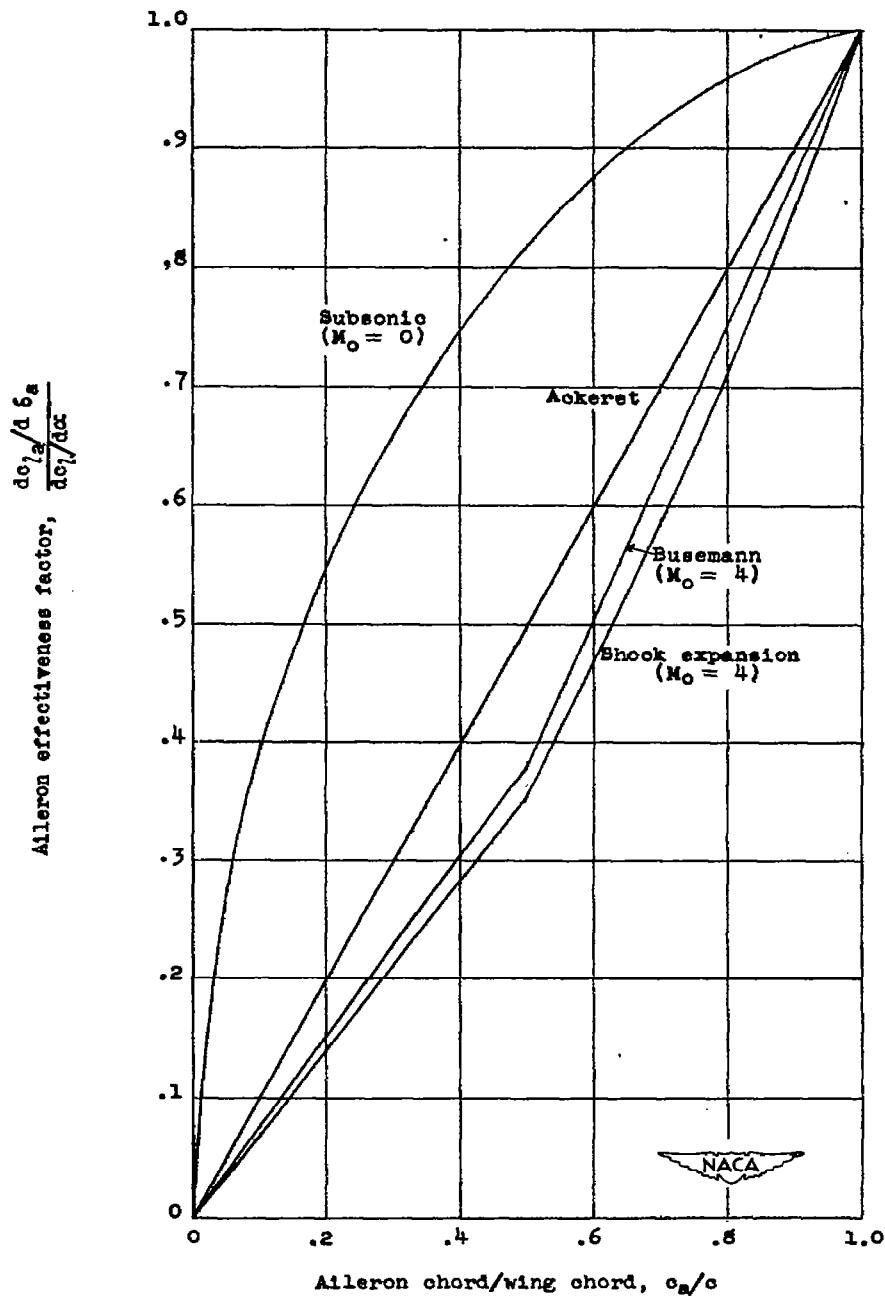
Figure 2.- Aileron effectiveness as a function of the ratio of aileron chord to wing chord for an uncambered wedge airfoil having maximum thickness at midchord and trailing-edge aileron. $\frac{t}{c} = 0.05$. (Curves with exception of Busemann curve are from figure 9, reference 5.)
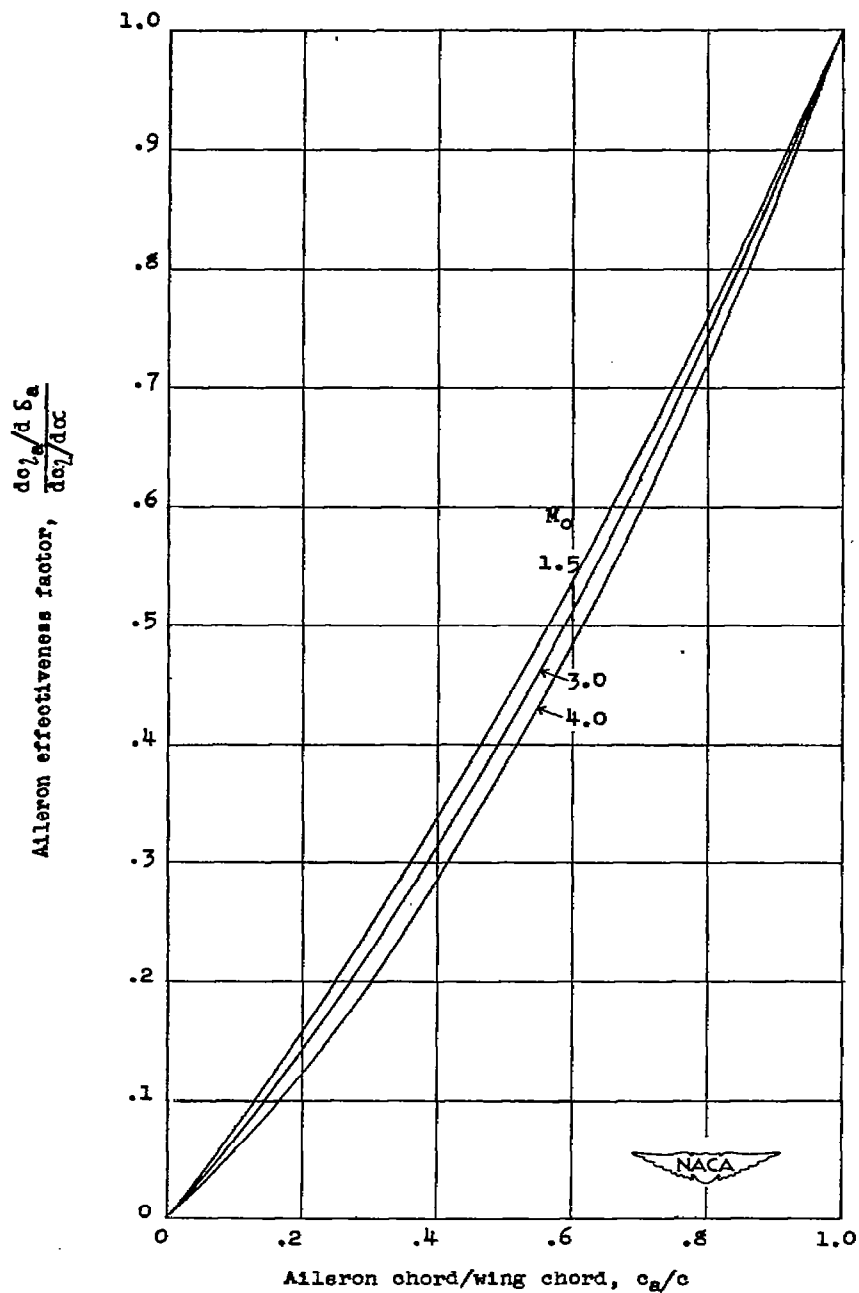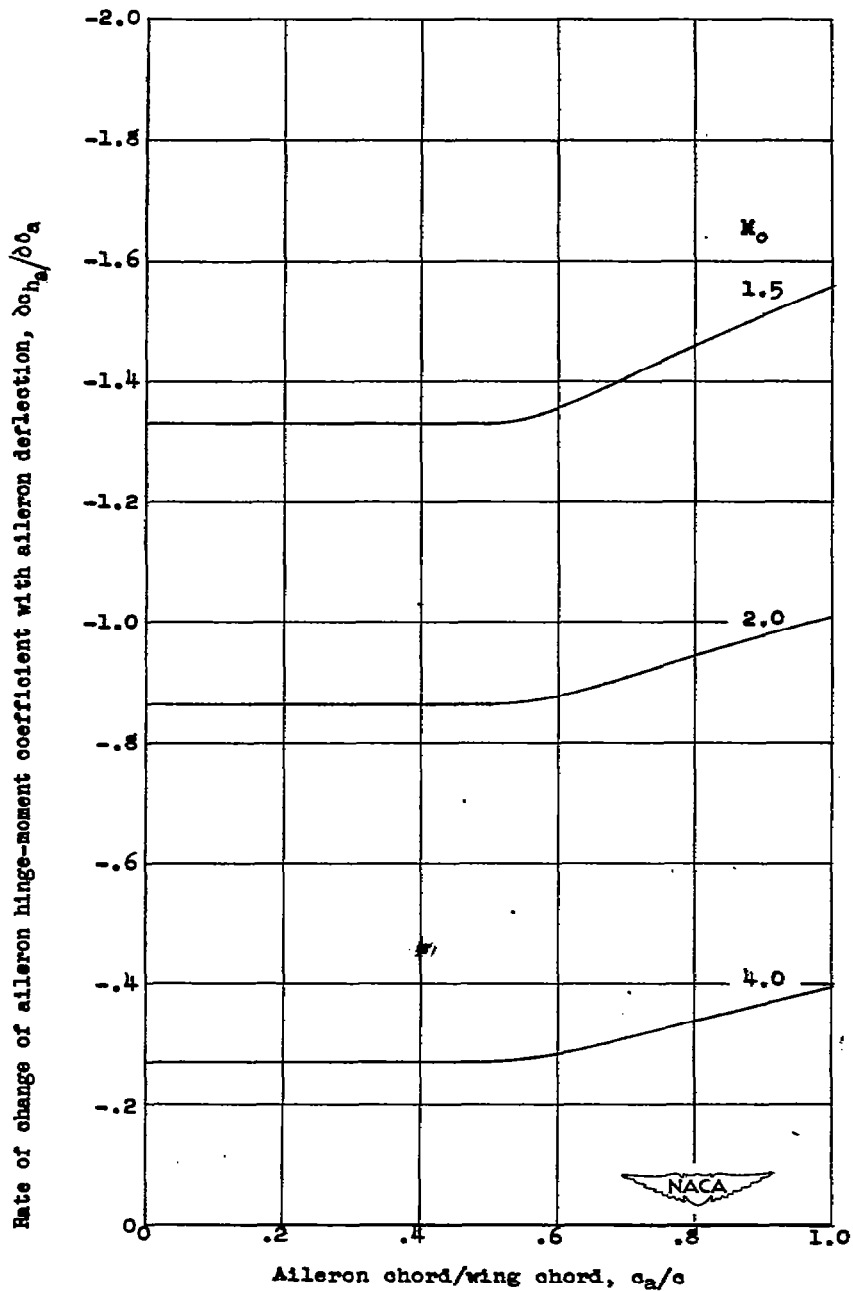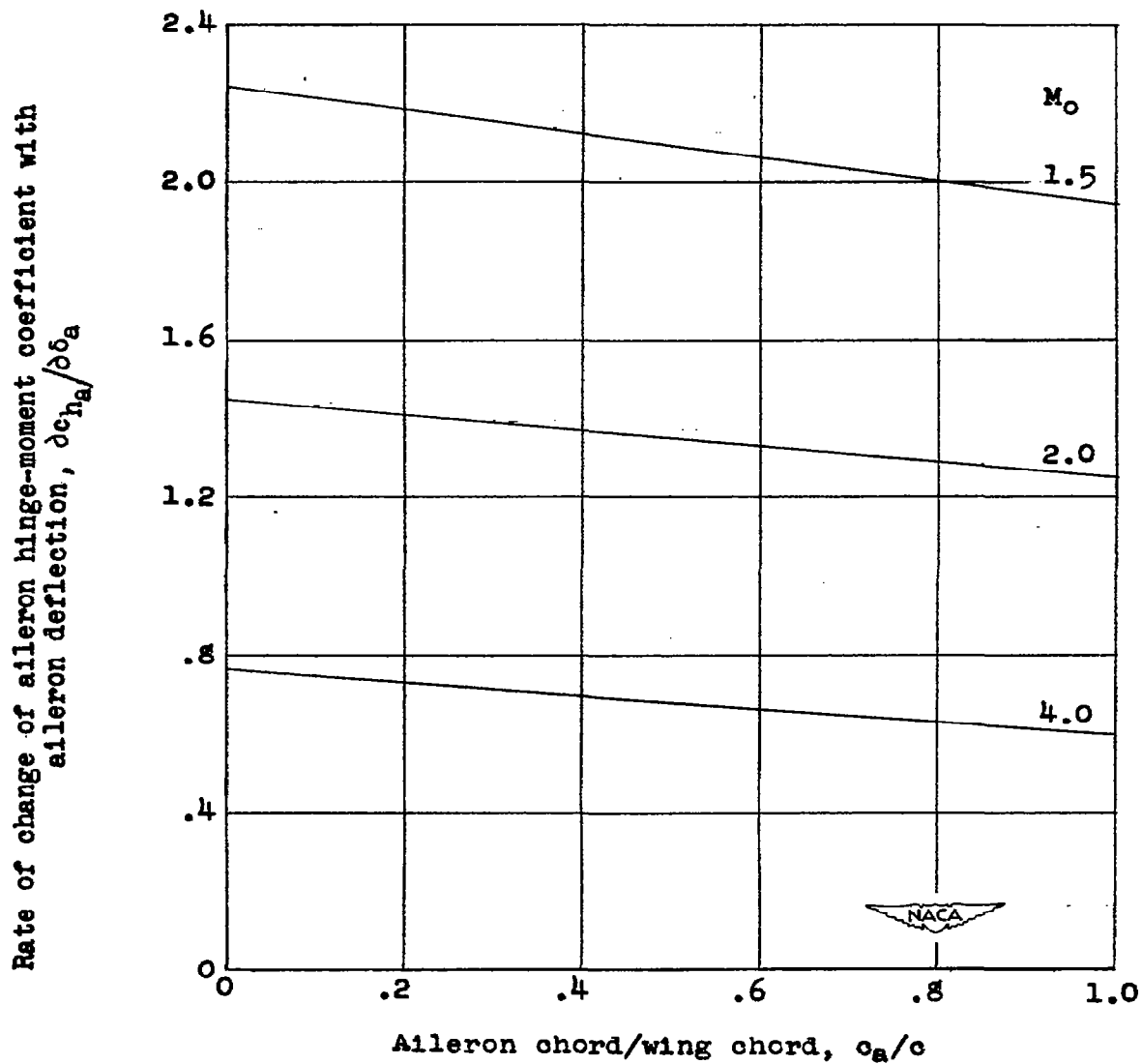
(a) $\dfrac{t}{c} = 0.05.$

Figure 3.- Aileron effectiveness as a function of the ratio of aileron chord to wing chord for an uncambered parabolic airfoil having maximum thickness at midchord and trailing-edge aileron.
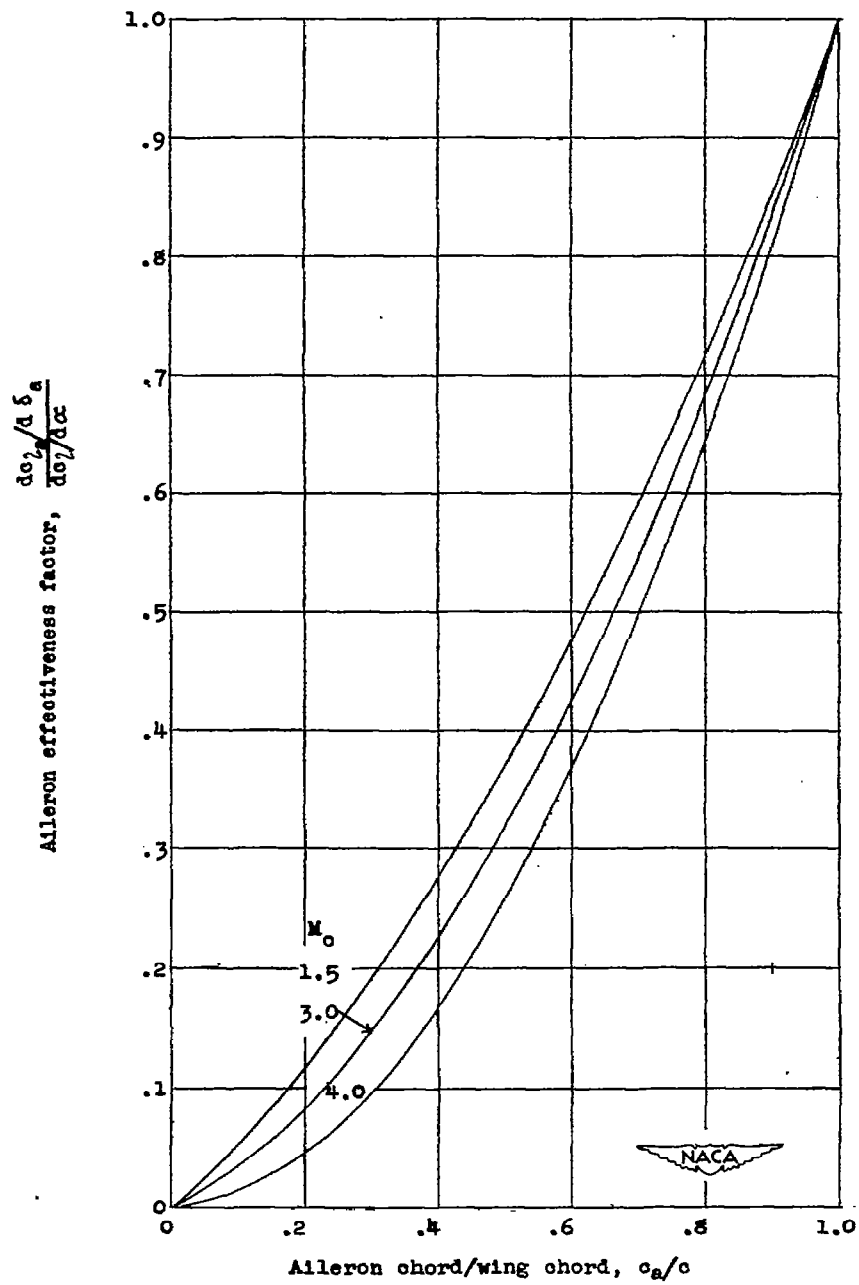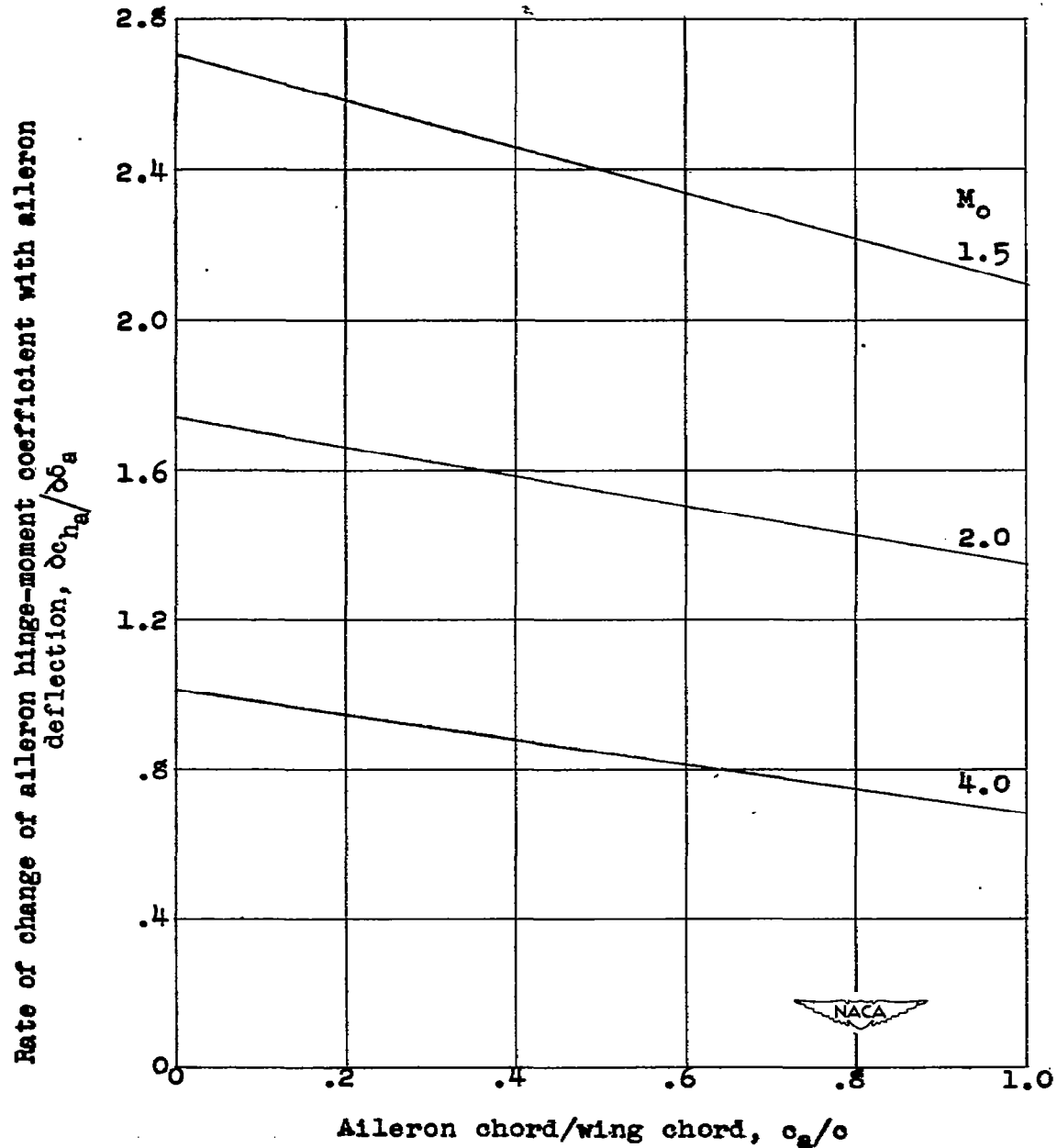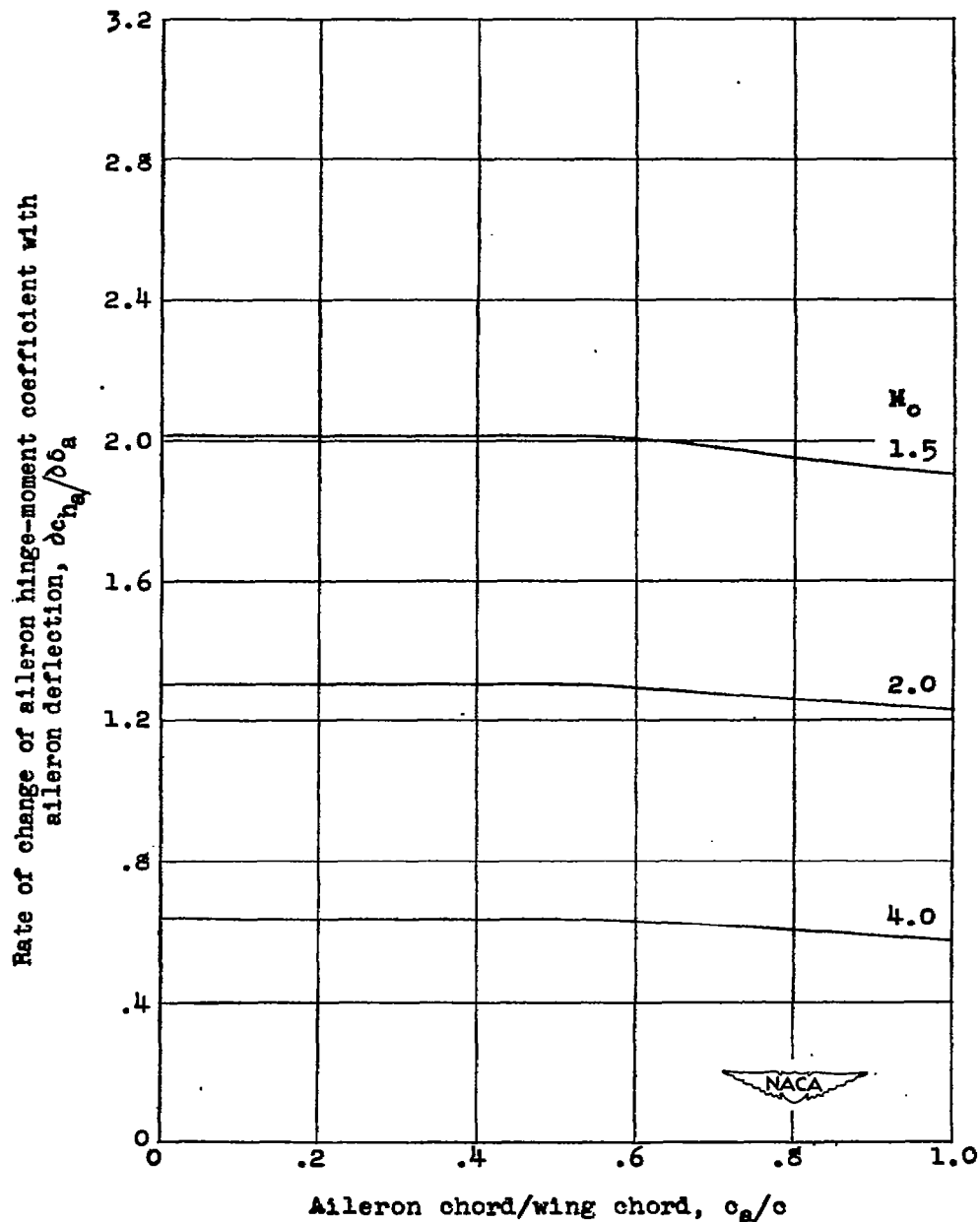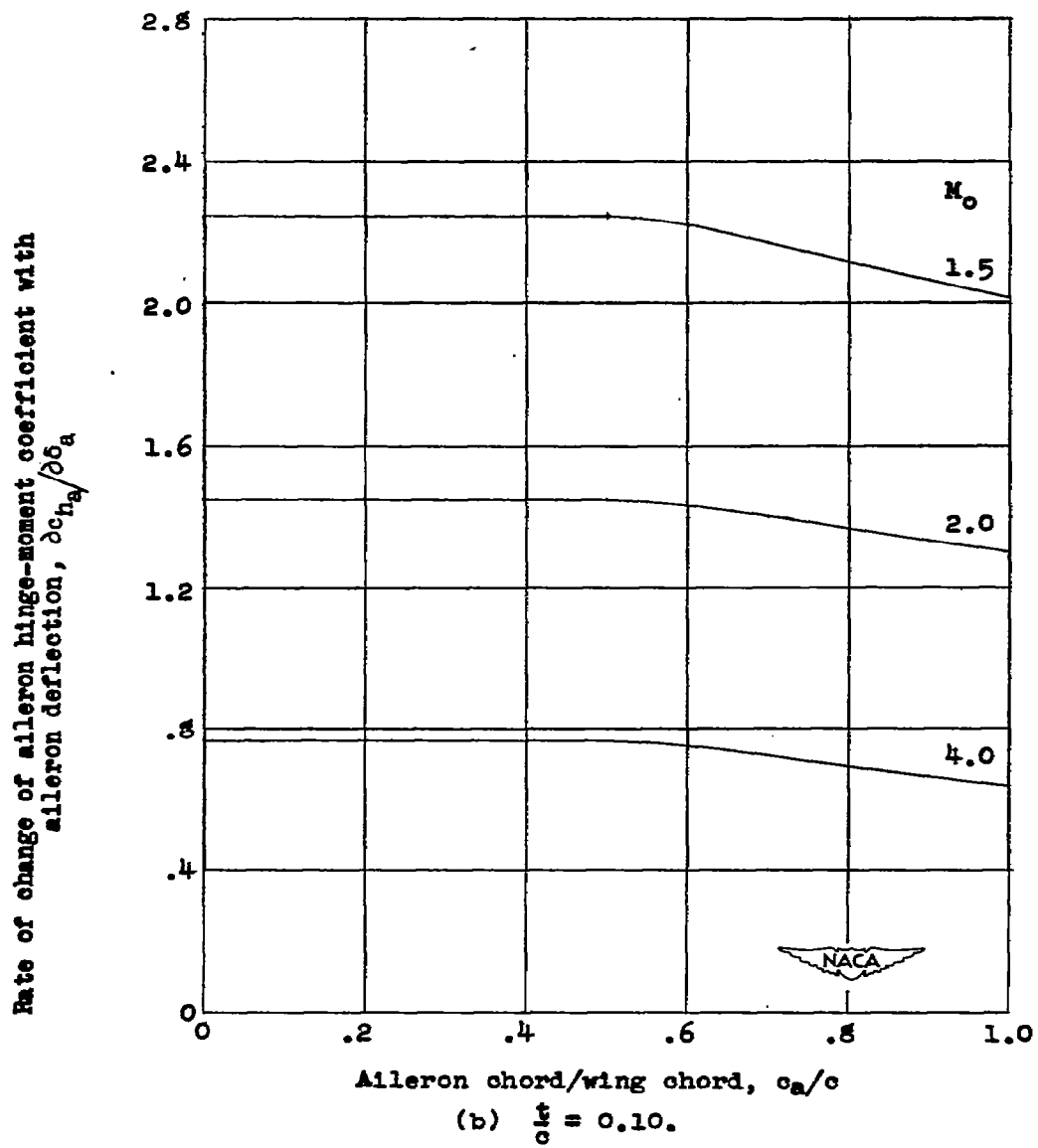
(b) $\frac{t}{c} = 0.10.$

Figure 3.- Concluded.
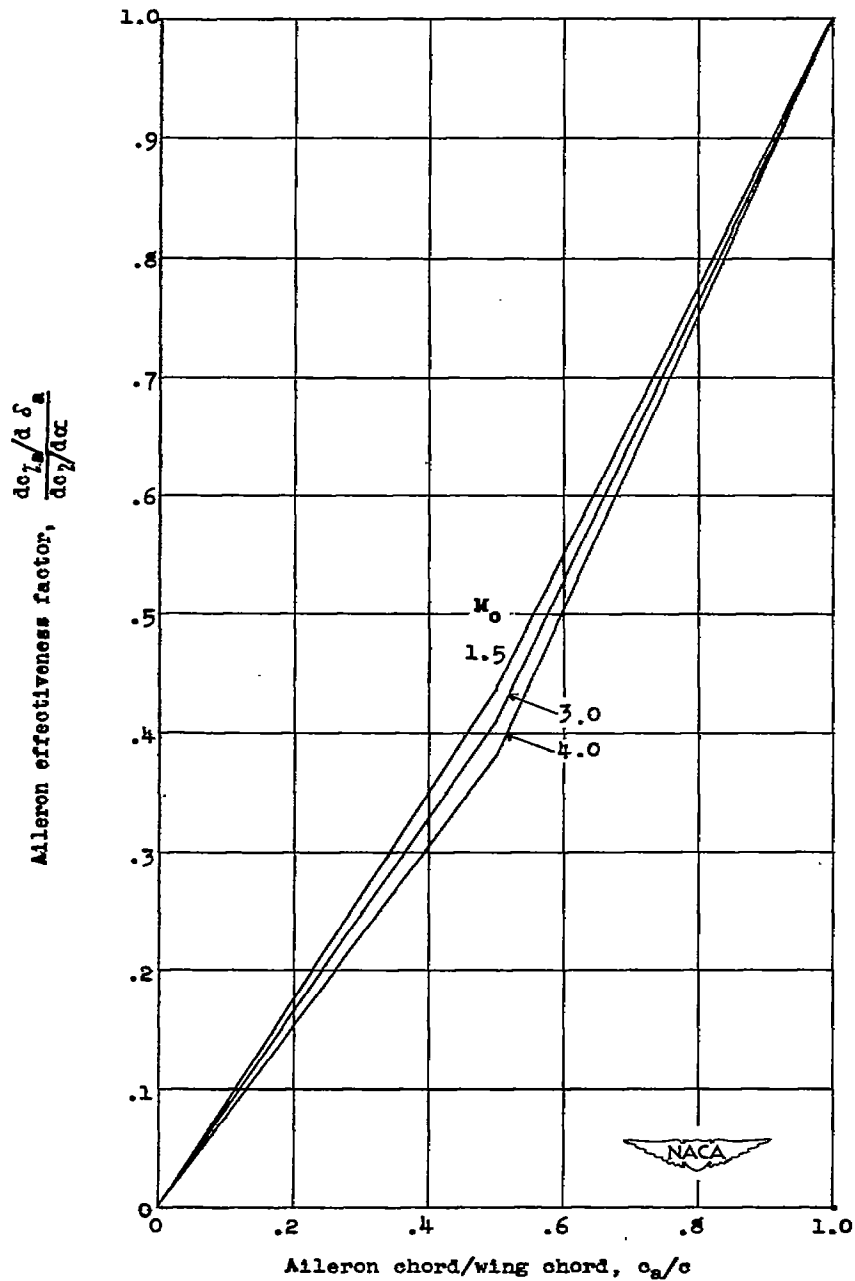
(a) $\frac{t}{c}$ = 0.05.

Figure 4.- Aileron effectiveness as a function of
the ratio of aileron chord to wing chord for an
uncambered wedge airfoil having maximum thickness
at midchord and trailing-edge aileron.
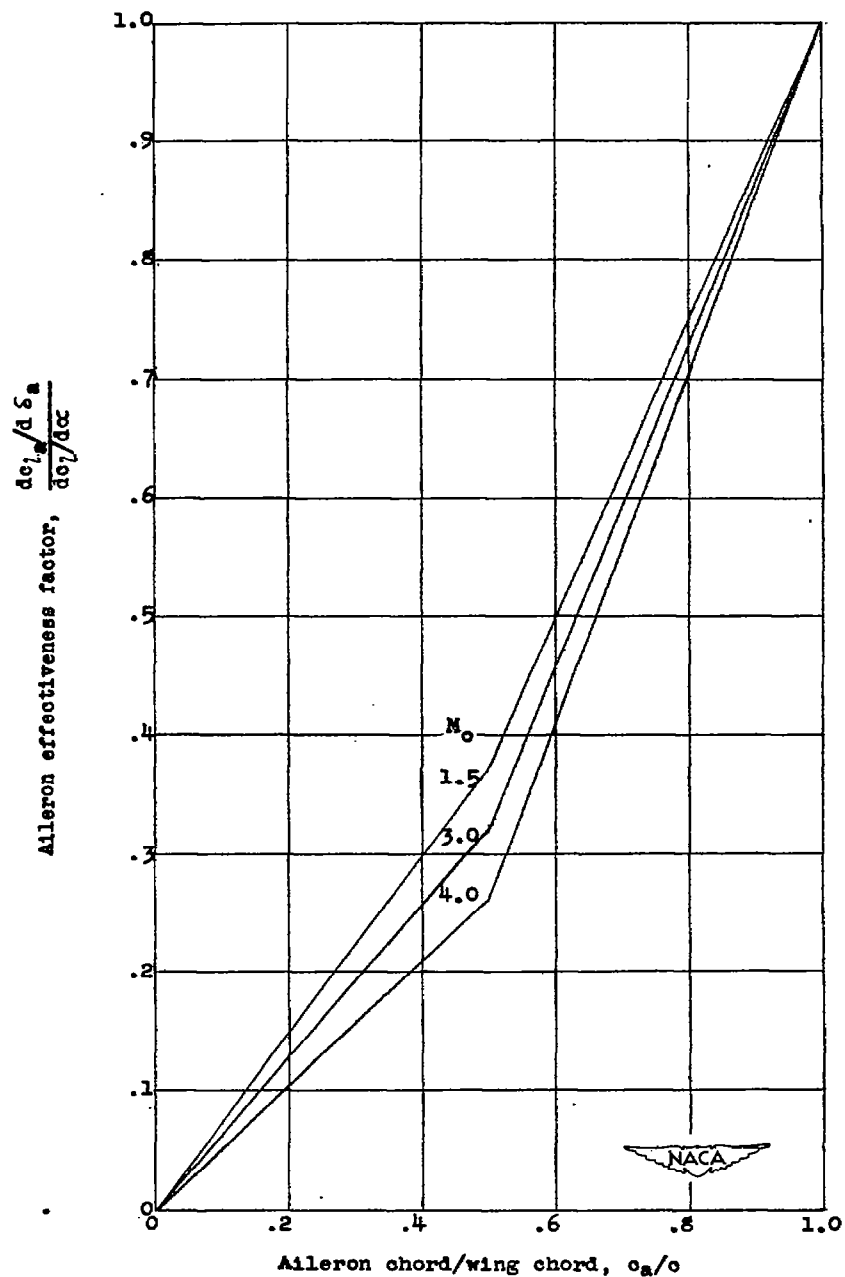
(b) $\frac{t}{c} = 0.10$.

Figure 4.- Concluded.
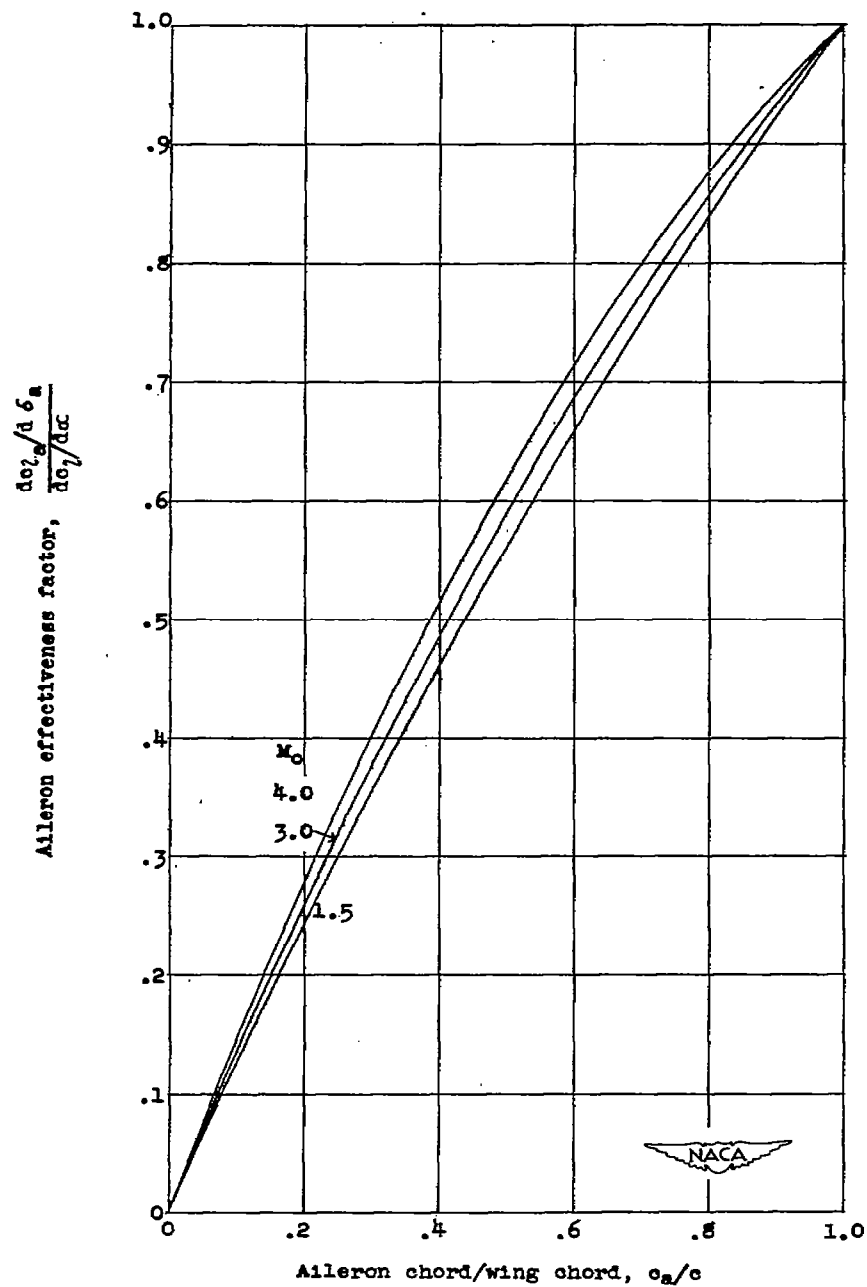
(a) $\frac{t}{c} = 0.05$.

Figure 5.- Aileron effectiveness as a function of
the ratio of aileron chord to wing chord for an
uncambered parabolic airfoil having maximum
thickness at midchord and leading-edge aileron.
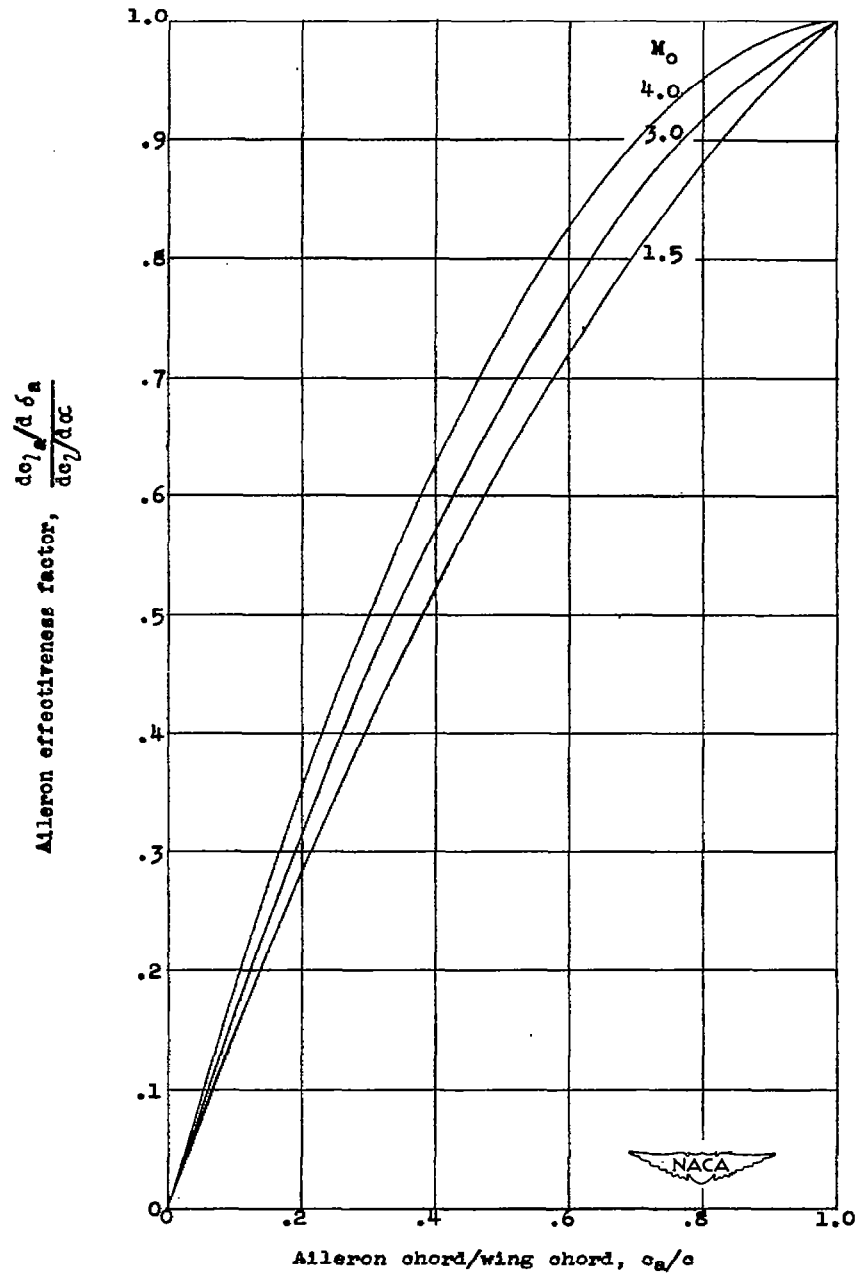
(b) $\frac{t}{c} = 0.10.$

Figure 5.- Concluded.

(a) $\frac{t}{c} = 0.05.$
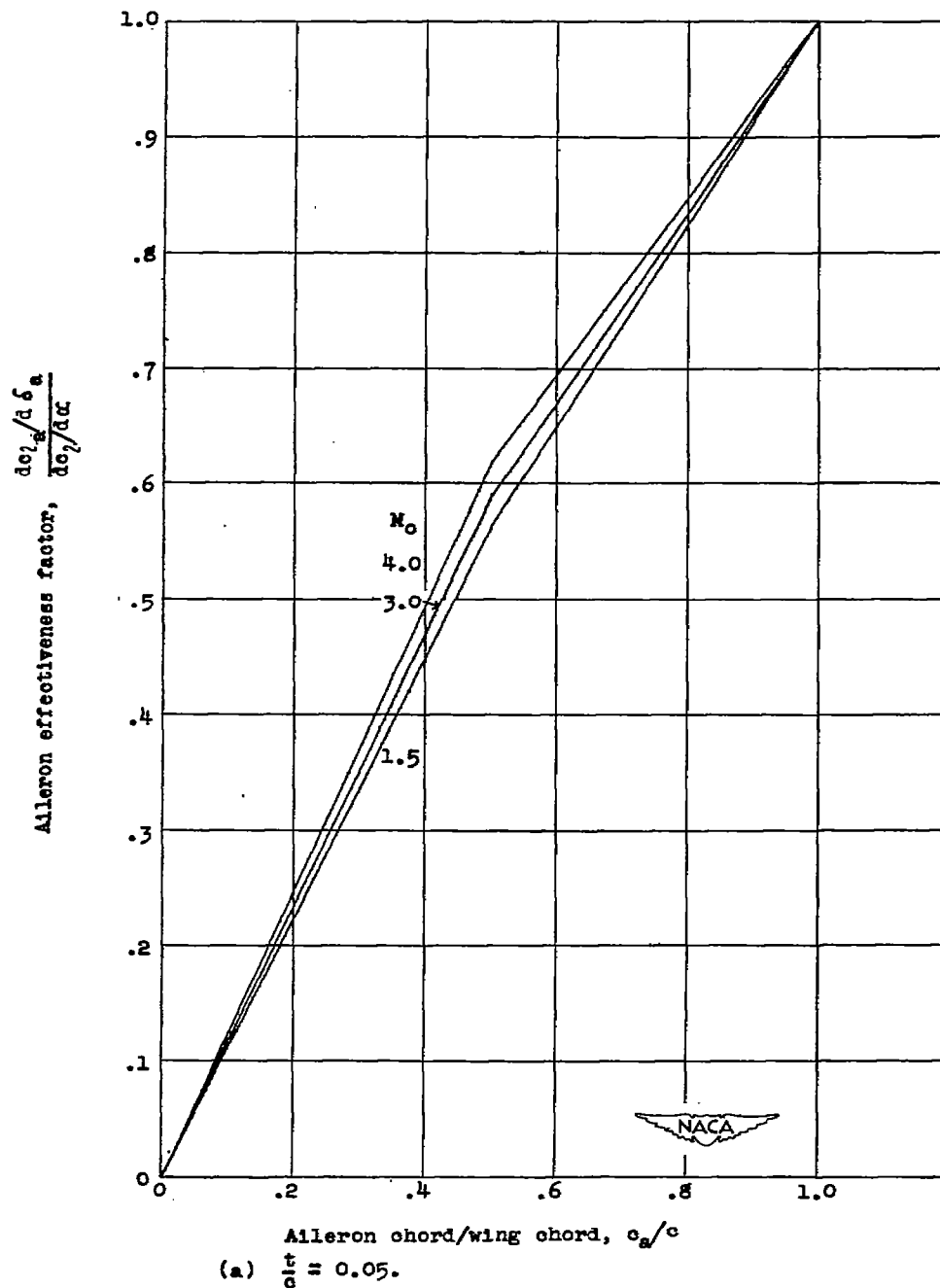
Figure 6.- Aileron effectiveness as a function of
the ratio of aileron chord to wing chord for an
uncambered wedge airfoil having maximum thickness at
midchord and leading-edge aileron.

Aileron effectiveness factor, $\dfrac{dc_{l_a}/d\delta_a}{dc_l/d\alpha}$

Aileron chord/wing chord, c_a/c
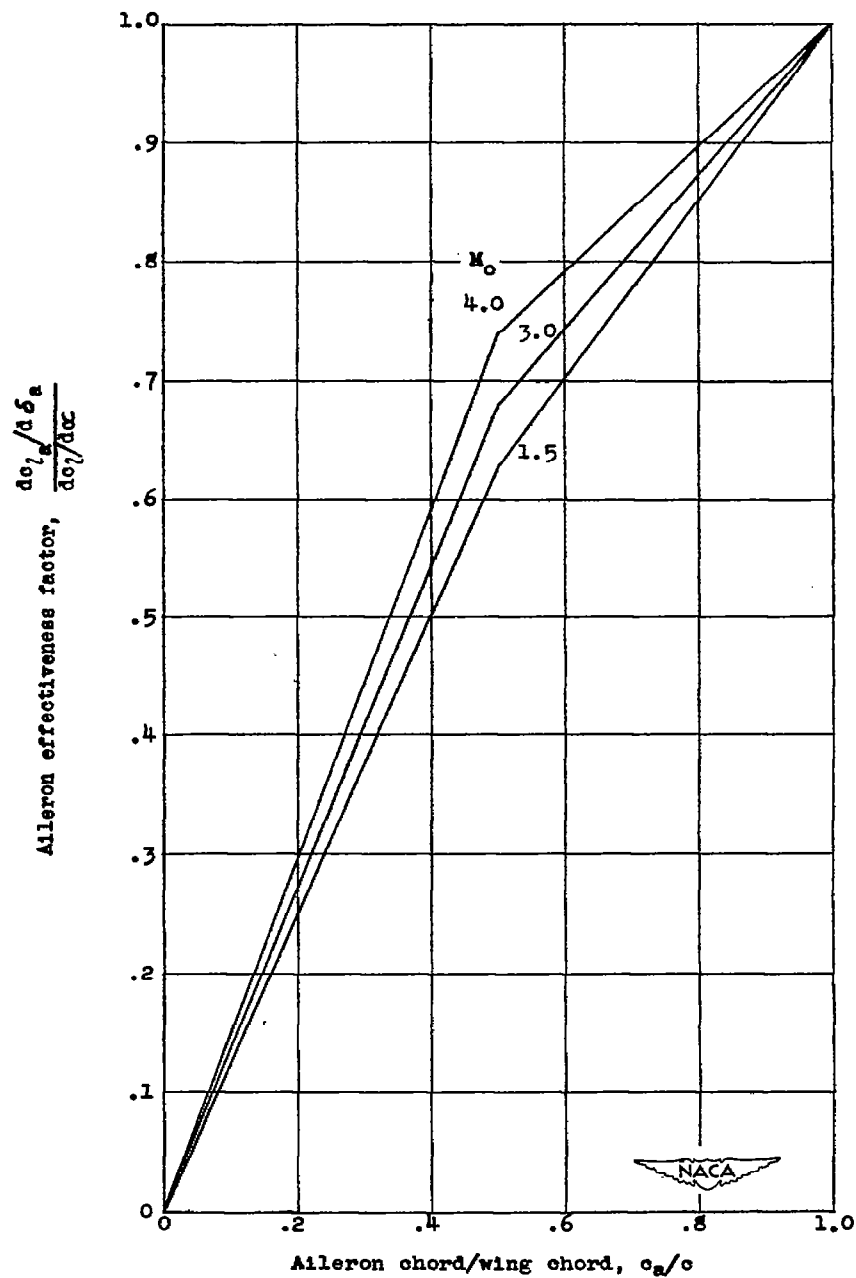
(b) $\dfrac{t}{c} = 0.10.$

Figure 6.- Concluded.
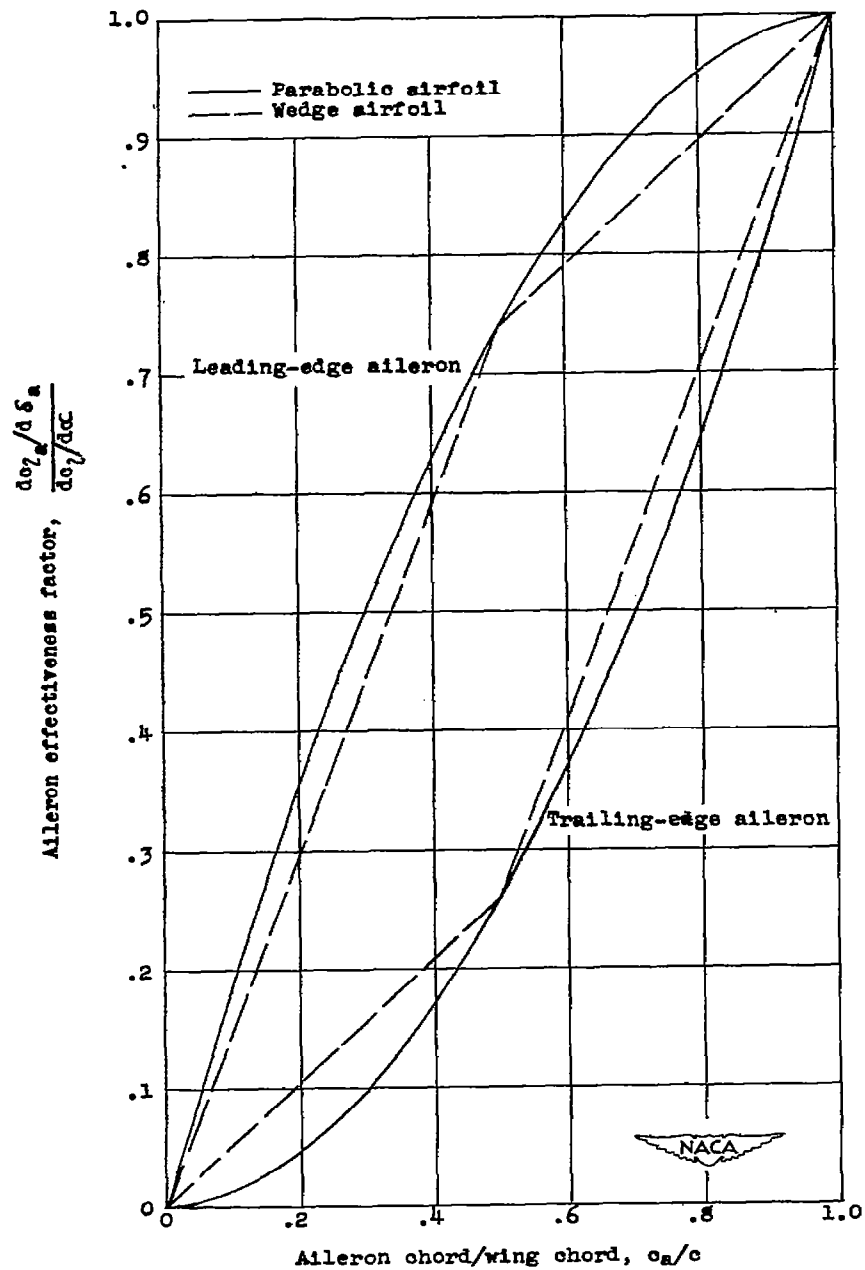
Figure 7.— Aileron effectiveness as a function of the ratio of aileron chord to wing chord for uncambered airfoils having maximum thickness at midchord. $M_0 = 4.0$; $\frac{t}{c} = 0.10$.
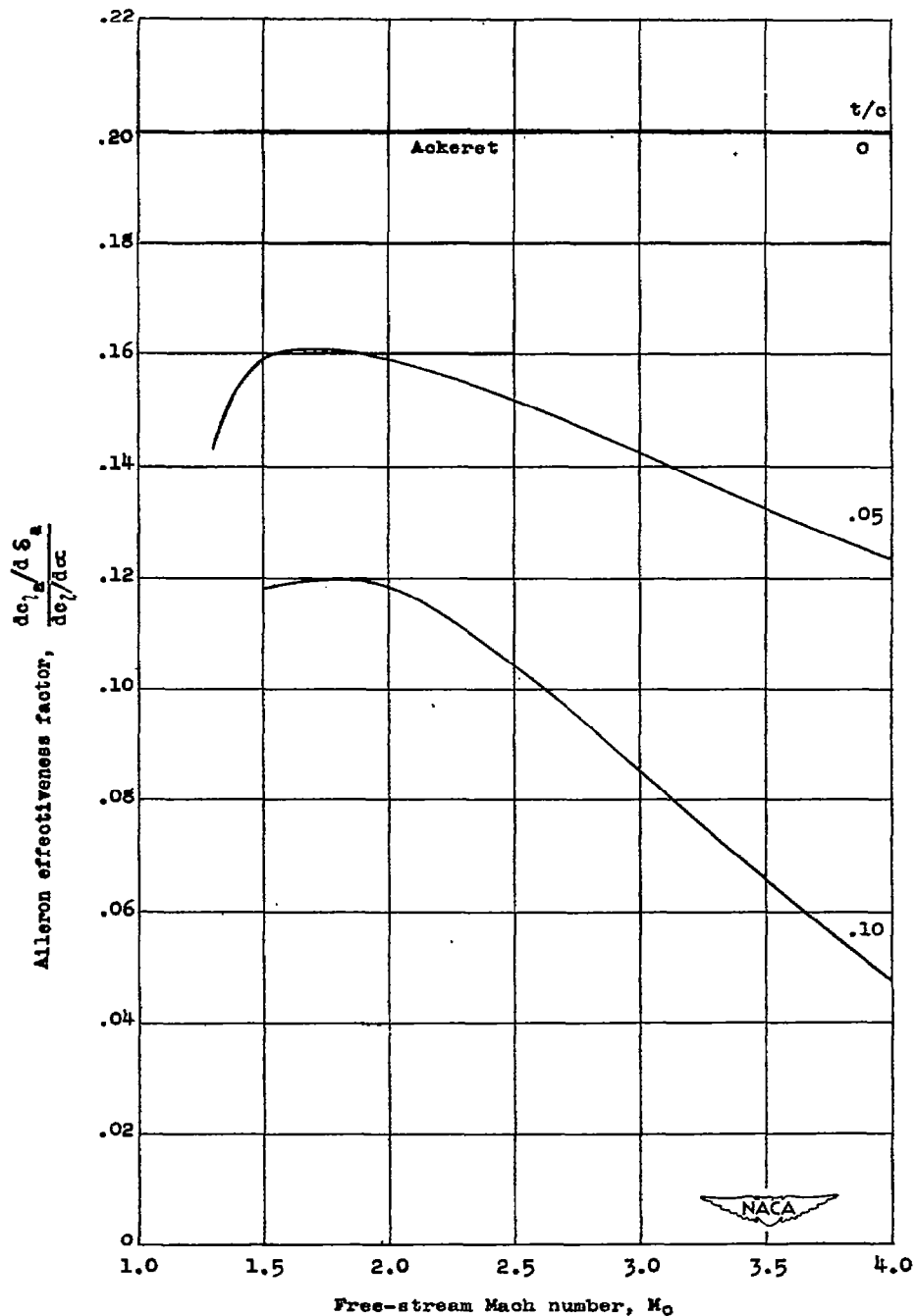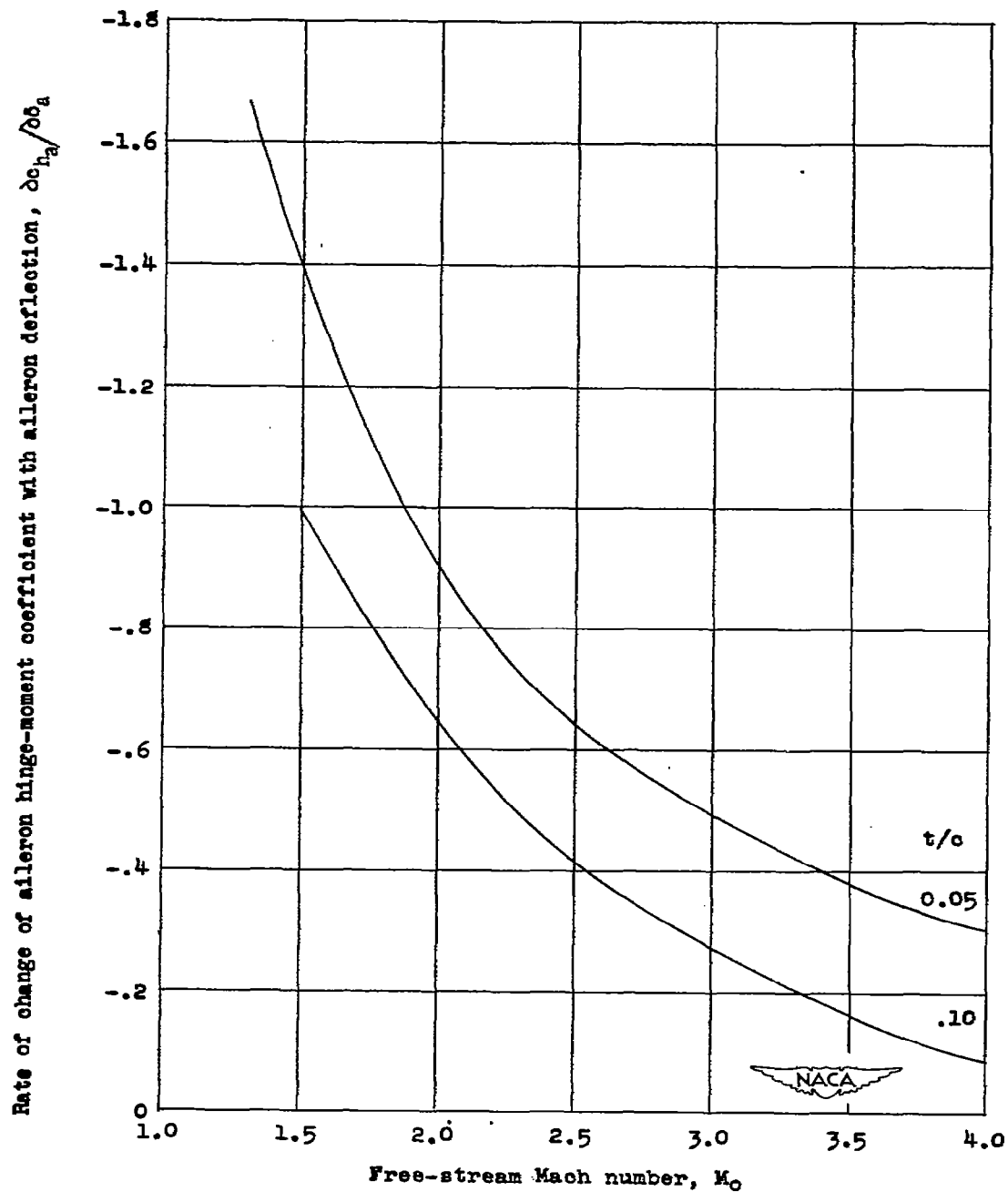
Figure 8.- Aileron effectiveness as a function of the free-
   stream Mach number for an uncambered parabolic airfoil
   having maximum thickness at midchord and trailing-edge
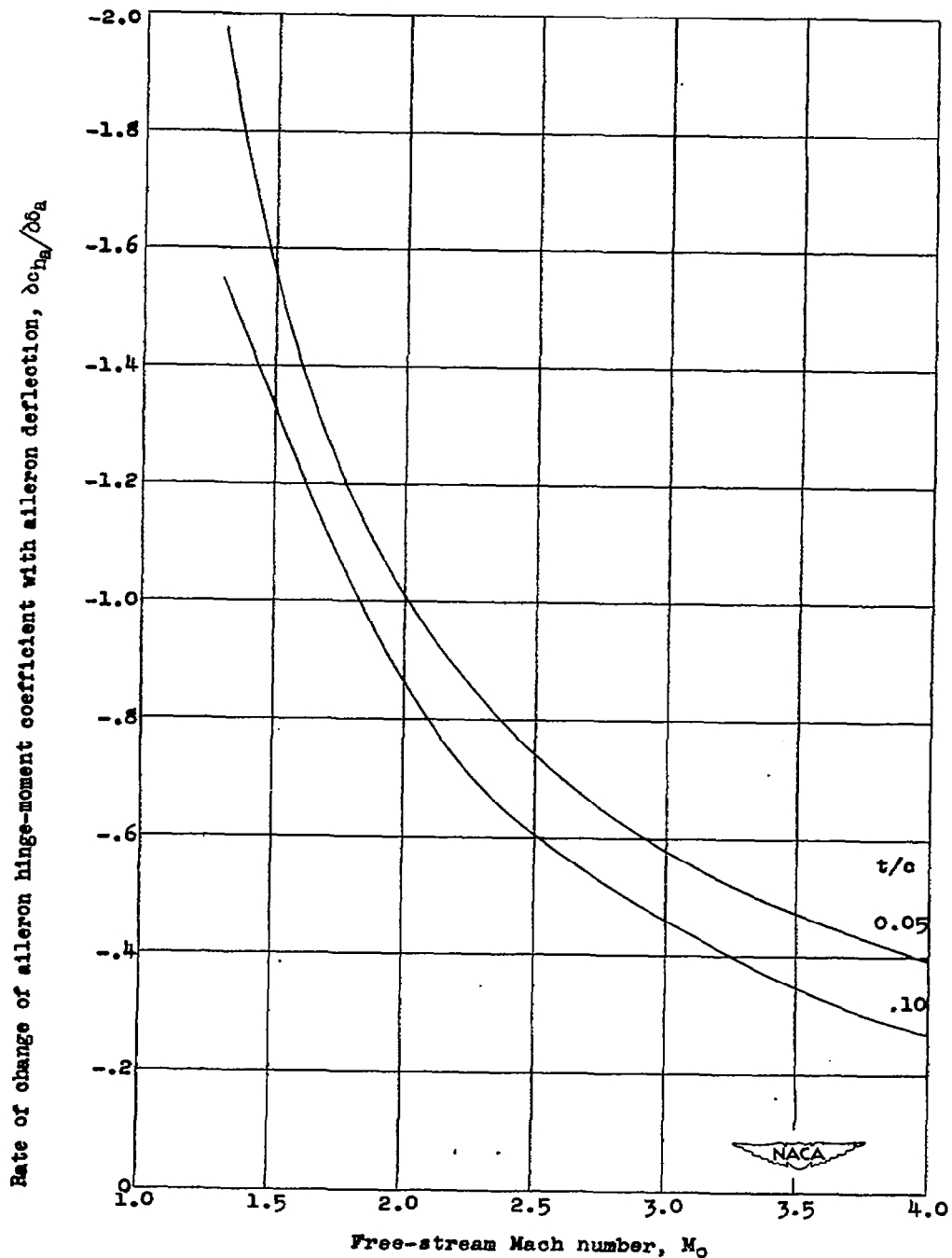   aileron. $\frac{c_a}{c} = 0.2.$
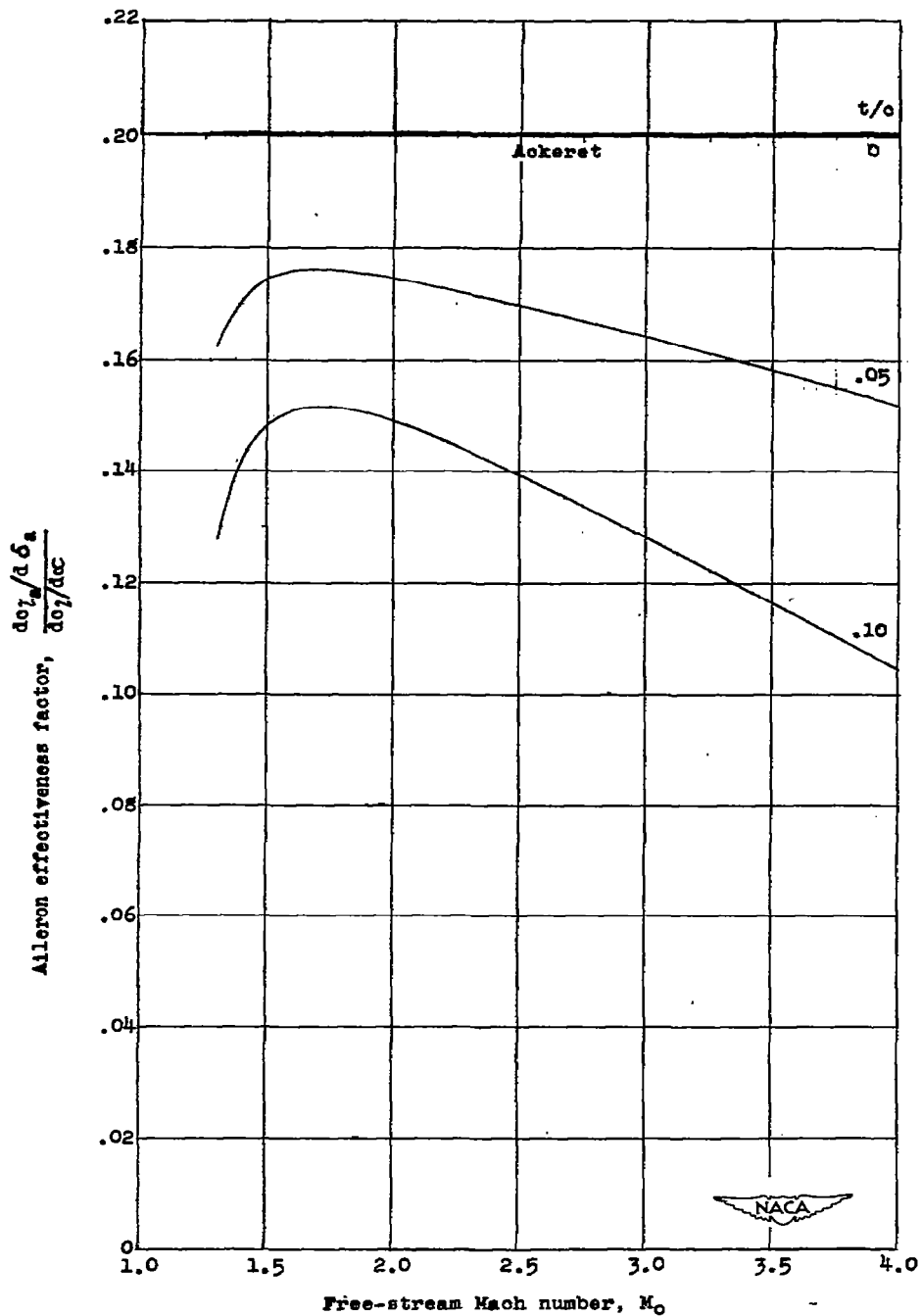
Figure 9.- Aileron effectiveness as a function of the free-stream
Mach number for an uncambered wedge airfoil having maximum
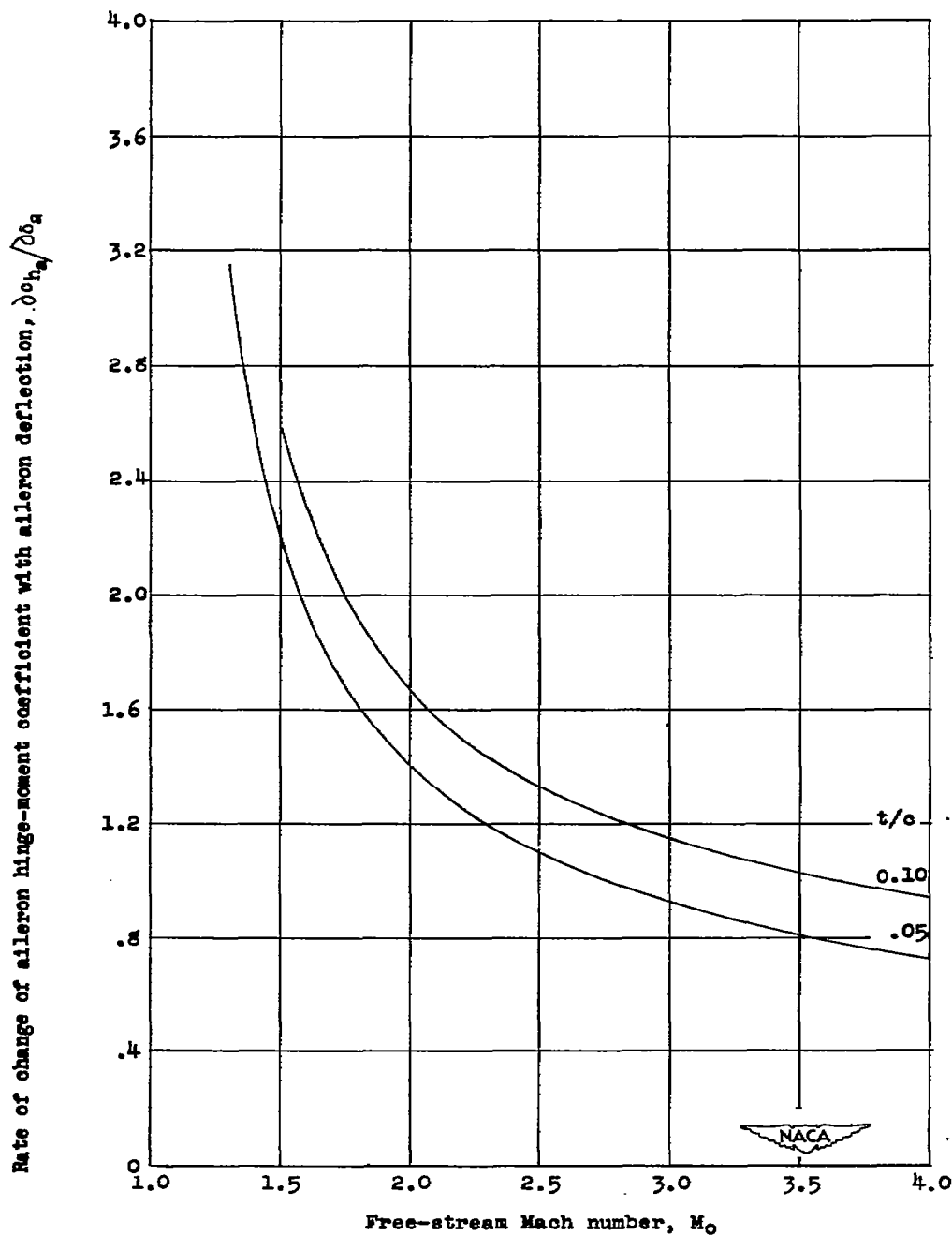thickness at midchord and trailing-edge aileron. $\frac{c_a}{c} = 0.2$.
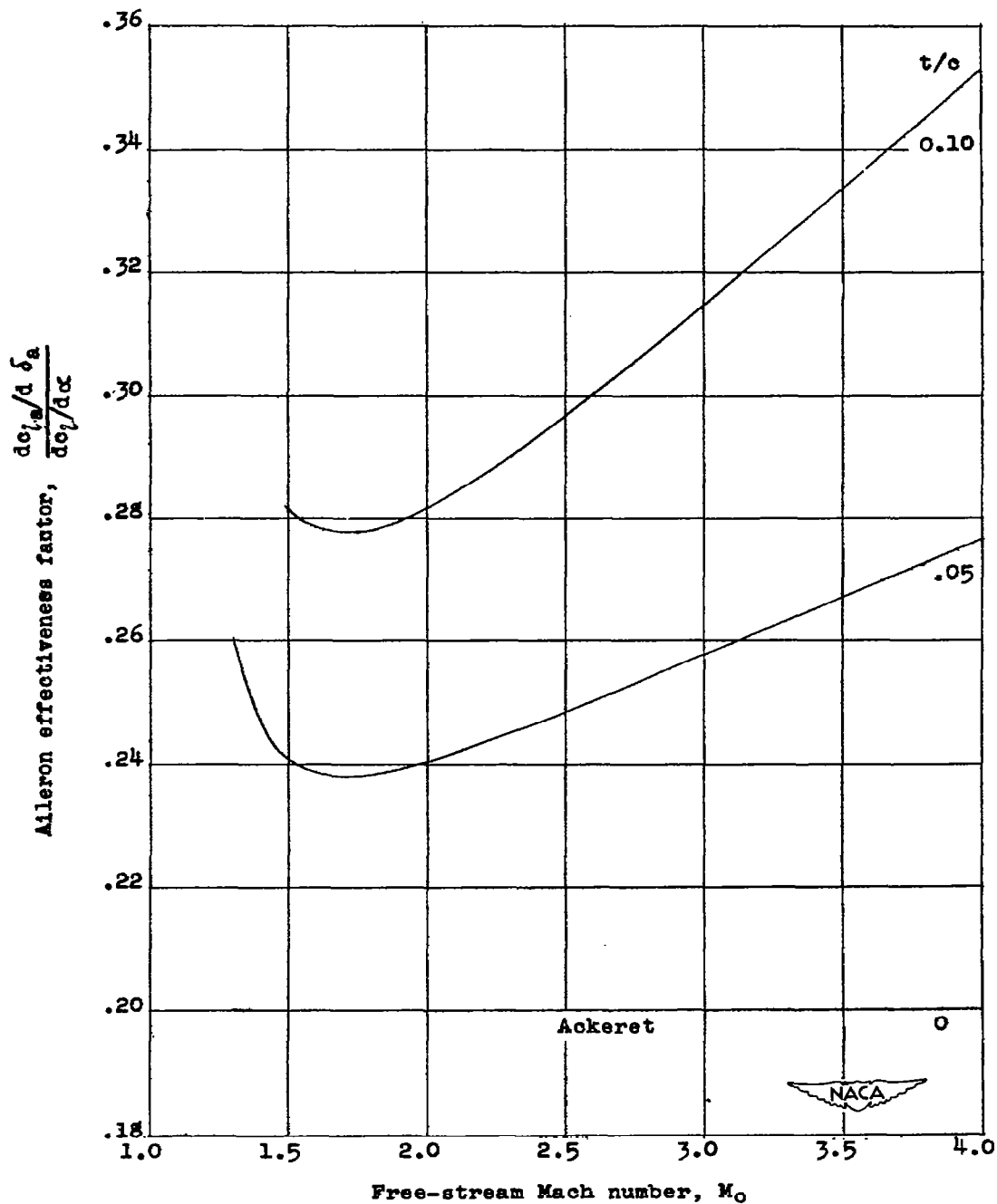
Figure 10.- Aileron effectiveness as a function of the free-stream Mach number for an uncambered parabolic airfoil having maximum thickness at midchord and leading-edge aileron. $\frac{c_a}{c} = 0.2$.
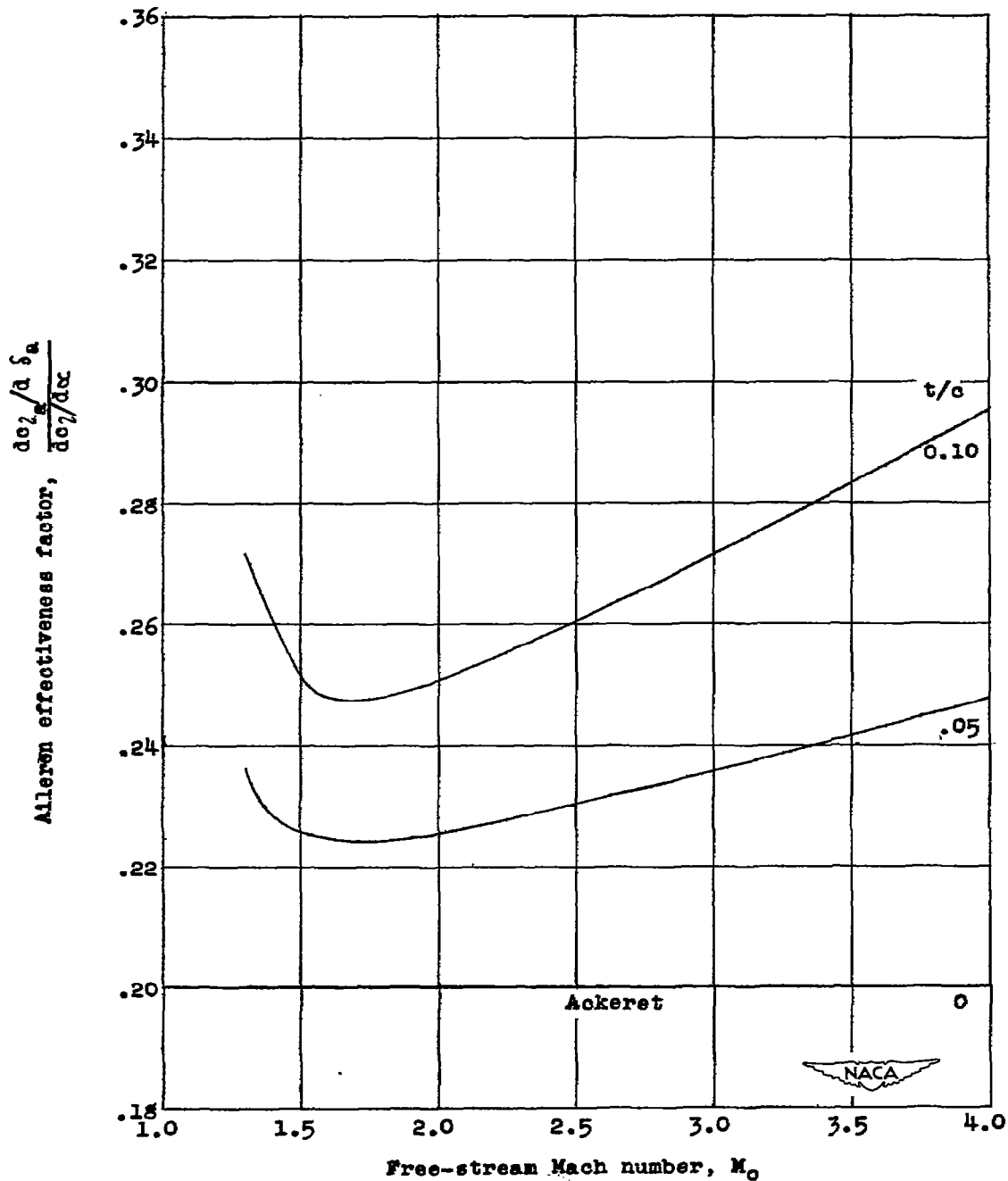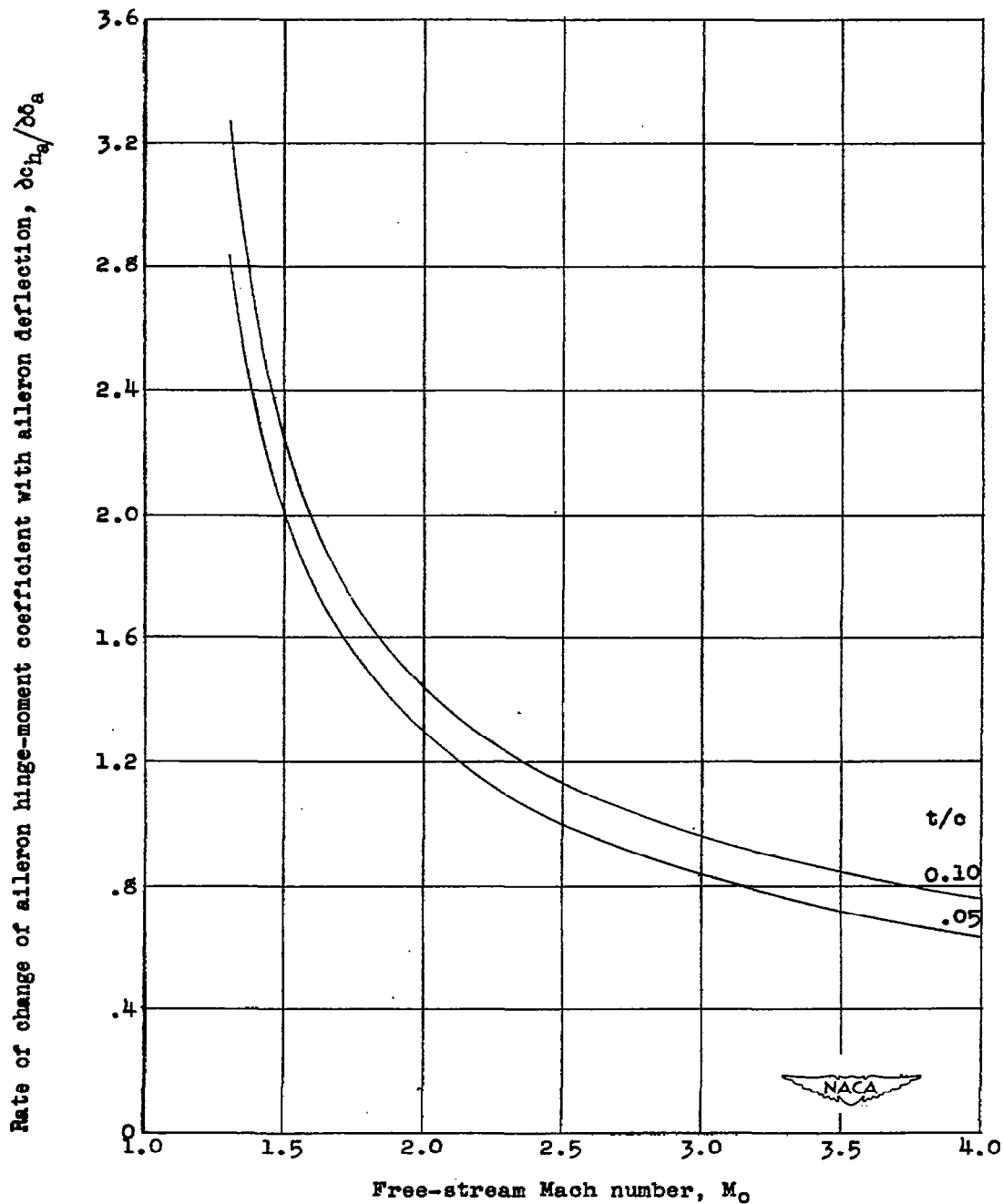
Figure 11.- Aileron effectiveness as a function of the free-stream Mach number for an uncambered wedge airfoil having maximum thickness at midchord and leading-edge aileron. $\frac{c_a}{c} = 0.2$.
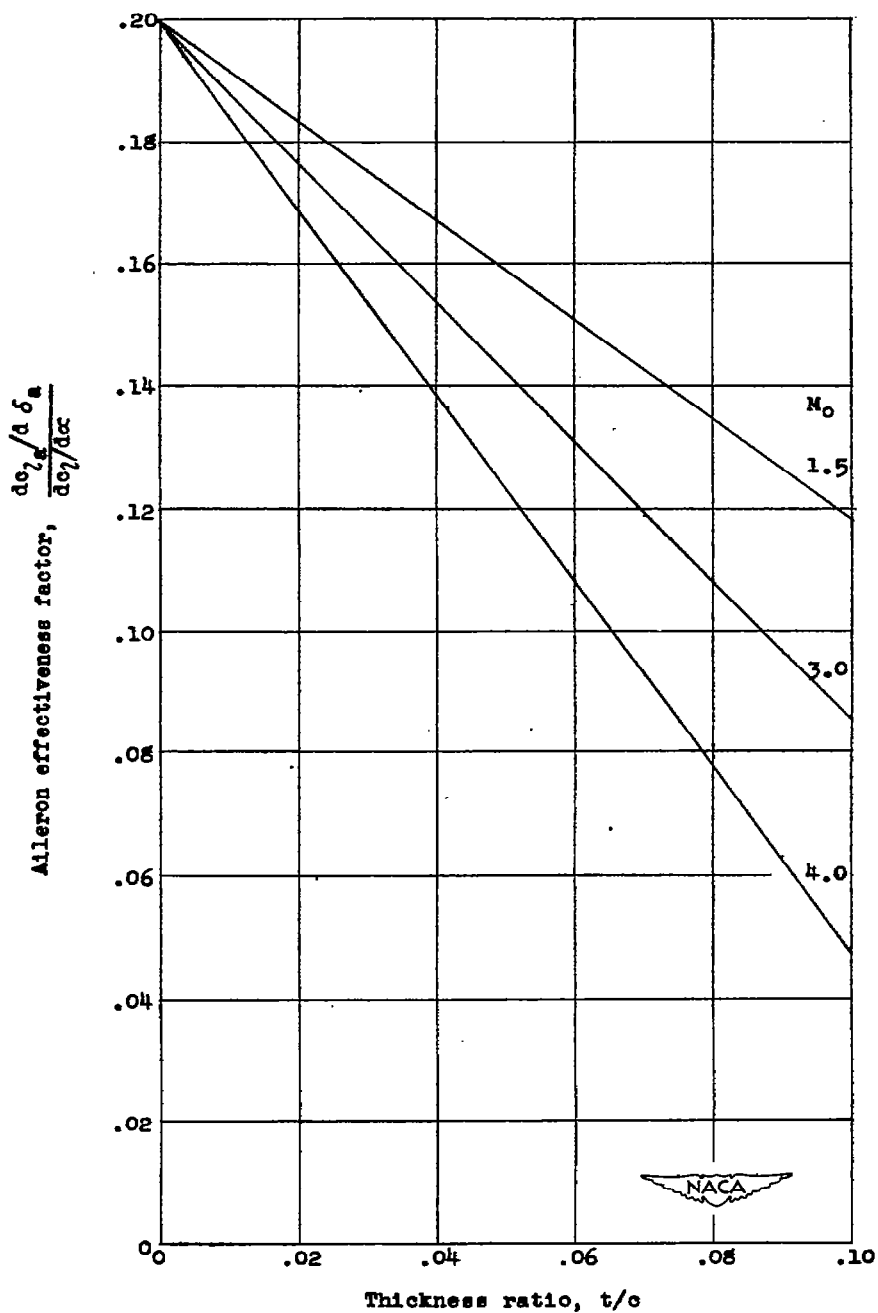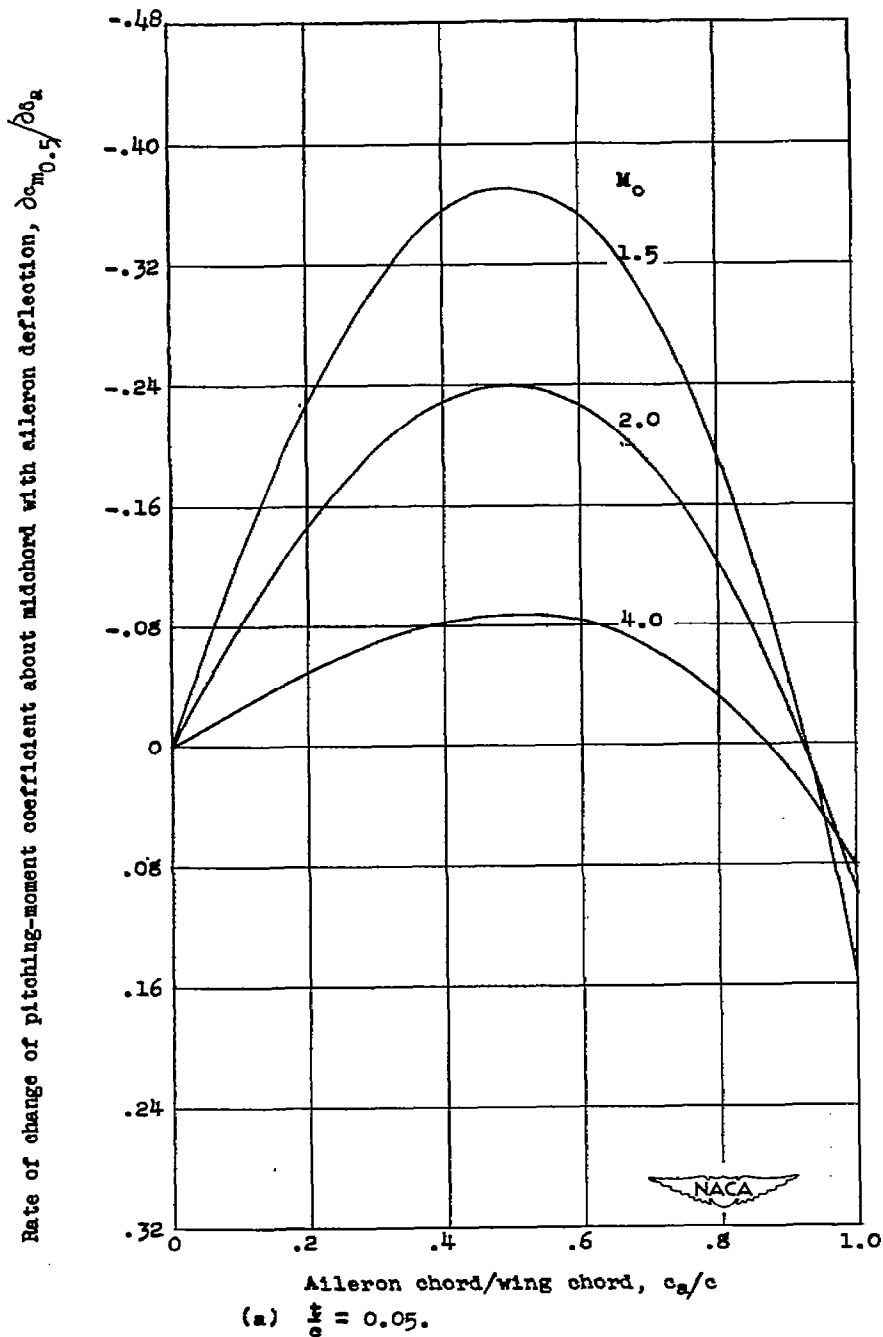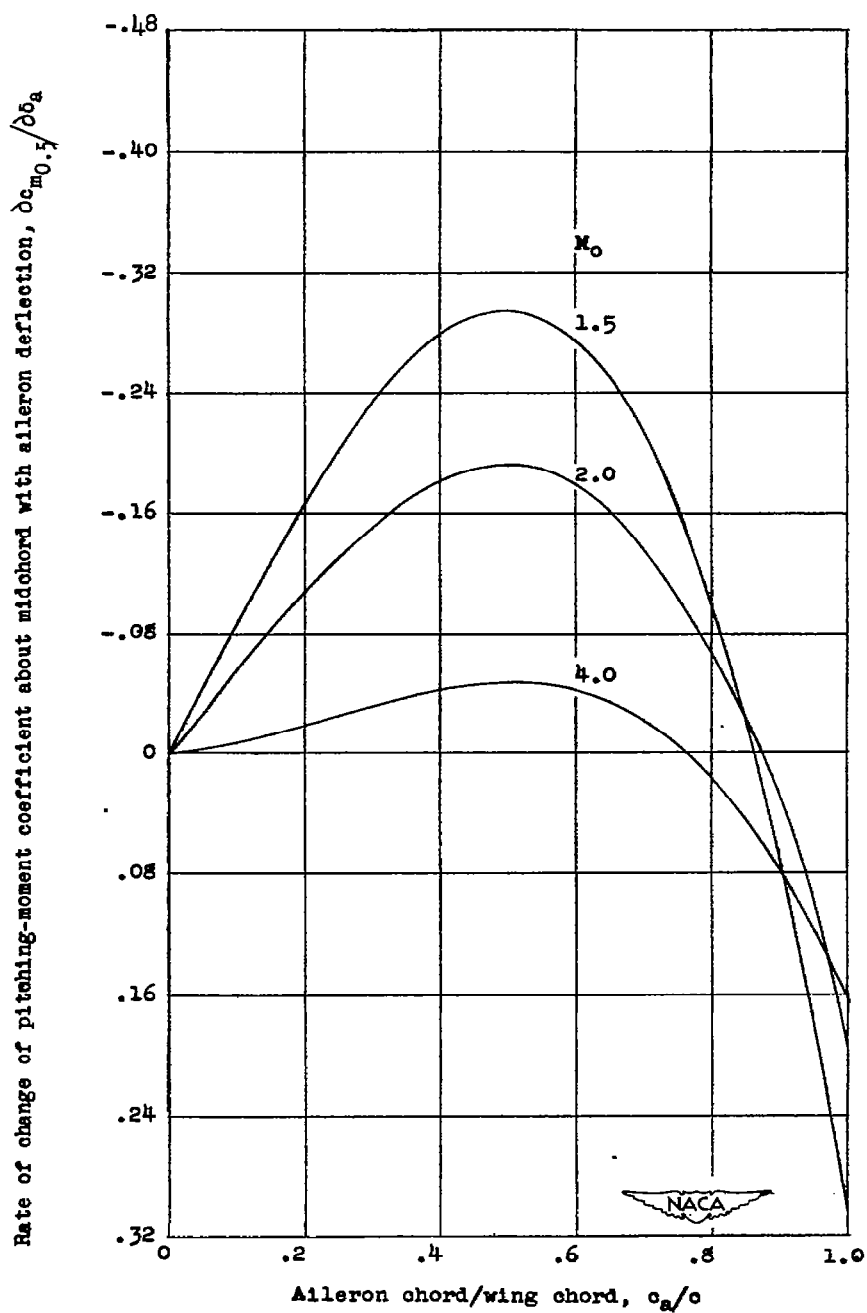
(a) Trailing-edge aileron.

Figure 12.- Aileron effectiveness as a function of
thickness ratio for an uncambered parabolic air-
foil having maximum thickness at midchord. $\frac{c_a}{c} = 0.2$.
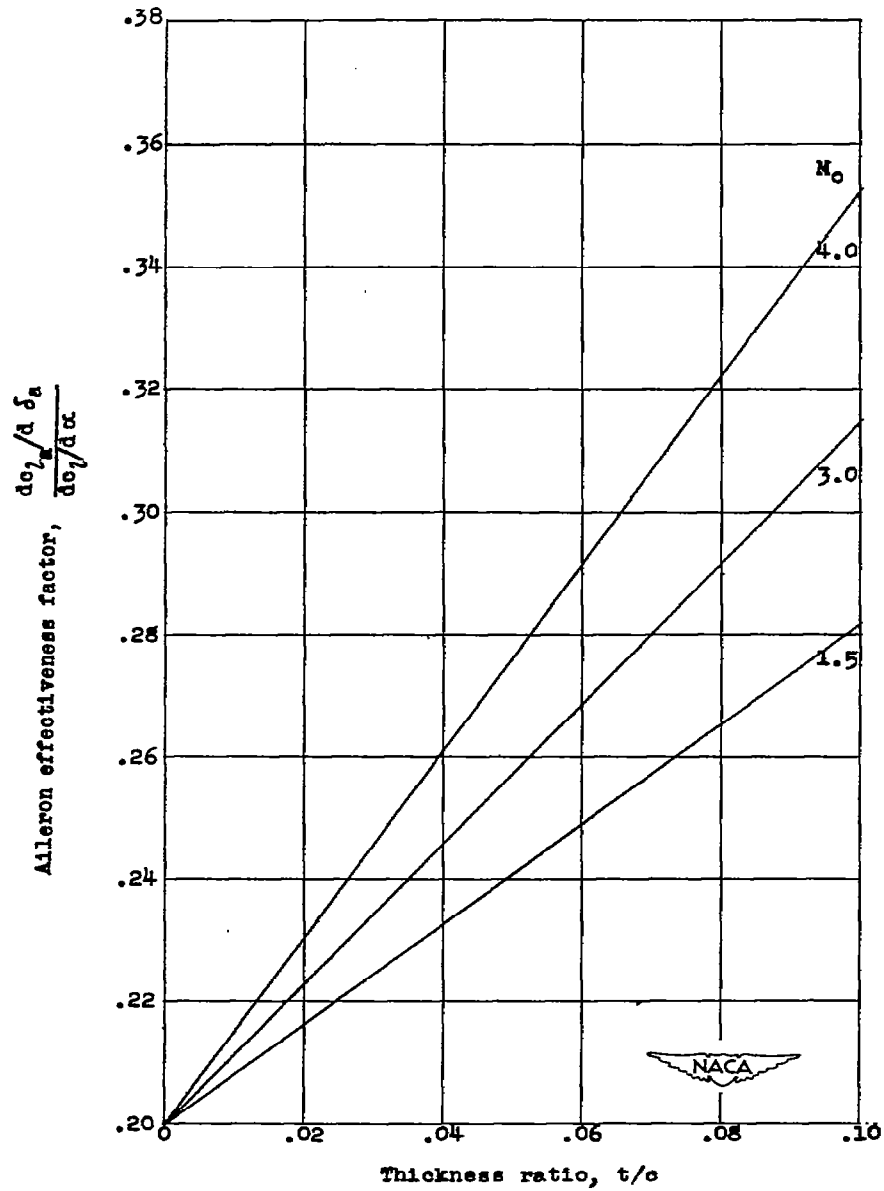
(b) Leading-edge aileron.

Figure 12.- Concluded.
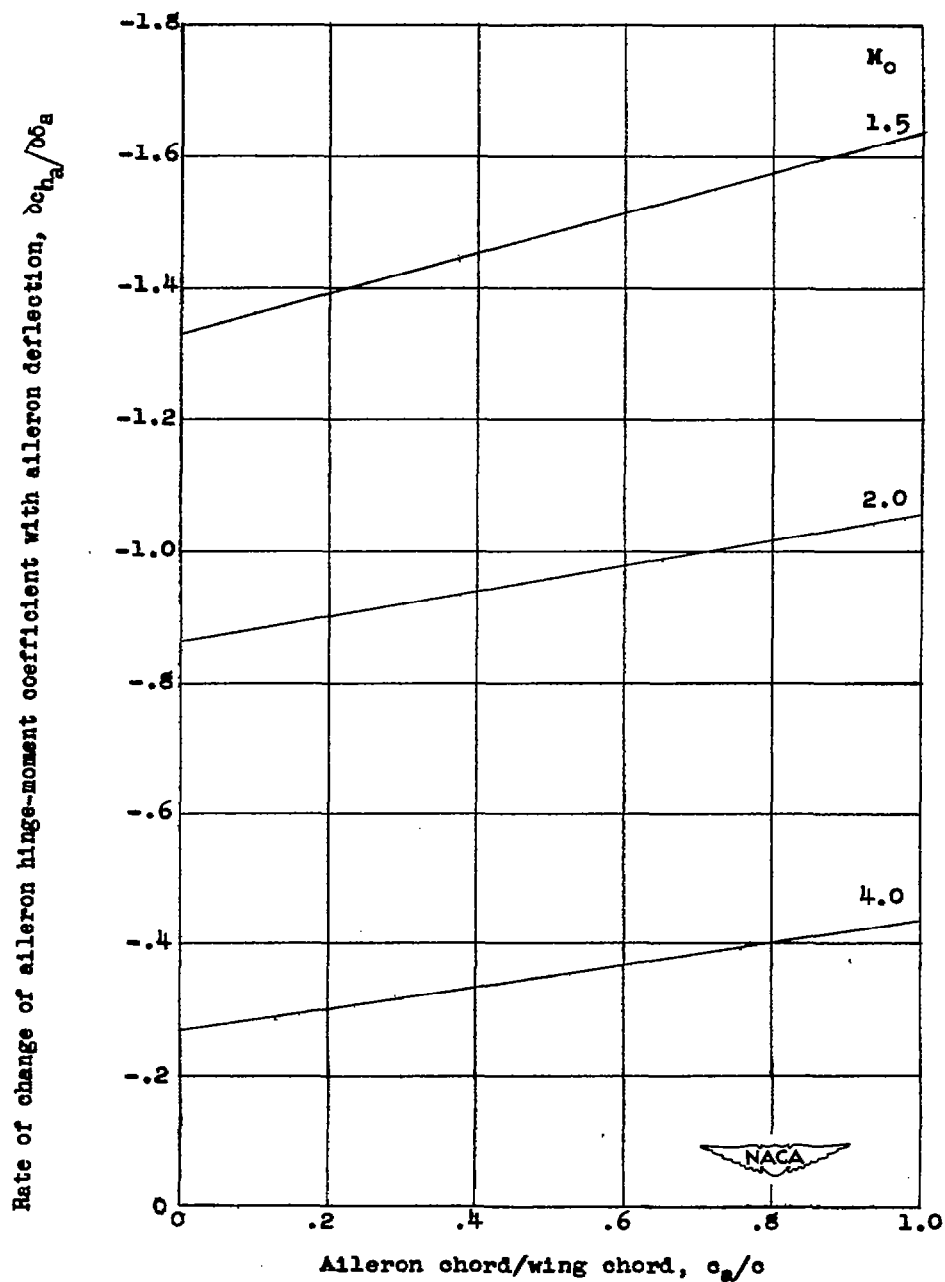
(a) $\frac{t}{c} = 0.05$.

Figure 13.- Rate of change of aileron hinge-moment
coefficient with aileron deflection as a
function of the ratio of aileron chord to wing
chord for an uncambered parabolic airfoil having
maximum thickness at midchord and trailing-edge aileron.
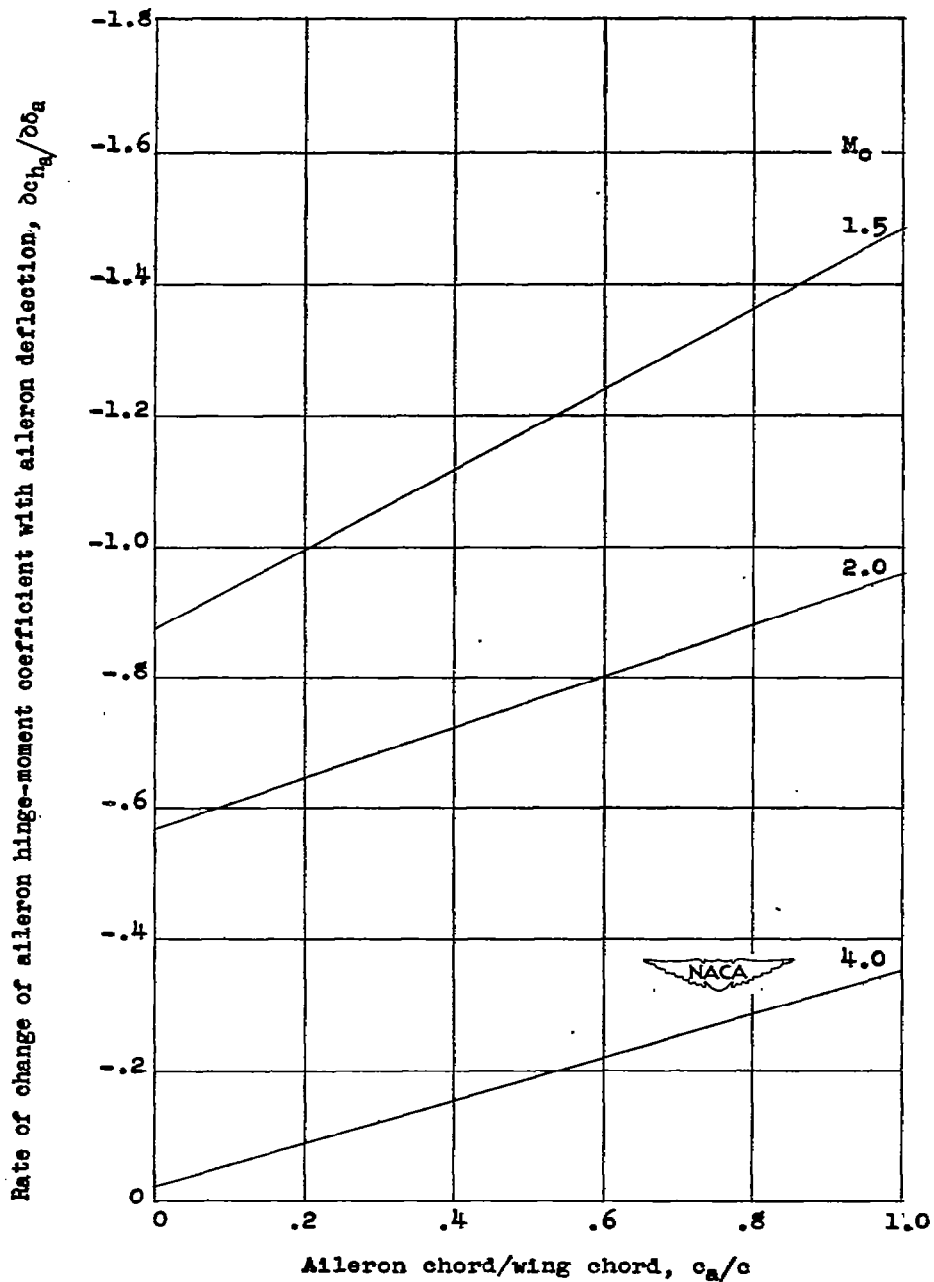
(b) $\frac{t}{c} = 0.10.$

Figure 13.- Concluded.
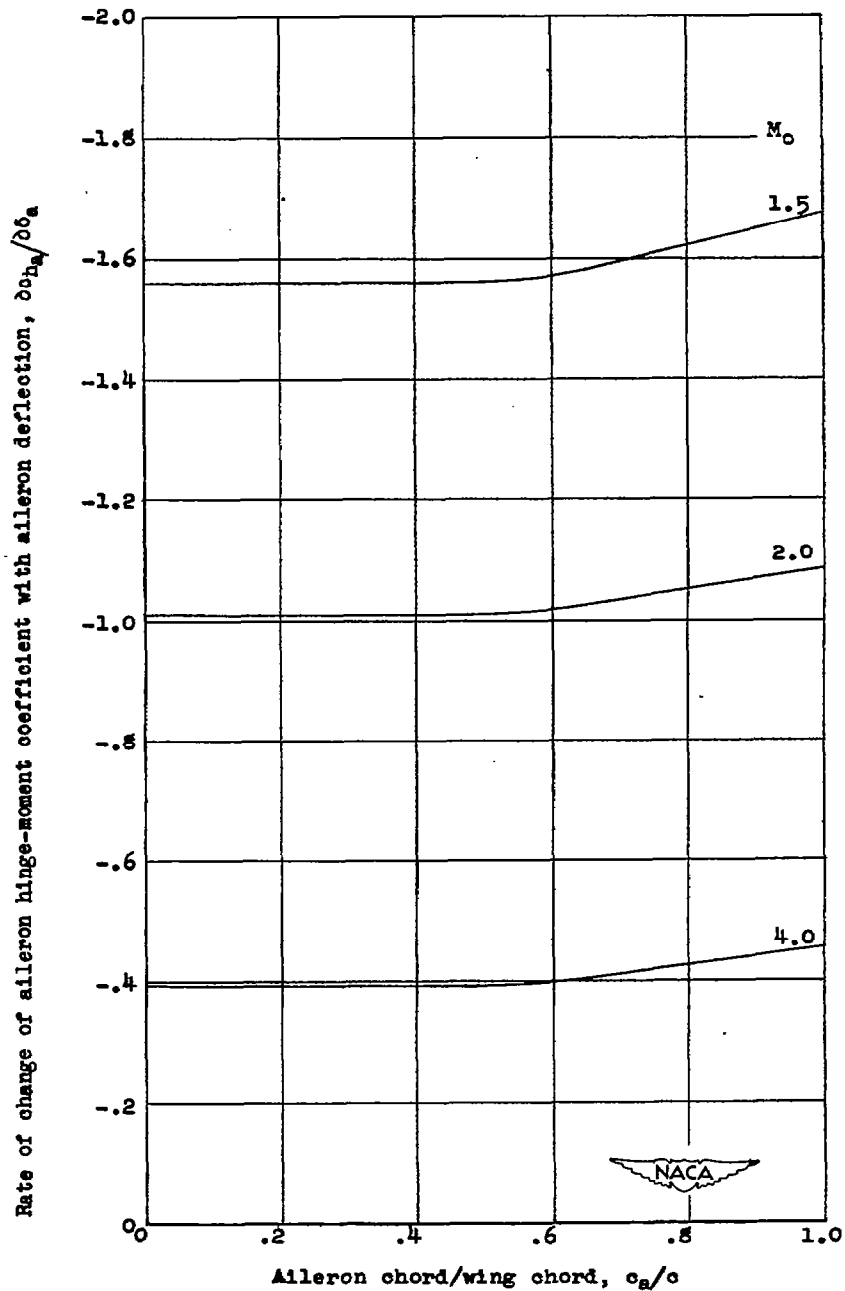
(a) $\dfrac{t}{c} = 0.05$.

Figure 14.- Rate of change of aileron hinge-moment coefficient with aileron deflection as a function of the ratio of aileron chord to wing chord for an uncambered wedge airfoil having maximum thickness at midchord and trailing-edge aileron.

(b) $\frac{t}{c} = 0.10.$

Figure 14.- Concluded.

(a) $\frac{t}{c} = 0.05.$

Figure 15.- Rate of change of aileron hinge-moment
   coefficient with aileron deflection as a
   function of the ratio of aileron chord to wing chord
   for an uncambered parabolic airfoil having maximum
   thickness at midchord and leading-edge aileron.

(b) $\dfrac{t}{c} = 0.10$.

Figure 15.- Concluded.
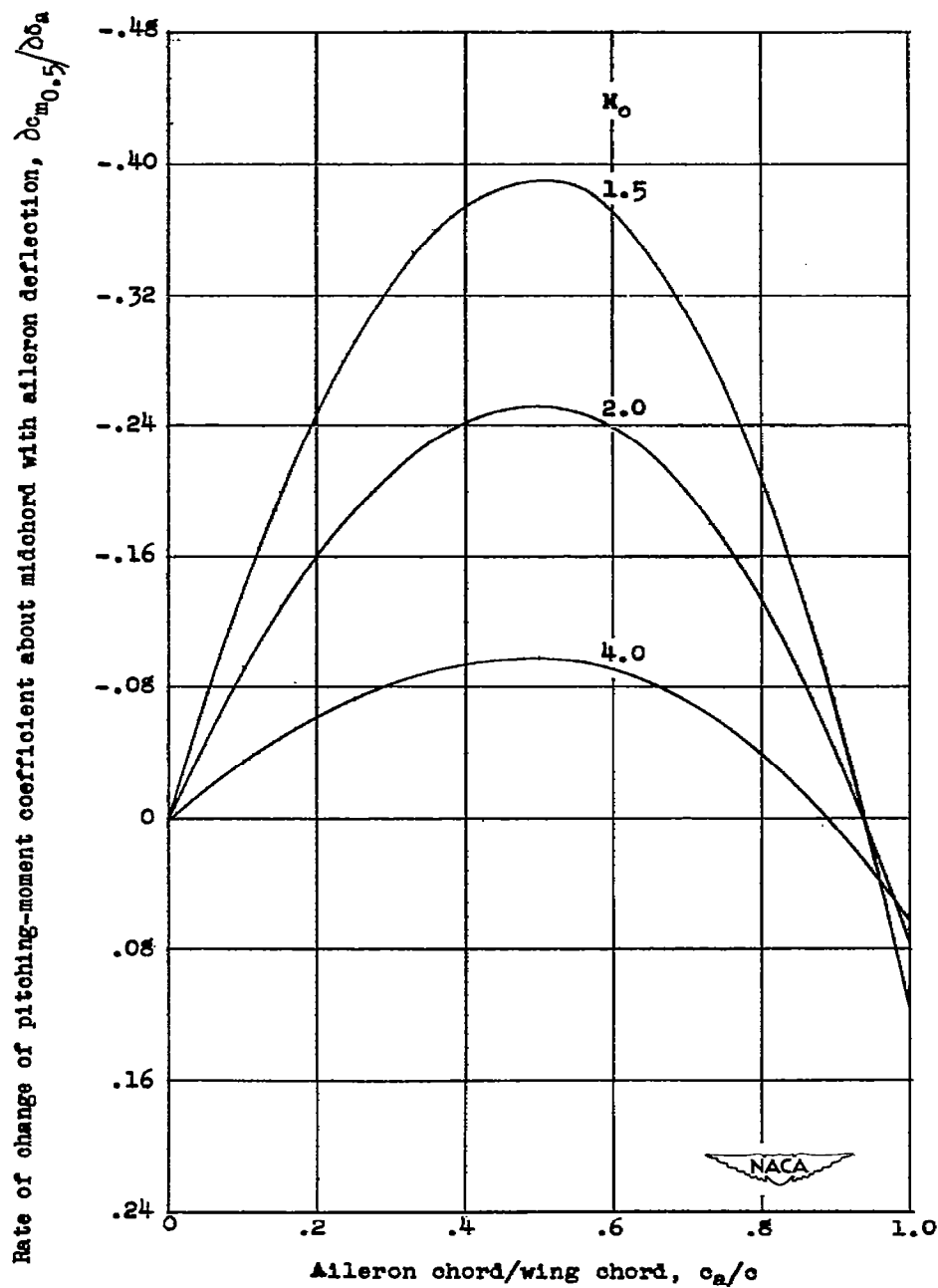
(a) $\frac{t}{c} = 0.05.$

Figure 16.- Rate of change of aileron hinge-moment
coefficient with aileron deflection as a
function of the ratio of aileron chord to wing
chord for an uncambered wedge airfoil having
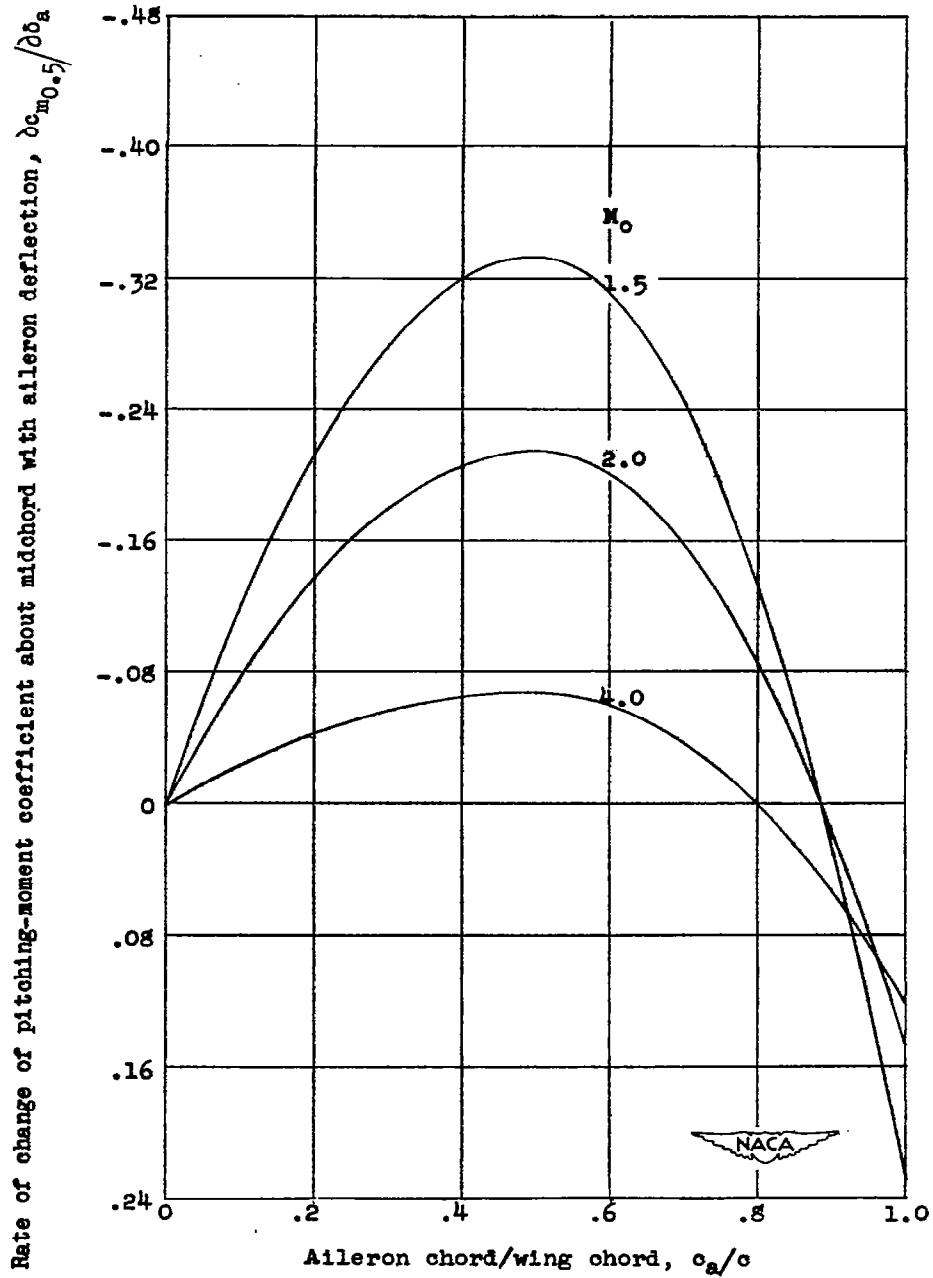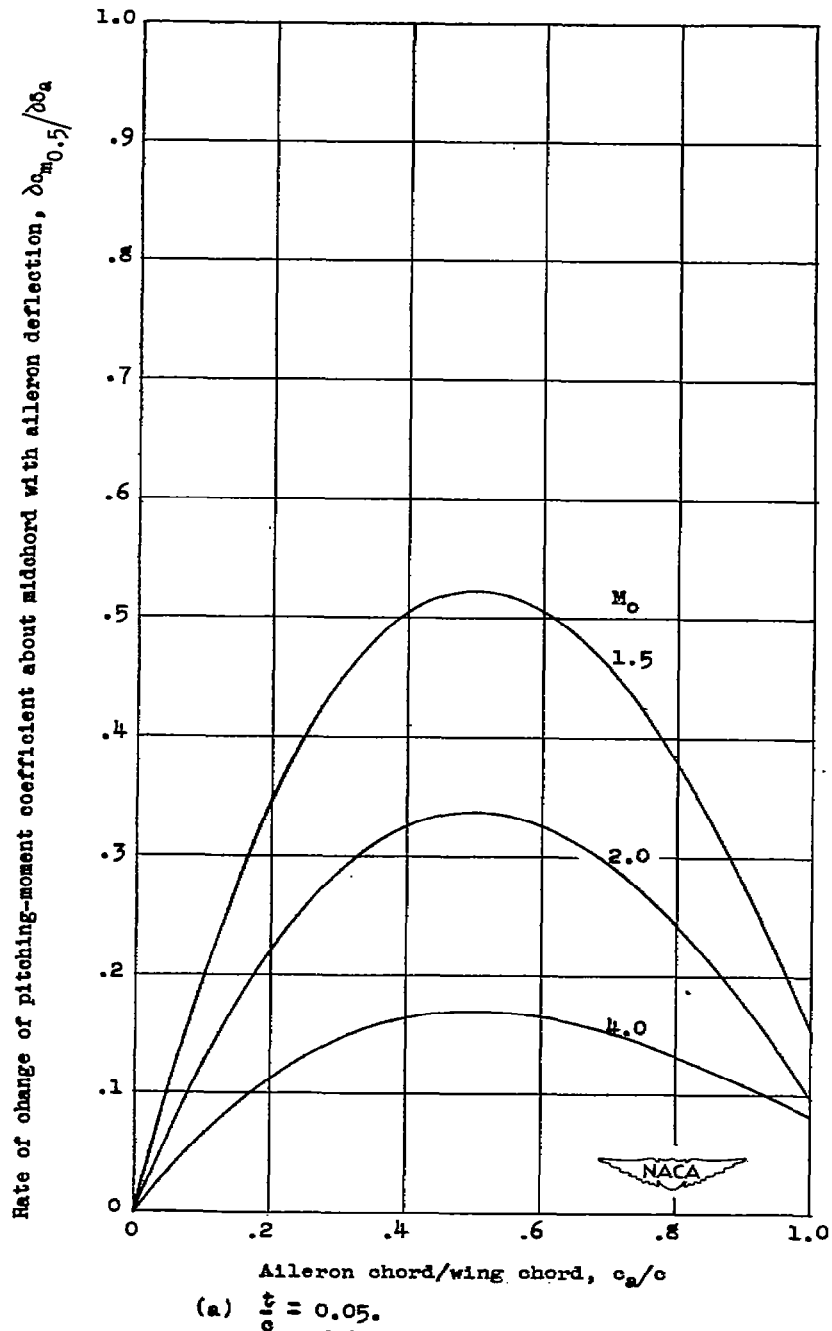maximum thickness at midchord and leading-edge
aileron.

(b) $\frac{t}{c} = 0.10.$

Figure 16.- Concluded.
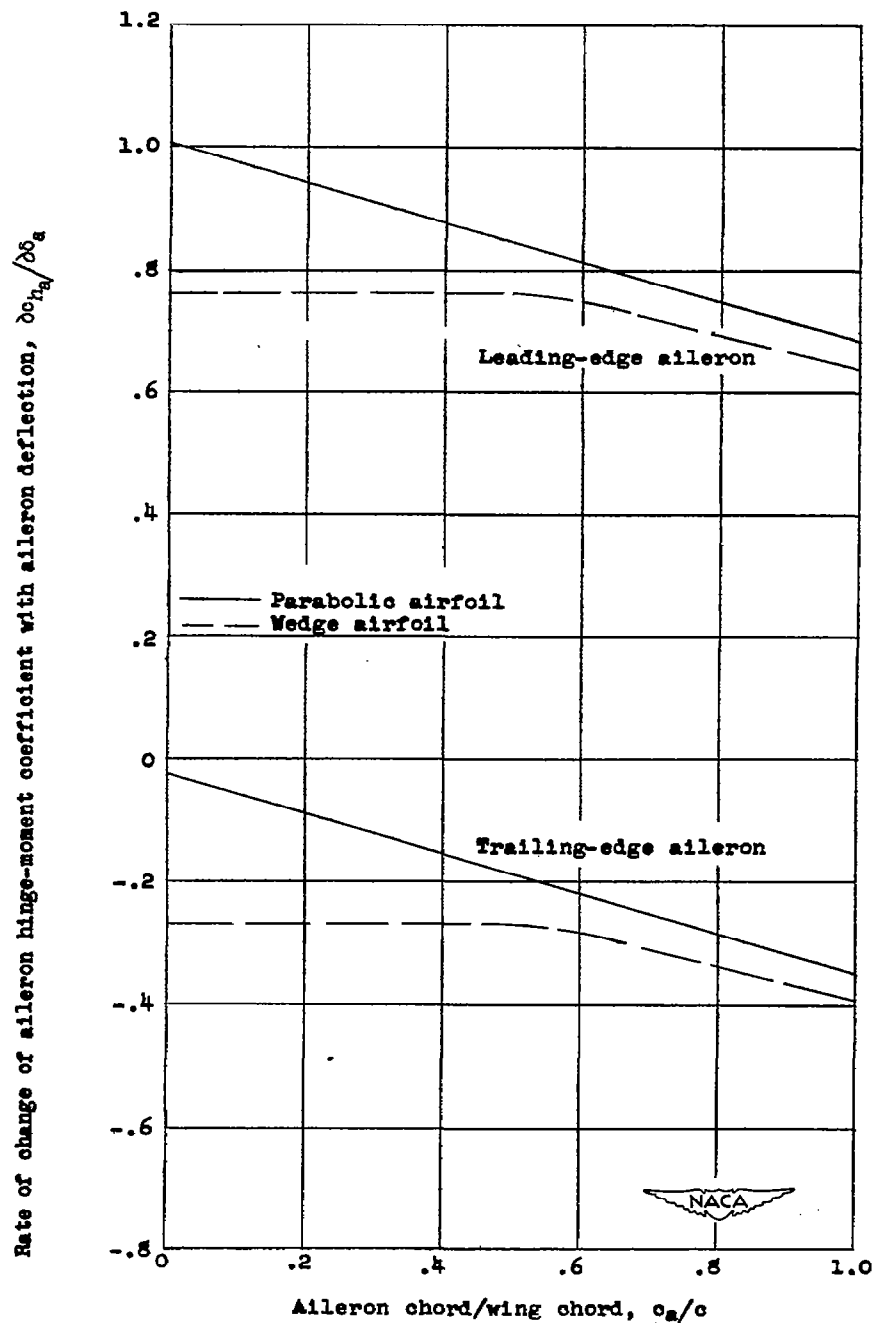
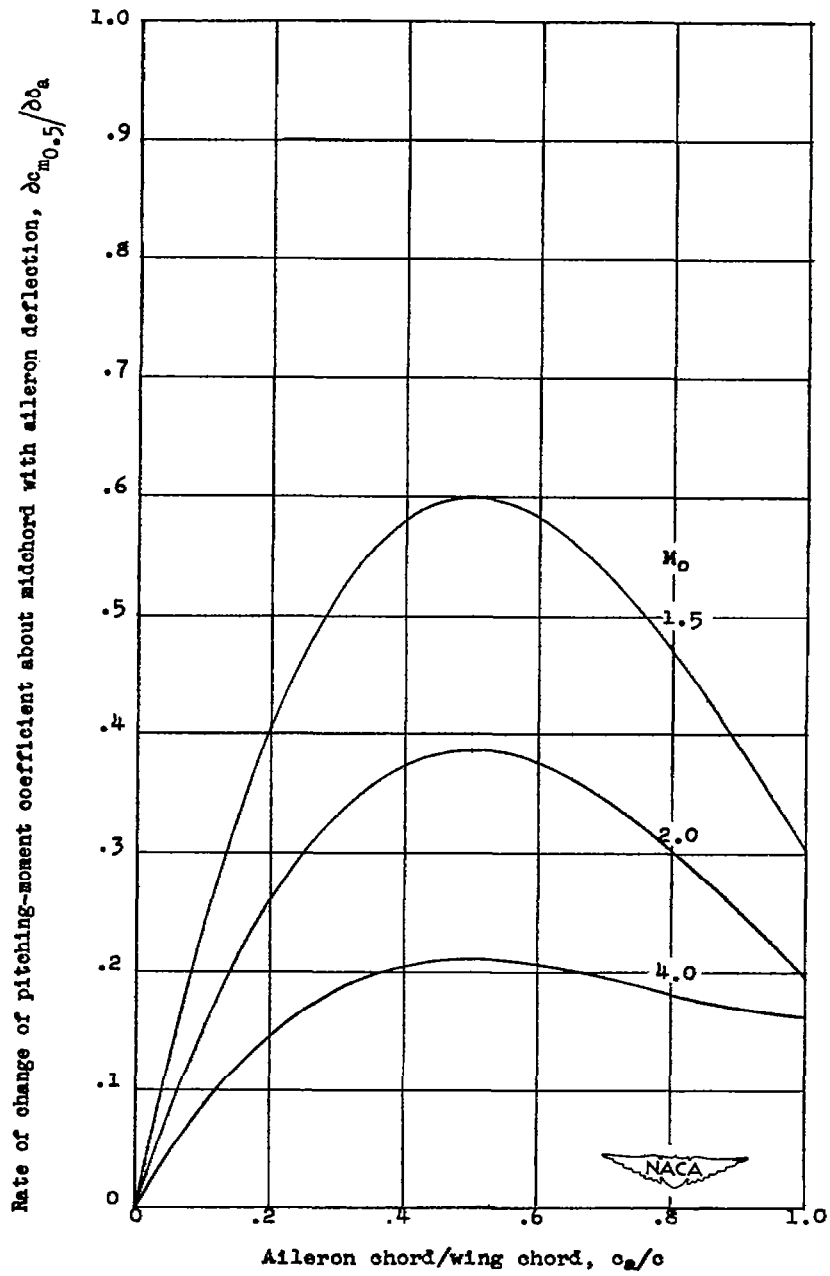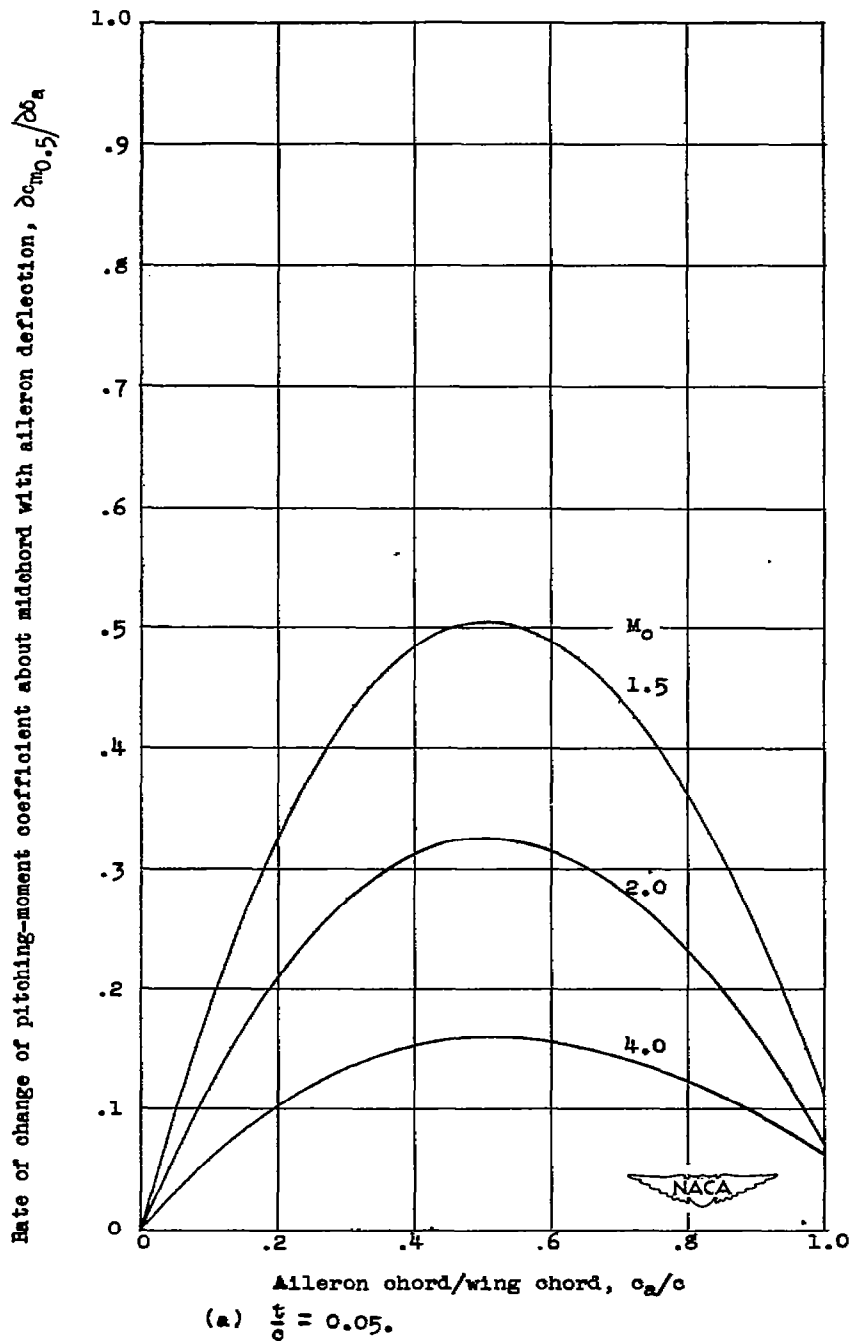Figure 17.- Rate of change of aileron hinge-moment
coefficient with aileron deflection as a
function of the ratio of aileron chord to wing
chord for uncambered airfoils having maximum
thickness at midchord. $M_0 = 4.0$; $\frac{t}{c} = 0.10$.

Figure 18.- Rate of change of aileron hinge-moment coefficient
with aileron deflection as a function of free-stream
Mach number for an uncambered parabolic airfoil having
maximum thickness at midchord and trailing-edge aileron.
$\frac{c_a}{c} = 0.2.$

Figure 19.- Rate of change of aileron hinge-moment coefficient
   with aileron deflection as a function of free-stream
   Mach number for an uncambered wedge airfoil having maximum
   thickness at midchord and trailing-edge aileron. $\frac{c_a}{c}$ = 0.2.

Figure 20.- Rate of change of aileron hinge-moment coefficient
with aileron deflection as a function of free-stream
Mach number for an uncambered parabolic airfoil having
maximum thickness at midchord and leading-edge aileron.
$\frac{c_a}{c} = 0.2.$

Figure 21.- Rate of change of aileron hinge-moment coefficient with aileron deflection as a function of free-stream Mach number for an uncambered wedge airfoil having maximum thickness at midchord and leading-edge aileron. $\frac{c_a}{c} = 0.2$.
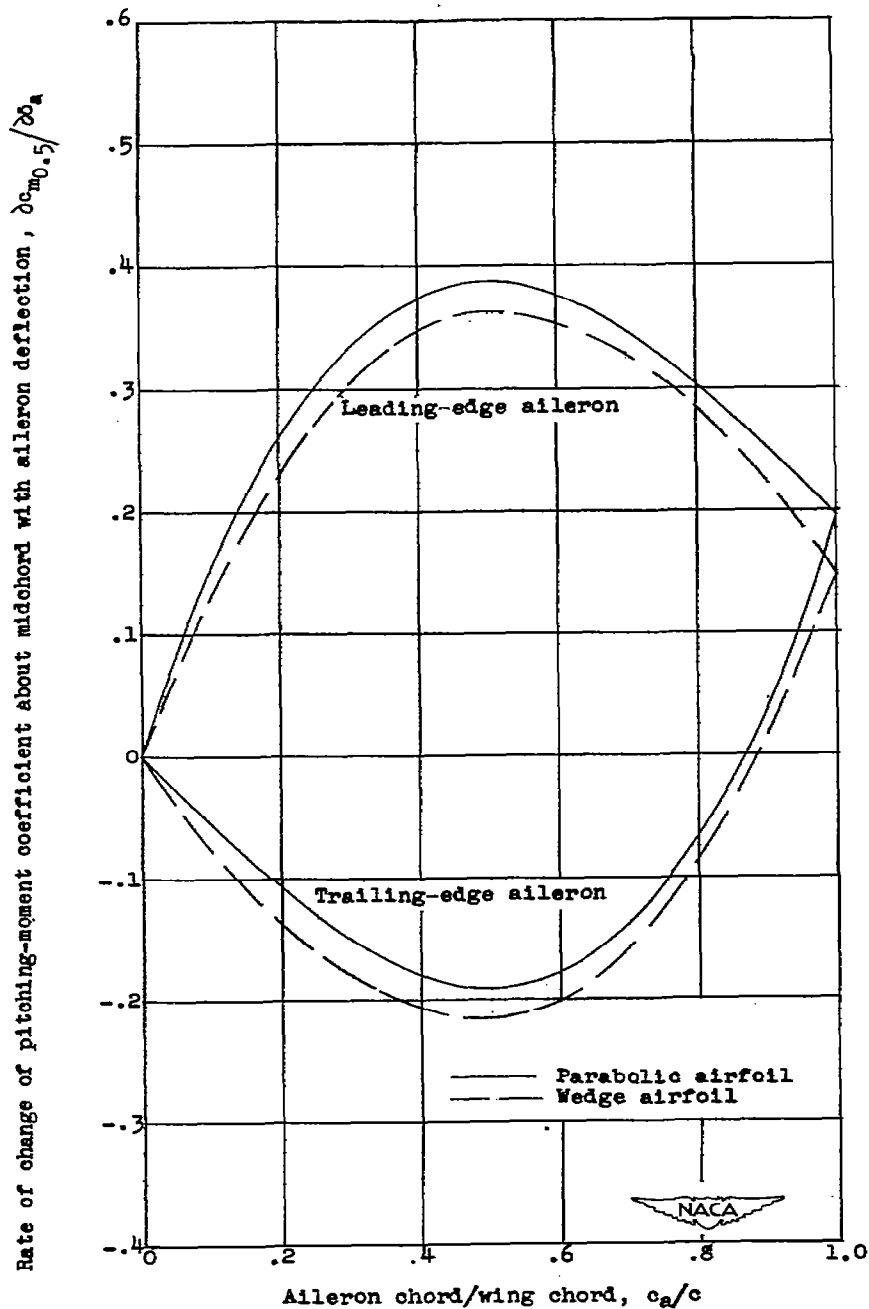
(a) $\frac{t}{c} = 0.05$.
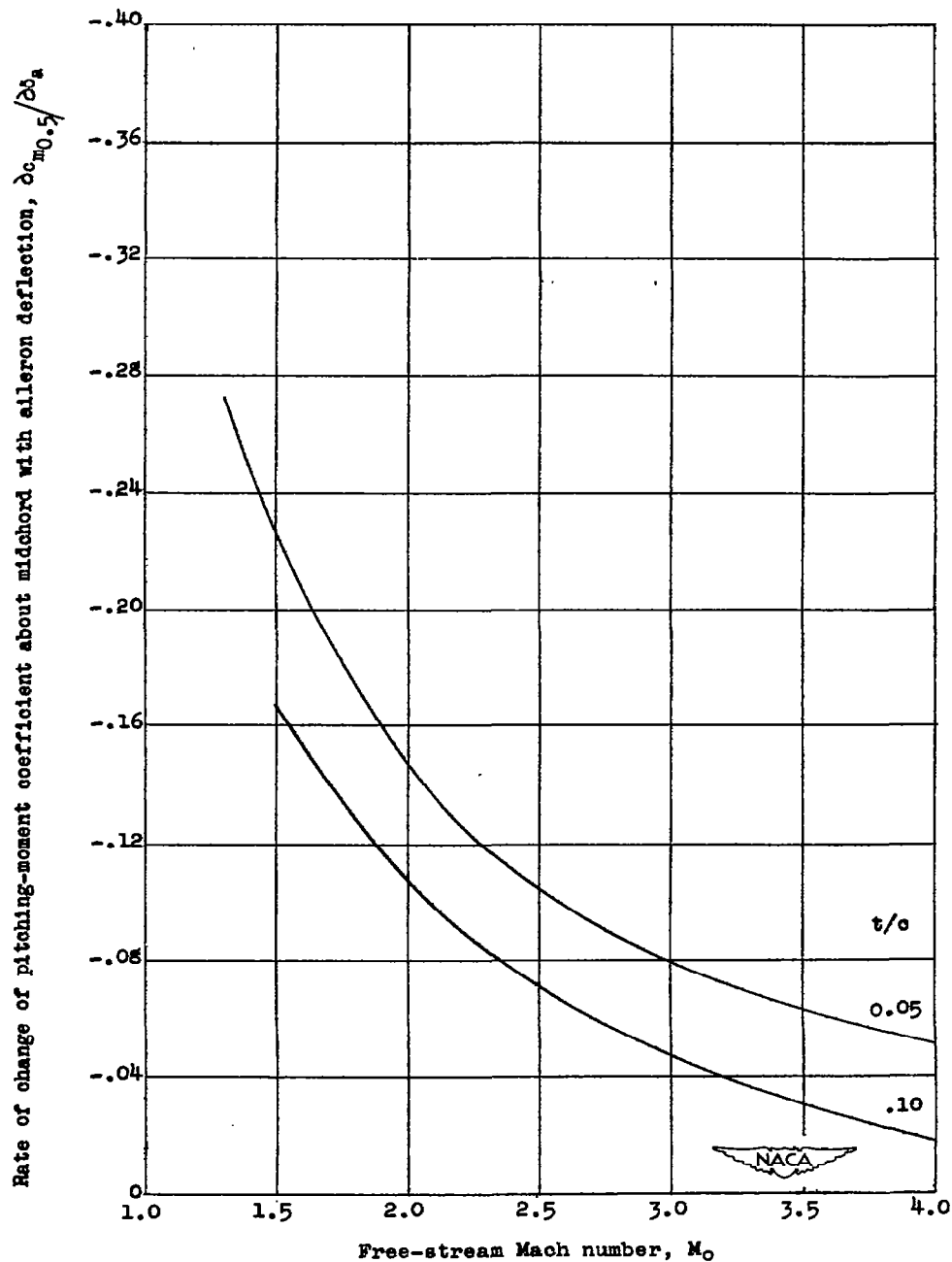
Figure 22.- Rate of change of pitching-moment coefficient
about midchord with aileron deflection as a
function of the ratio of aileron chord to wing chord
for an uncambered parabolic airfoil having maximum
thickness at midchord and trailing-edge aileron.

(b) $\frac{t}{c} = 0.10.$

Figure 22.- Concluded.

(a) $\frac{t}{c} = 0.05$.
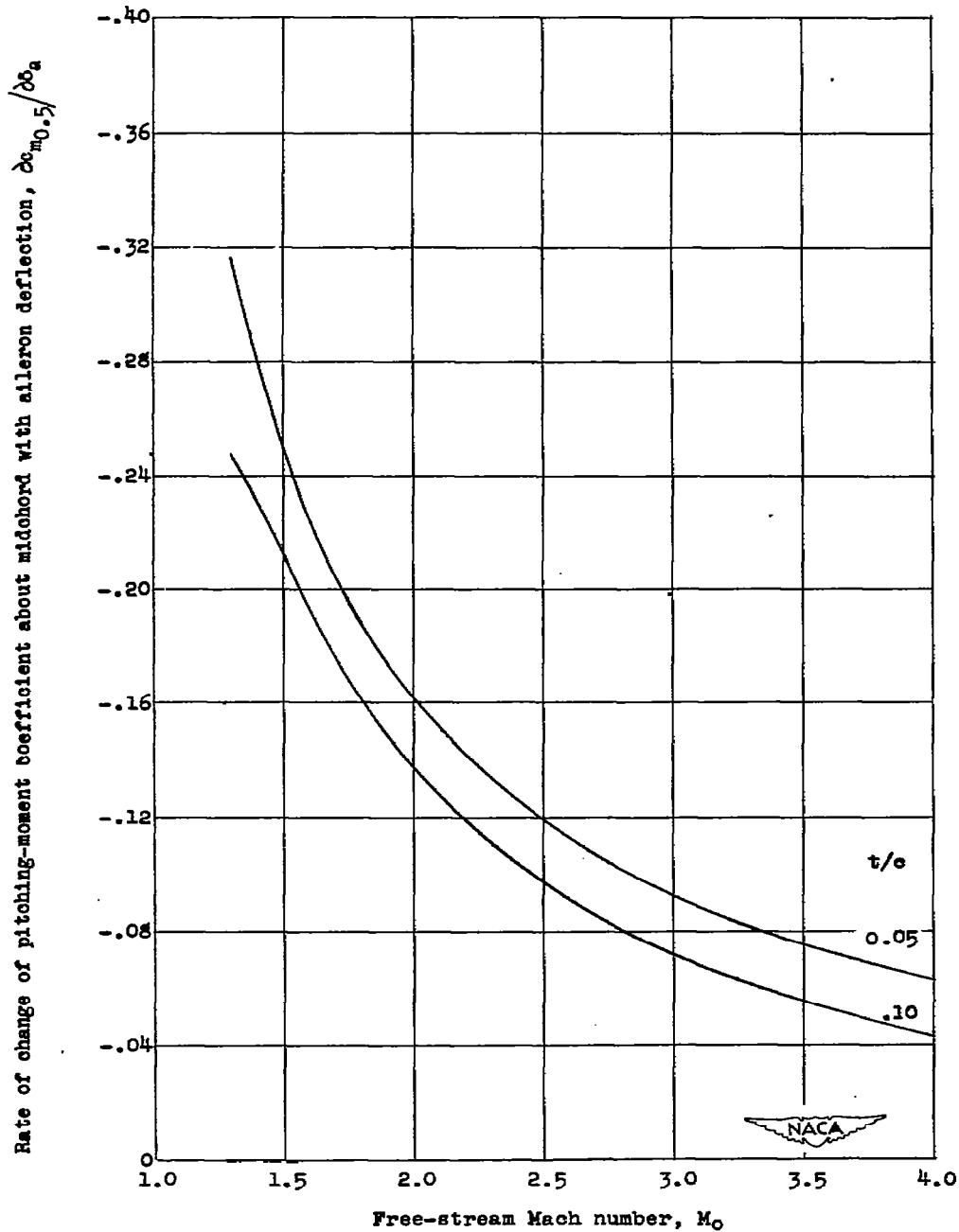
Figure 23.- Rate of change of pitching-moment coefficient
about midchord with aileron deflection as a
function of the ratio of aileron chord to wing chord
for an uncambered wedge airfoil having maximum
thickness at midchord and trailing-edge aileron.

(b) $\dfrac{t}{c} = 0.10.$

Figure 23.- Concluded.

(a) $\frac{t}{c} = 0.05.$
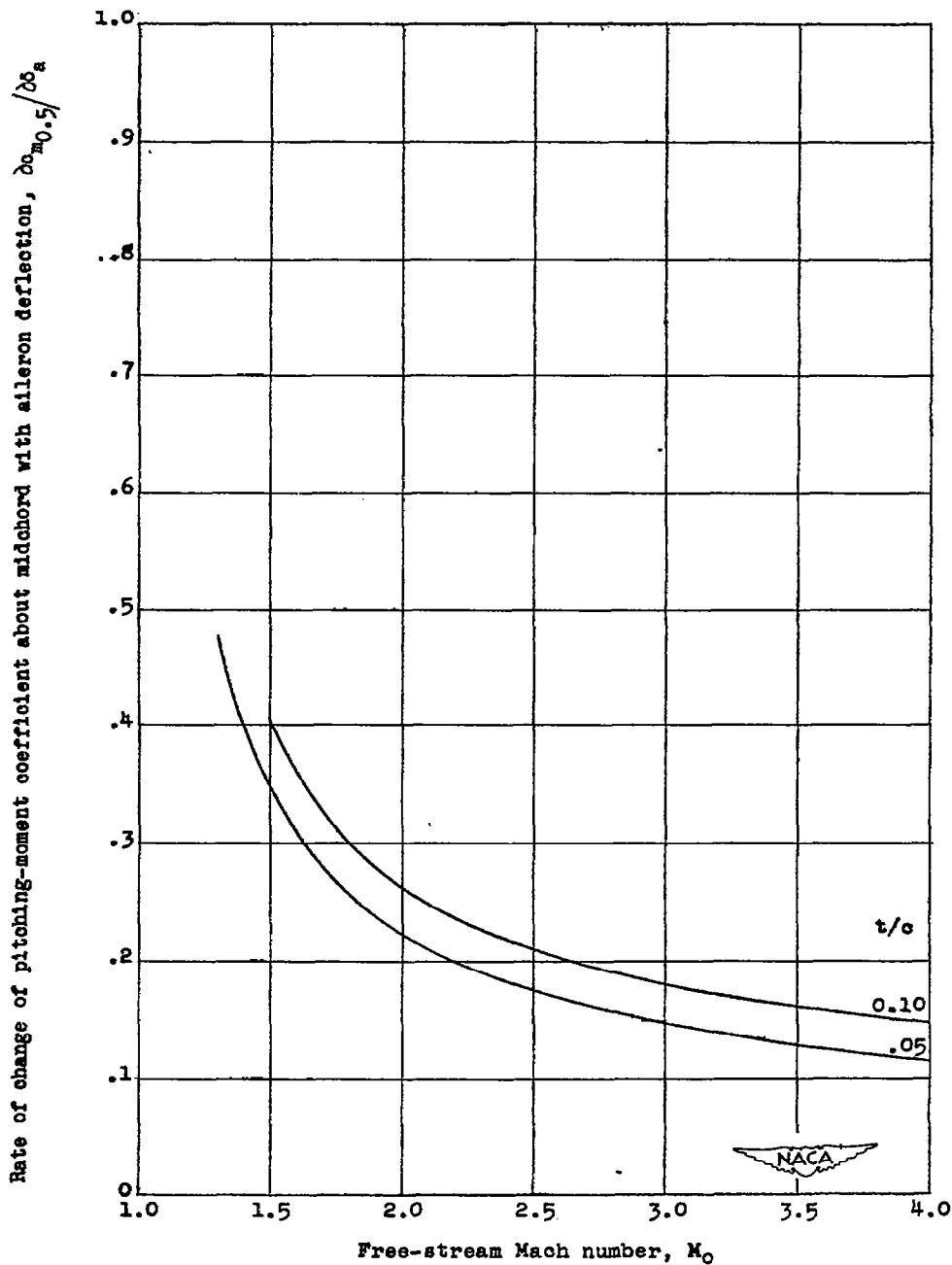
Figure 24.- Rate of change of pitching-moment coefficient
about midchord with aileron deflection as a
function of the ratio of aileron chord to wing chord
for an uncambered parabolic airfoil having maximum
thickness at midchord and leading-edge aileron.

(b) $\frac{t}{c} = 0.10$.

Figure 24.- Concluded.

(a) $\frac{t}{c} = 0.05.$

Figure 25.- Rate of change of pitching-moment coefficient
   about midchord with aileron deflection as a
   function of the ratio of aileron chord to wing chord
   for an uncambered wedge airfoil having maximum thickness
   at midchord and leading-edge aileron.
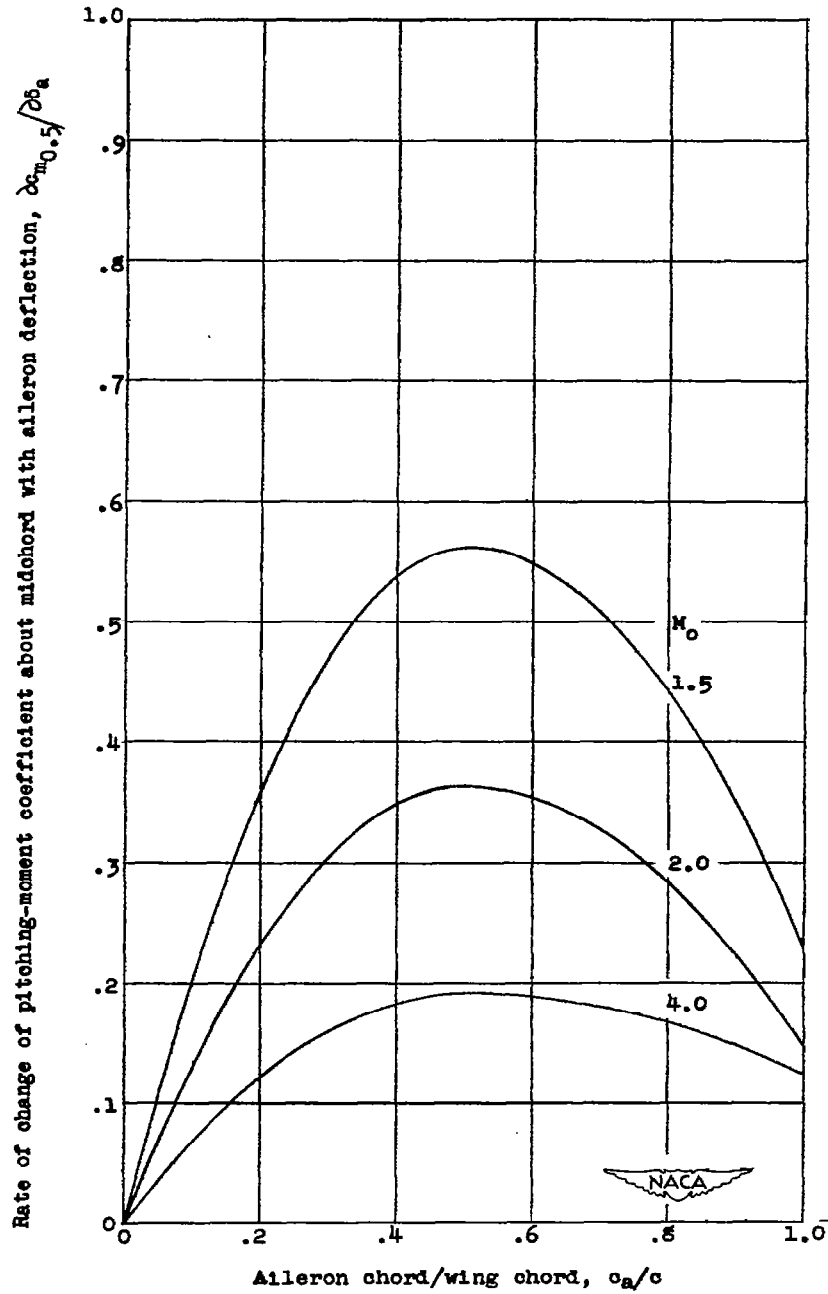
(b) $\frac{t}{c} = 0.10$.

Figure 25.- Concluded.

Figure 26.- Rate of change of pitching-moment coefficient
about midchord with aileron deflection as a
function of the ratio of aileron chord to wing chord
for uncambered airfoils having maximum thickness at
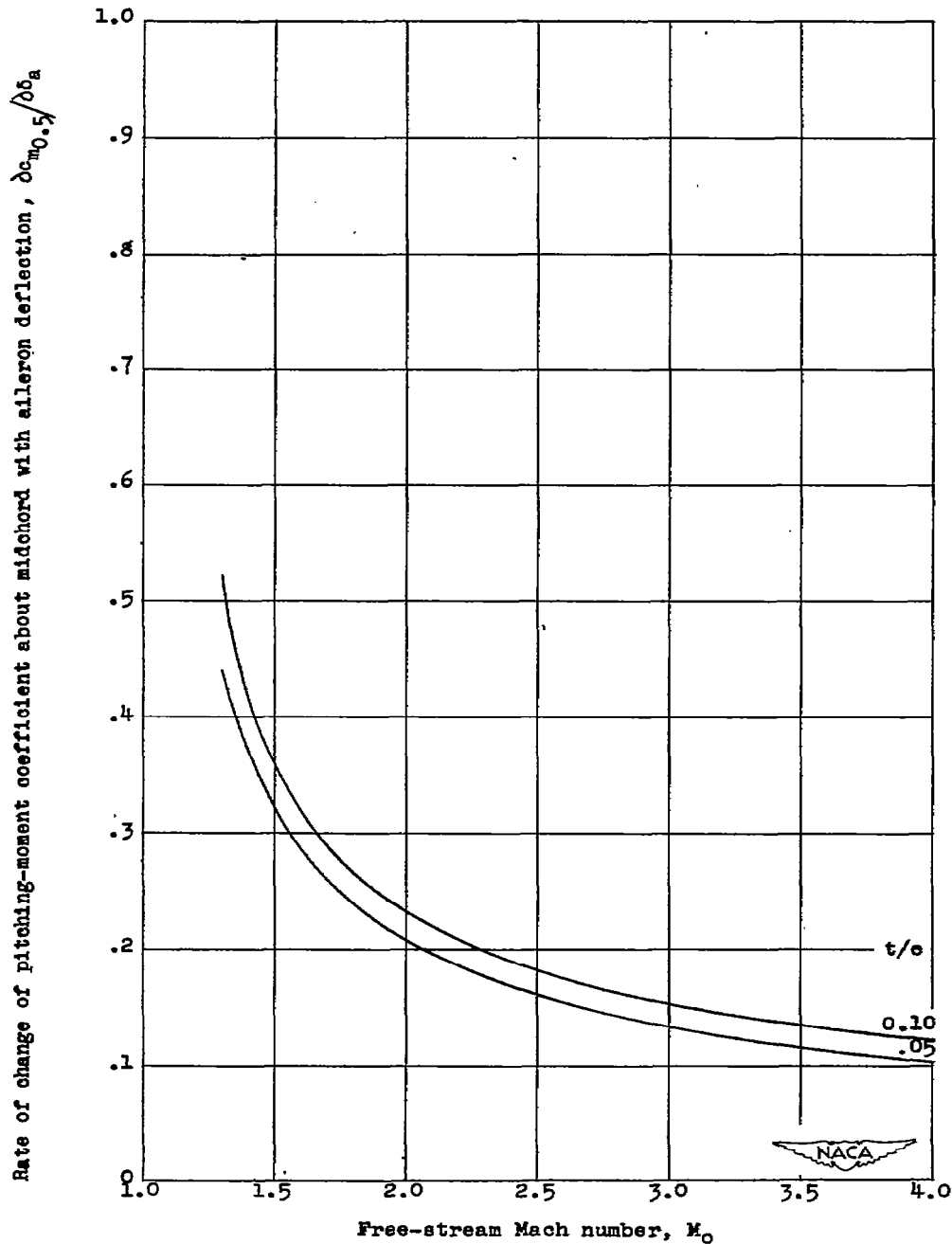midchord. $M_0 = 2.0$; $\frac{t}{c} = 0.10$.

Figure 27.- Rate of change of pitching-moment coefficient about
   midchord with aileron deflection as a function of free-
   stream Mach number for an uncambered parabolic airfoil having
   maximum thickness at midchord and trailing-edge aileron.
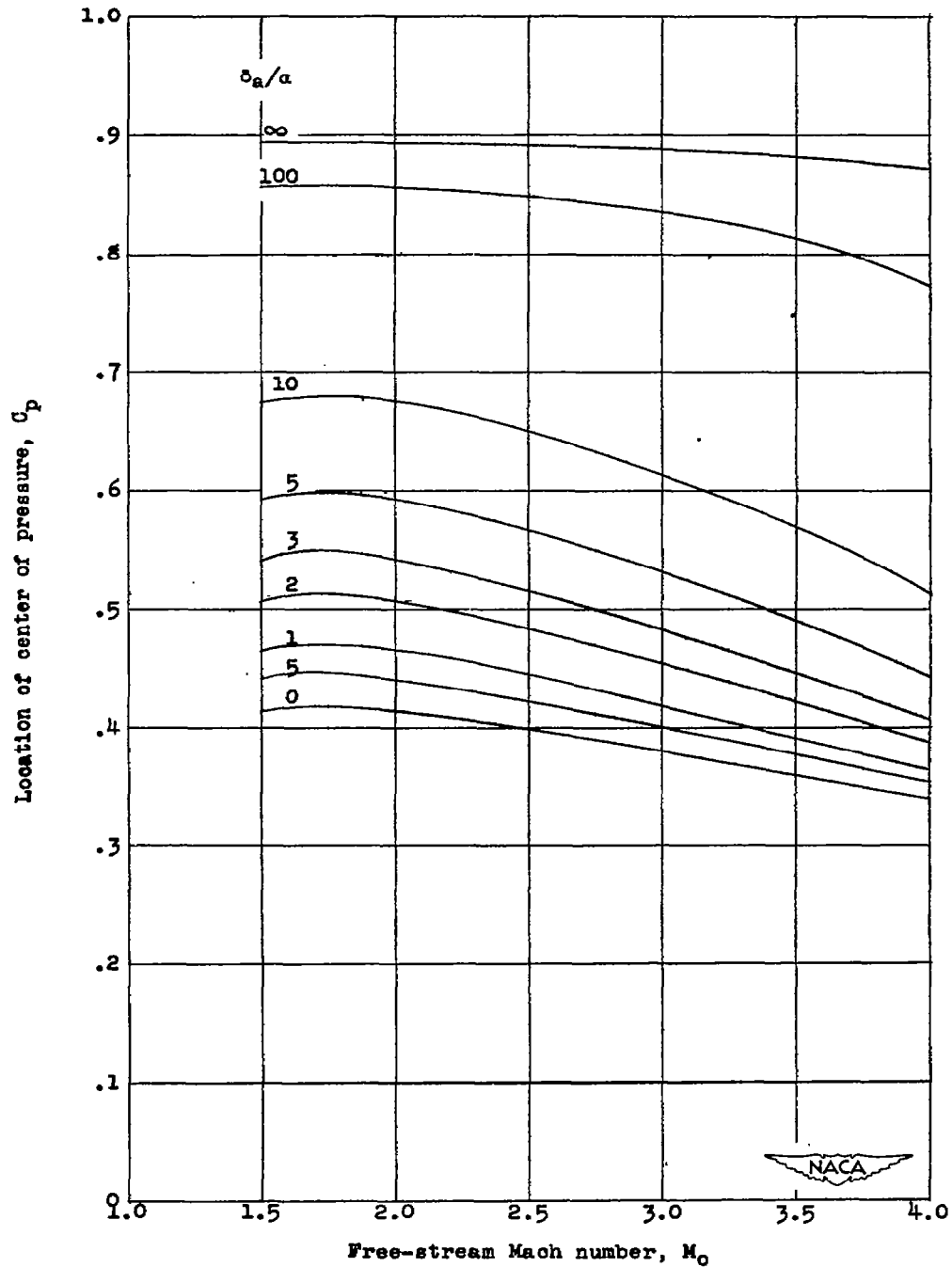 $\frac{c_a}{c} = 0.2.$

Figure 28.- Rate of change of pitching-moment coefficient
    about midchord with aileron deflection as a
    function of free-stream Mach number for an uncambered
    wedge airfoil having maximum thickness at midchord
    and trailing-edge aileron. $\frac{c_a}{c} = 0.2.$

Figure 29.- Rate of change of pitching-moment coefficient about midchord with aileron deflection as a function of free-stream Mach number for an uncambered parabolic airfoil having maximum thickness at midchord and leading-edge aileron. $\frac{\delta a}{c} = 0.2$.

Figure 30.— Rate of change of pitching-moment coefficient about
midchord with aileron deflection as a function of free-
stream Mach number for an uncambered wedge airfoil having
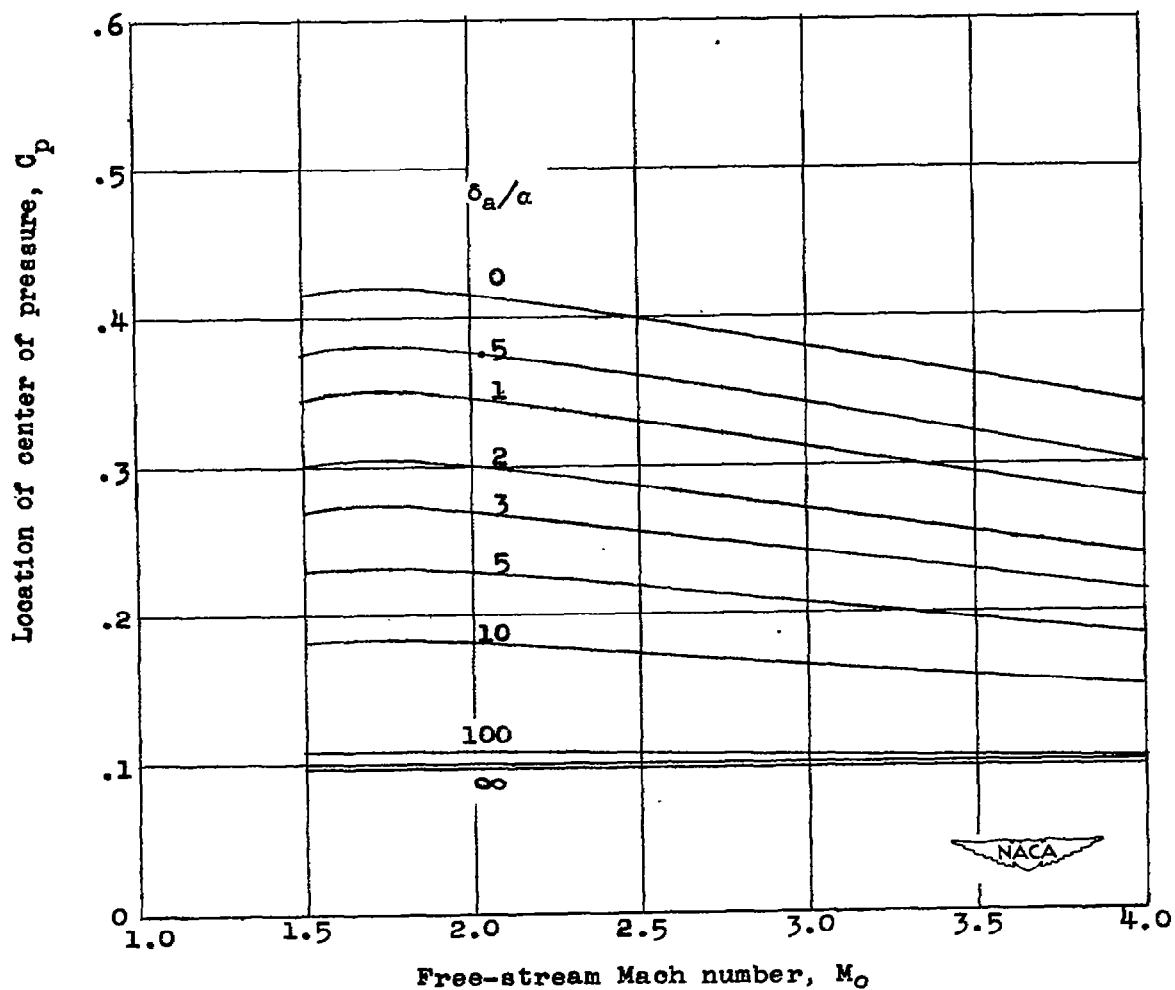maximum thickness at midchord and leading-edge aileron.
$\frac{c_a}{c} = 0.2$.

Figure 31.- Location of center of pressure as a function of free-stream Mach number for an uncambered parabolic airfoil having maximum thickness at midchord and trailing-edge aileron. $\frac{c_a}{c} = 0.2$; $\frac{t}{c} = 0.10$.
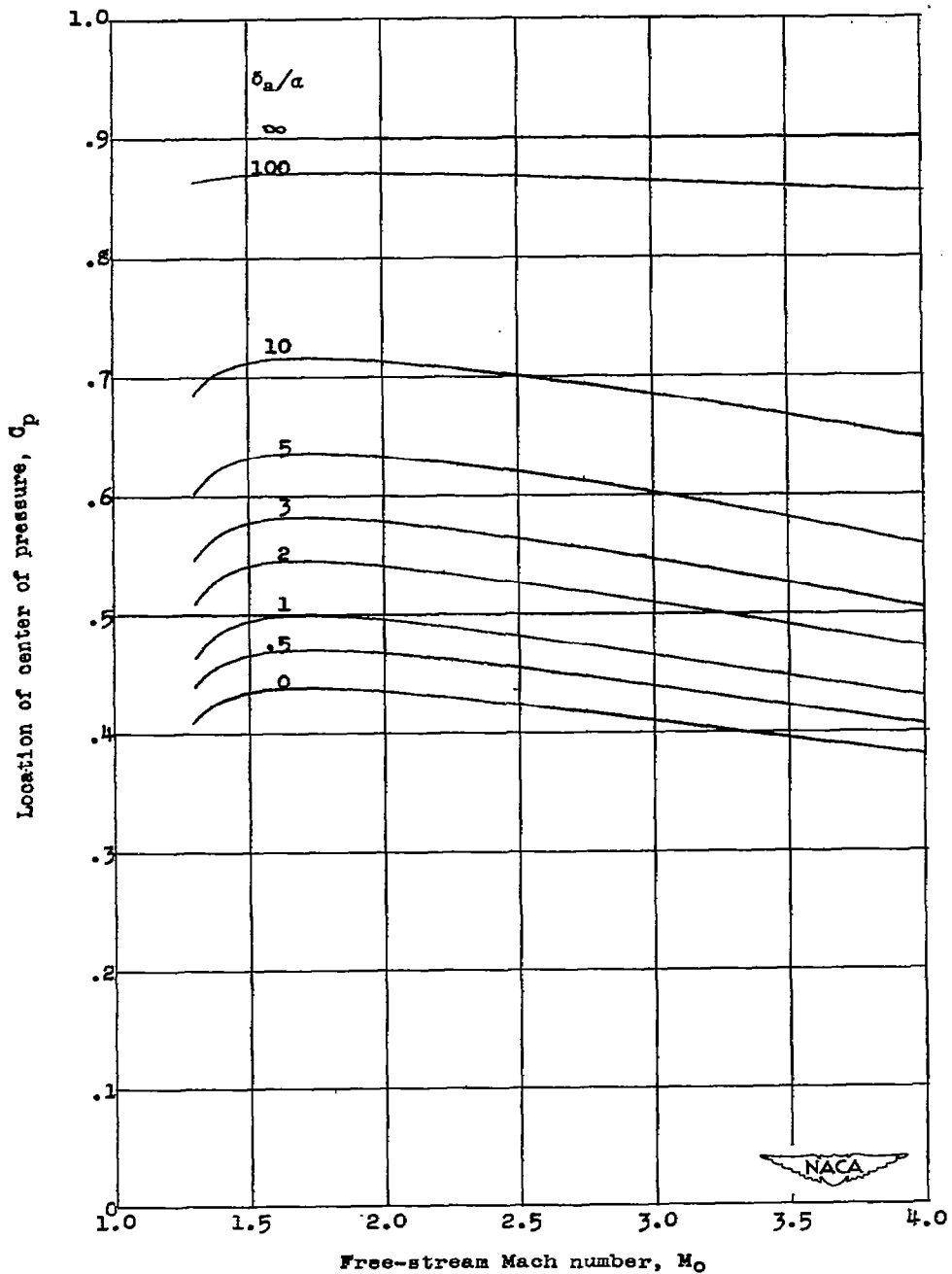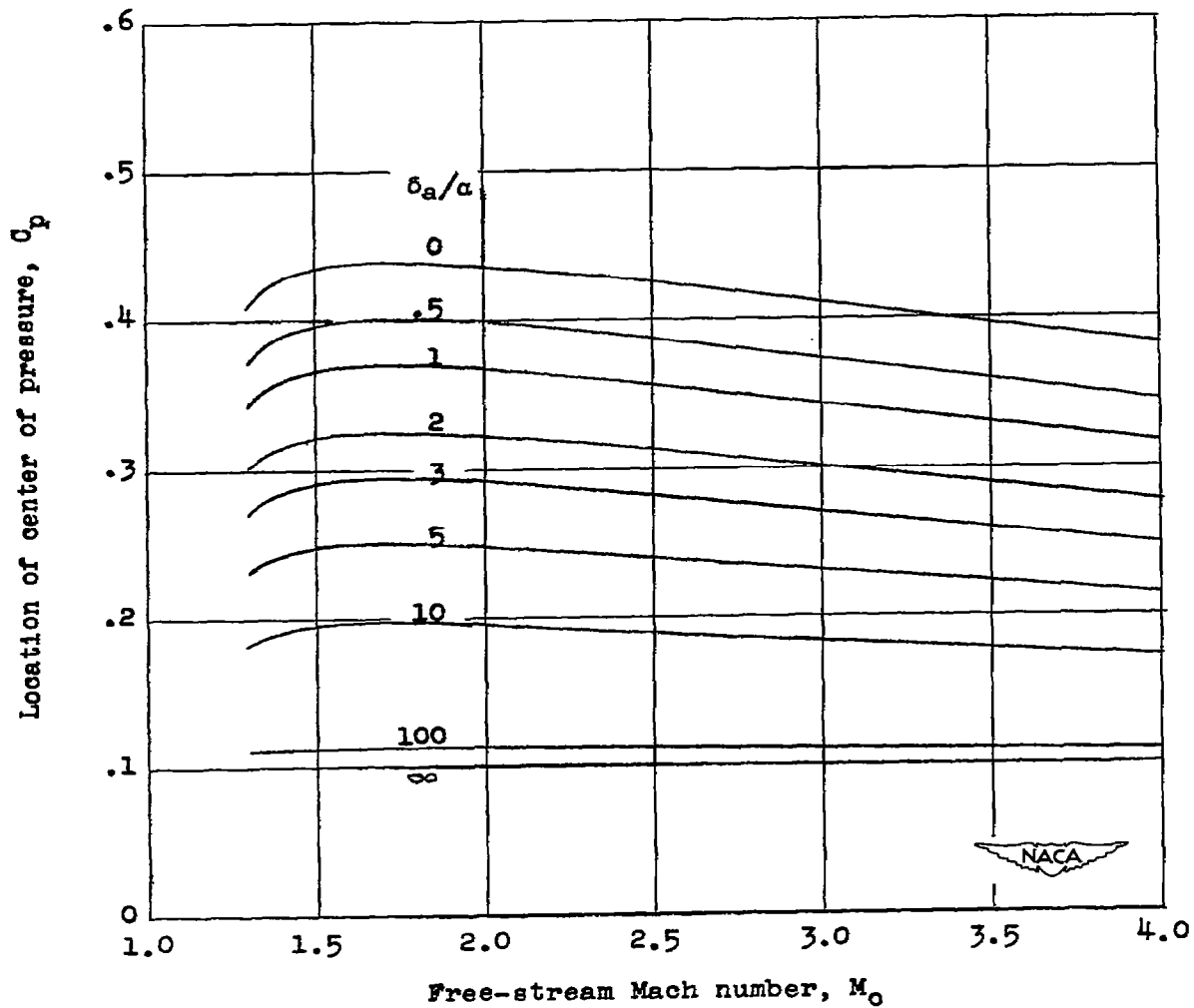
Figure 32.- Location of center of pressure as a function of free-stream Mach number for an uncambered wedge airfoil having maximum thickness at midchord and trailing-edge aileron. $\frac{c_a}{c} = 0.2$; $\frac{t}{c} = 0.10$.
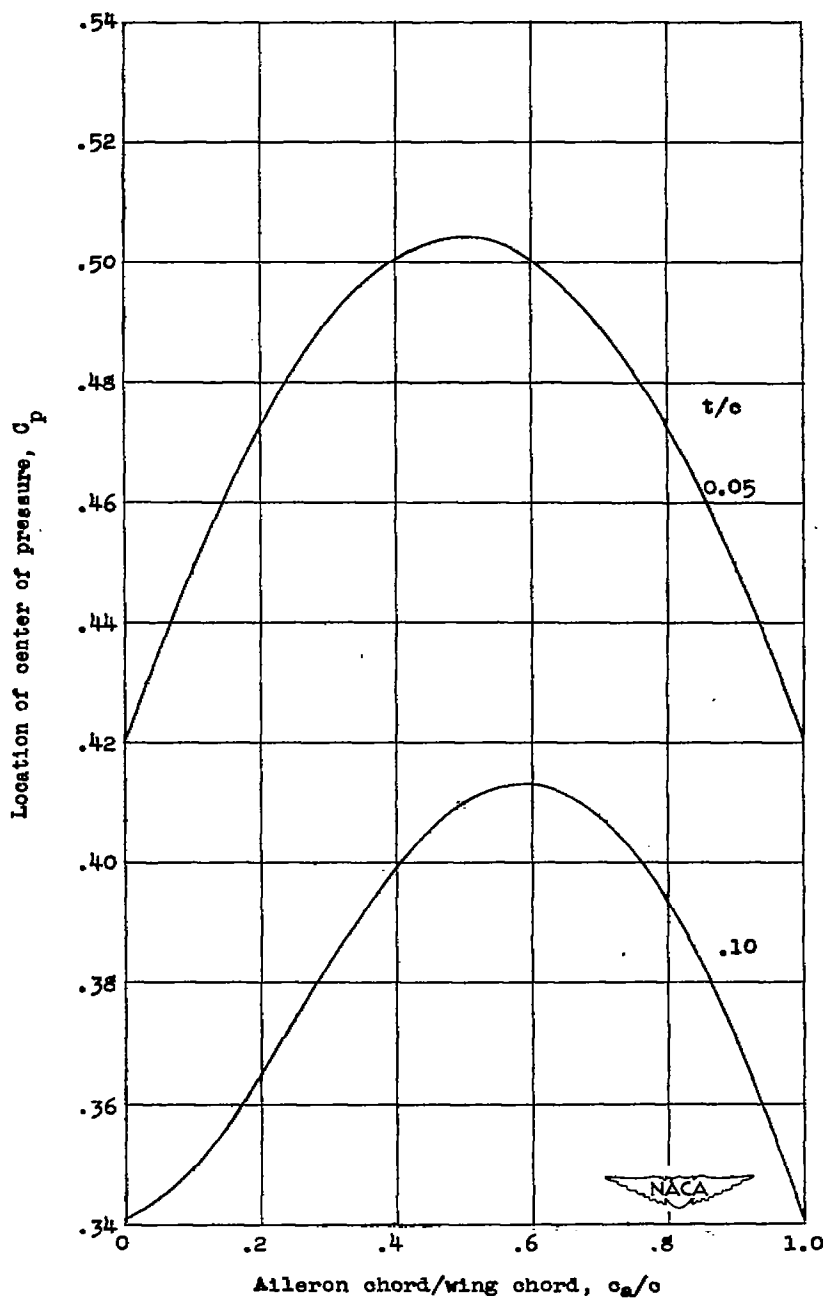
Figure 33.- Location of center of pressure as a function of free-stream Mach number for an uncambered parabolic airfoil having maximum thickness at midchord and leading-edge aileron. $\frac{c_a}{c} = 0.2$; $\frac{t}{c} = 0.10$.

Figure 34.- Location of center of pressure as a function of free-stream Mach number for an uncambered wedge airfoil having maximum thickness at midchord and leading-edge aileron. $\frac{c_a}{c} = 0.2$; $\frac{t}{c} = 0.10$.

Figure 35.- Location of center of pressure as a
function of the ratio of aileron chord to wing
chord for an uncambered parabolic airfoil having
maximum thickness at midchord and trailing-edge
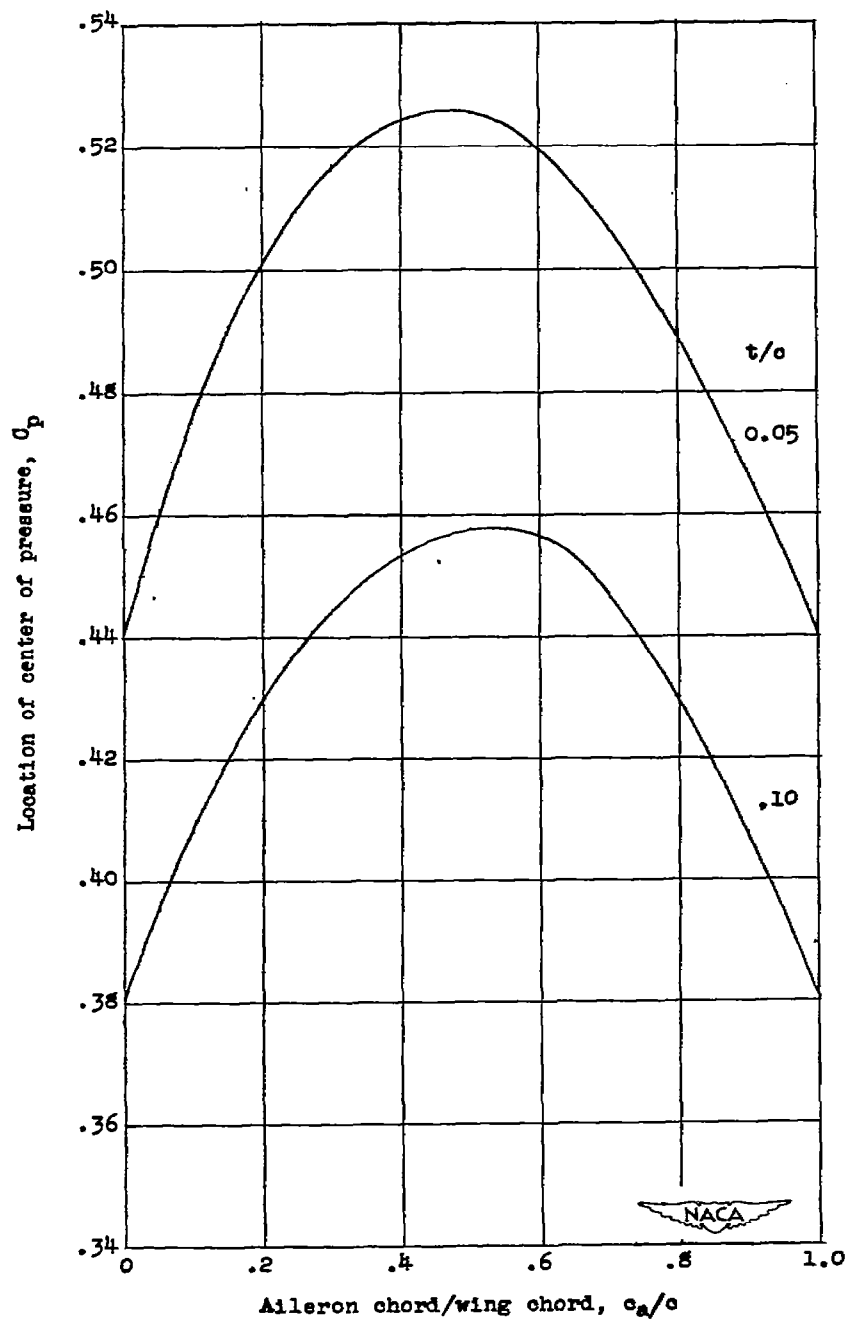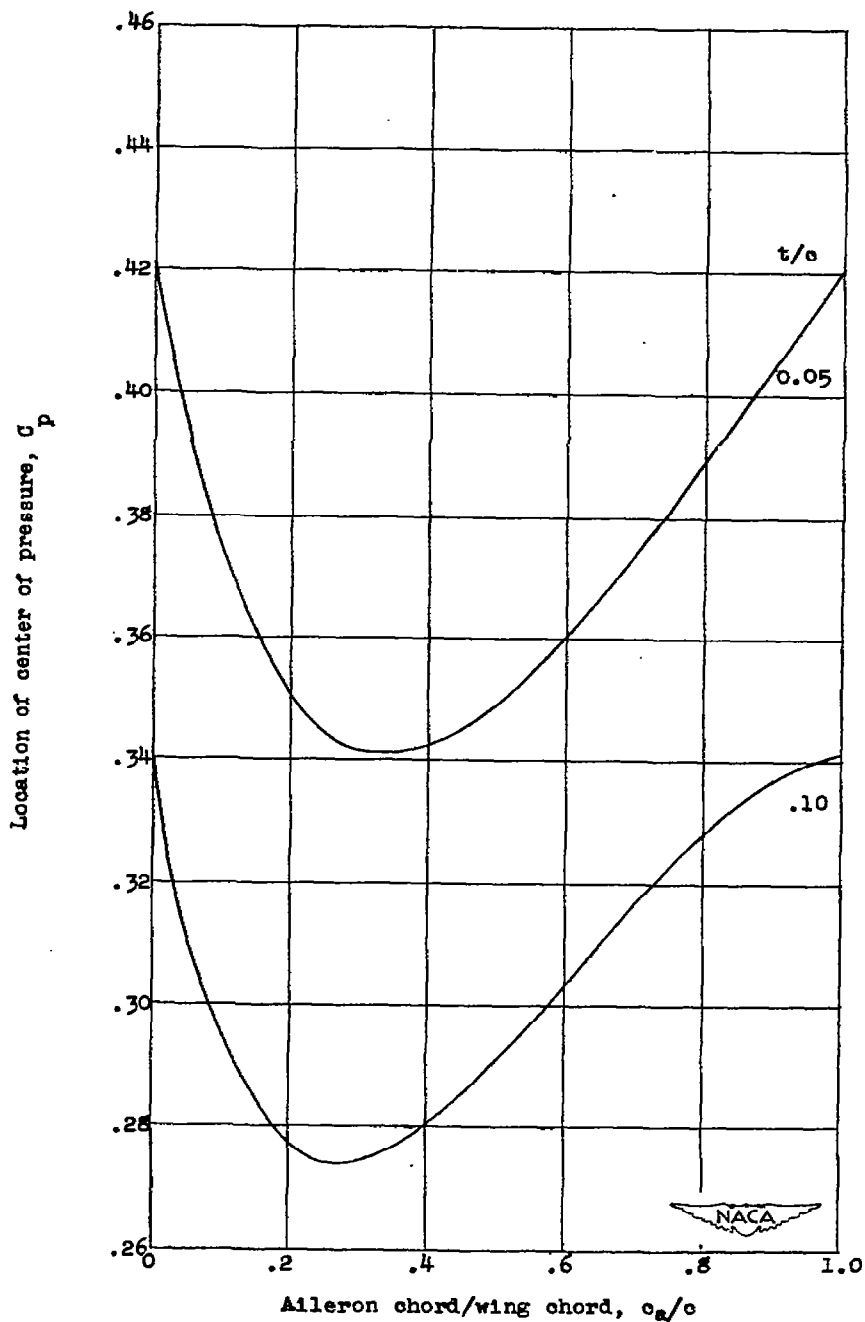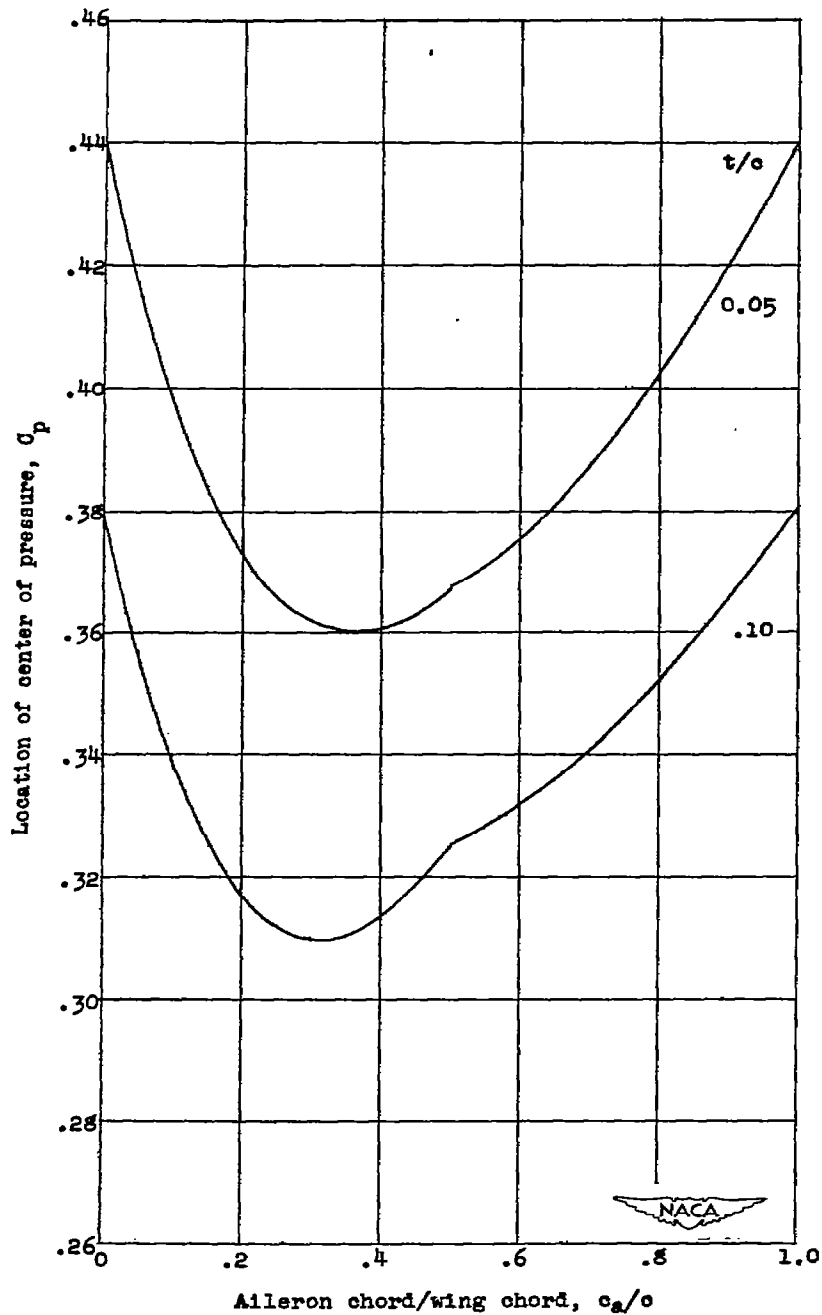aileron. $M_0 = 4.0$; $\frac{\delta_a}{\alpha} = 1.0$.

Figure 36.- Location of center of pressure as a function
of the ratio of aileron chord to wing chord for an
uncambered wedge airfoil having maximum thickness at
midchord and trailing-edge aileron. $M_O = 4.0$; $\frac{\delta_a}{\alpha} = 1.0$.

Figure 37.- Location of center of pressure as a function
of the ratio of aileron chord to wing chord for an
uncambered parabolic airfoil having maximum thickness
at midchord and leading-edge aileron. $M_o = 4.0$; $\frac{\delta_a}{\alpha} = 1.0$.

Figure 38.- Location of center of pressure as a function
of the ratio of aileron chord to wing chord for an
uncambered wedge airfoil having maximum thickness at
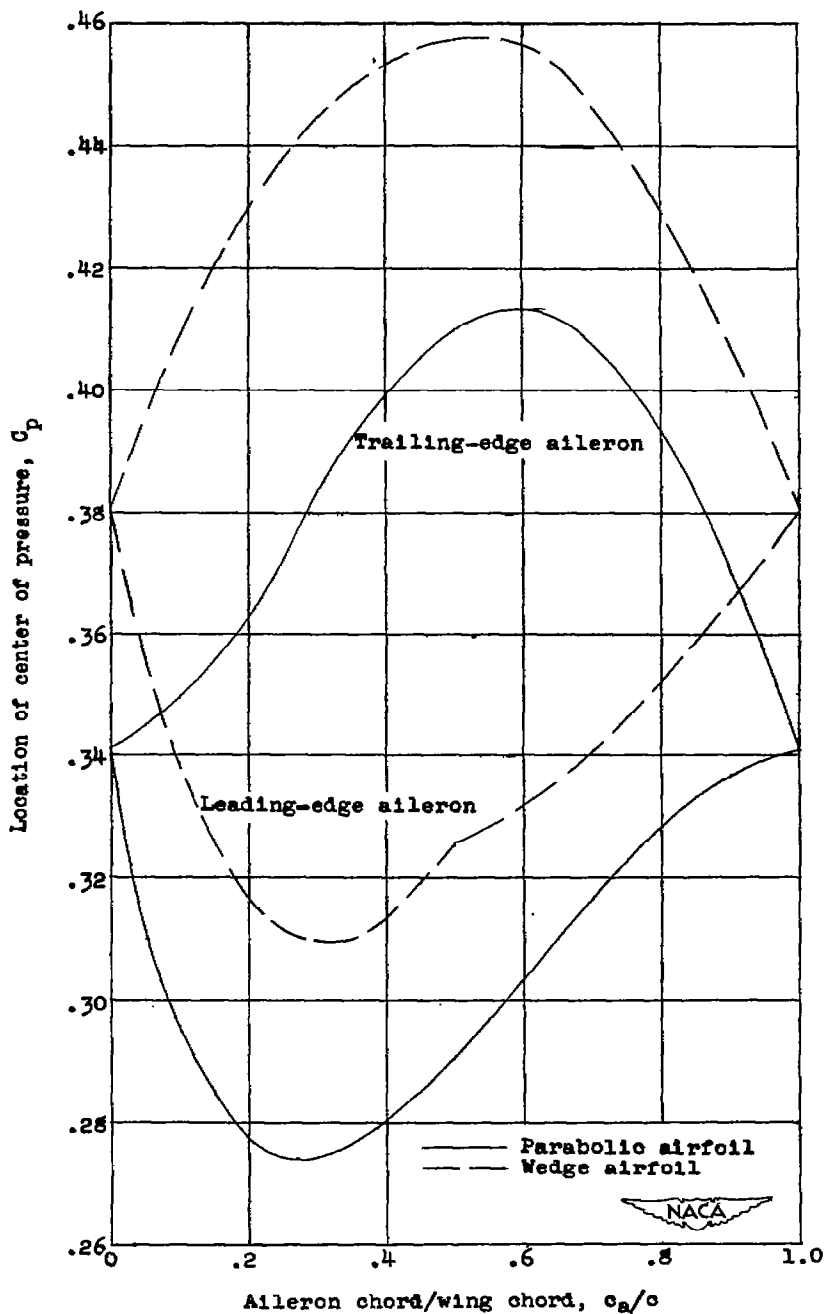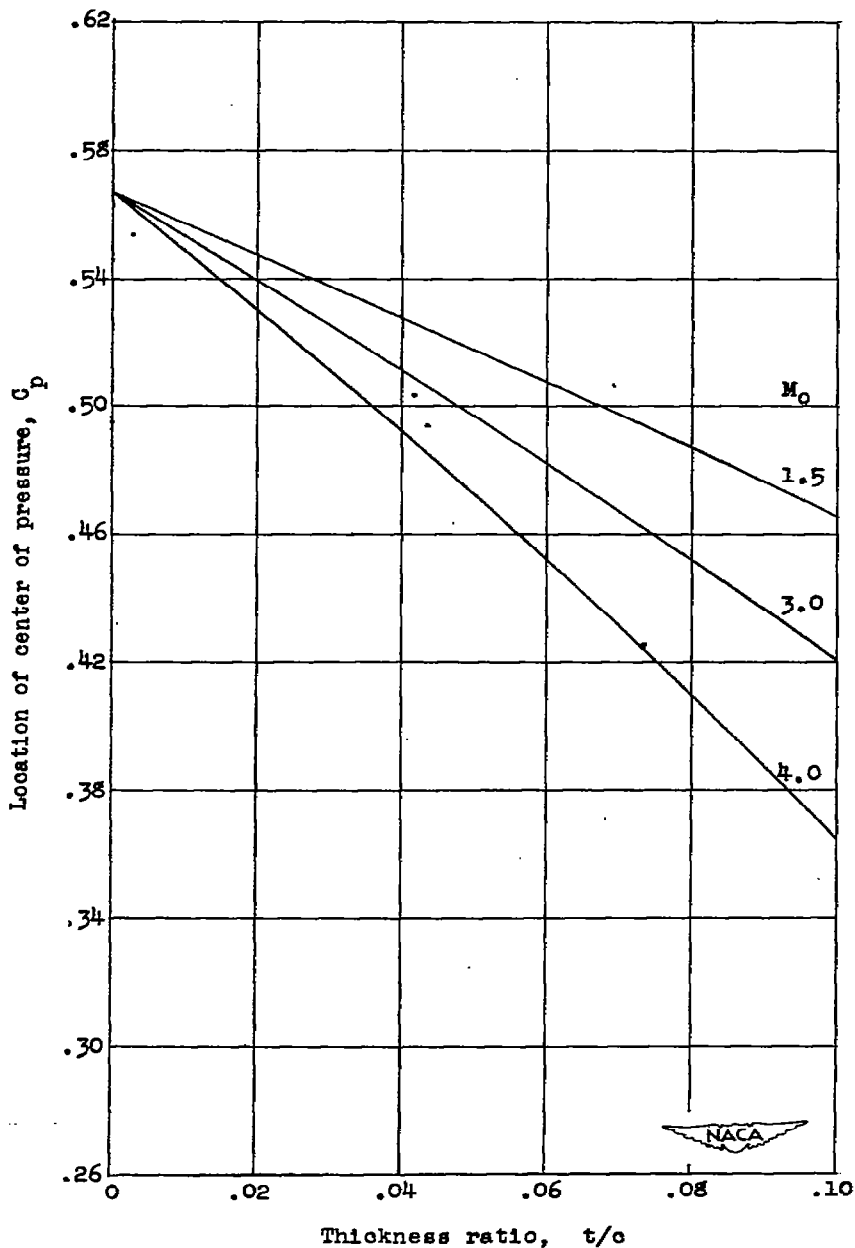midchord and leading-edge aileron. $M_o = 4.0$; $\frac{\delta_a}{\alpha} = 1.0$.

Figure 39.- Location of center of pressure as a function
of the ratio of aileron chord to wing chord for un-
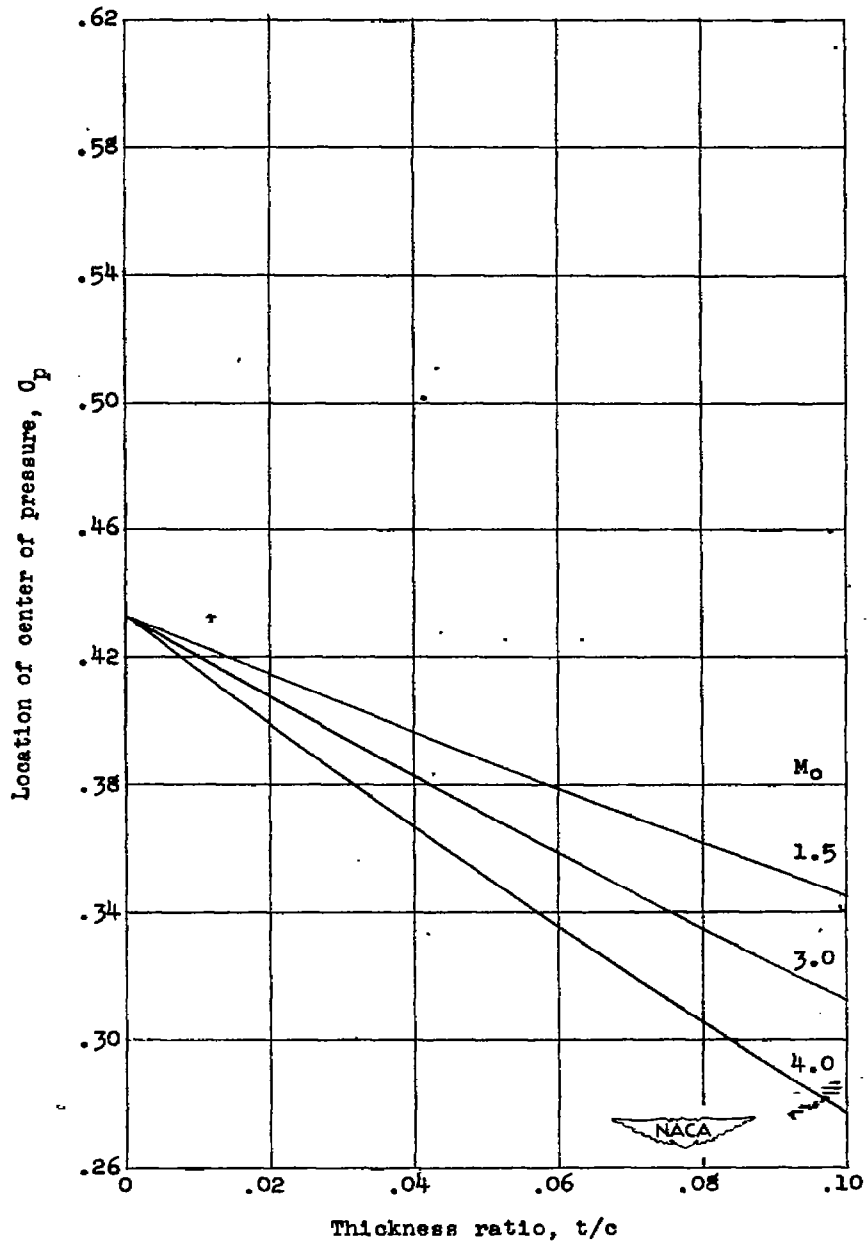cambered airfoils having maximum thickness at midchord.

$M_0 = 4.0$; $\frac{\delta_a}{\alpha} = 1.0$; $\frac{t}{c} = 0.10$.

(a) Trailing-edge aileron.

Figure 40.- Location of center of pressure as a function
of the thickness ratio for an uncambered parabolic
airfoil having maximum thickness at midchord.
$\frac{c_a}{c} = 0.2$; $\frac{\delta_a}{\alpha} = 1.0$.

Thickness ratio, t/c

(b) Leading-edge aileron.

Figure 40.- Concluded.